HOST UNIVERSITY: University of Queensland – University of Edinburgh

FACULTY: Engineering, Architecture and Information Technology[a] – College of Science and Engineering[b]

DEPARTMENT: School of Civil Engineering[a] – School of Engineering[b]

Academic Year 2022-2023

IGNITION AND FLAME SPREAD OF COMBUSTIBLE CEILINGS (DOWNWARD ORIENTED SURFACES)

Ahab Zahoor

Supervisor(s): Dr David Lange[a], Dr Rory Hadden[b], Dr Felix Wiesner[a], Dr Vinny Gupta[c]

(a) University of Queensland, Australia. (b) University of Edinburgh, United Kingdom.
(c) University of Sydney, Australia.

Master thesis submitted in the Erasmus+ Study Programme

International Master of Science in Fire Safety Engineering

Disclaimer

This thesis is submitted in partial fulfilment of the requirements for the degree of *The International Master of Science in Fire Safety Engineering (IMFSE)*. This thesis has never been submitted for any degree or examination to any other University/programme. The author(s) declare(s) that this thesis is original work except where stated. This declaration constitutes an assertion that full and accurate references and citations have been included for all material, directly included and indirectly contributing to the thesis. The author(s) gives (give) permission to make this master thesis available for consultation and to copy parts of this master thesis for personal use. In the case of any other use, the limitations of the copyright have to be respected, in particular with regard to the obligation to state expressly the source when quoting results from this master thesis. The thesis supervisor must be informed when data or results are used.

Read and approved,

(AHAB ZAHOOR)

(11th May, 2023)

Acknowledgement

I would like to express my sincere gratitude to my supervisor, Dr. David Lange, for his invaluable guidance and support throughout my research. His expertise in the field of fire science and his dedication to mentoring have been instrumental in shaping the research

I would also like to extend my thanks to my other supervisors, Dr. Felix Wiesner and Dr. Vinny Gupta, for their contributions and assistance in this project. Their expertise and support have been indispensable in helping me navigate the various challenges I encountered along the way.

I would thank Dr, Ishtiaq Warraich and Dr. Adnan Hamid, the professors from bachelor's university who wrote my letter recommendations for the IMFSE program. Dr Haroon ur Rasheed (Registrar, PIEAS) for all kinds of administrative help.

I would also like to acknowledge the contributions of Sergio Zarate, Julian Mendez, and Akshay Baheti, who provided invaluable assistance in carrying out the experiments and analysing the data. I appreciate Dr Qudsiah Ghazanfar for the love and emotional support.

I would like to extend my sincere gratitude to the International Master of Science in Fire Safety Engineering (IMFSE) Board and Dr. Grunde Jomaas for providing me with the opportunity to be part of this prestigious program. The knowledge and experiences I gained during this program have been invaluable to my personal and professional development. I am especially grateful to Prof. Bart Merci, Dr. Rory Hadden, and Lies Decroos for their guidance and support throughout thesis and my masters as well.

Finally, I would like to thank my family and friends for their constant love, and encouragement. Especially, Ahsan Rehman Khan, Abdul Moeed, Hateem Ghani and Khadija Siddique for the support, and my class fellows Muneeb Kazmi, Muneeb Khalid for the unconditional cooperation and these people are like a family away from home.

Abstract

This dissertation presents a methodology involving experimental setup and design, for the investigation of ignition and flame spread characteristics of combustible ceilings. The flame spread is an important parameter to study for understanding the fire growth and develop the design fires.

The experimental setup consisted of rectangular (1500mm x 500mm x150mm) CLT samples placed at a distance above a radiant panel. The radiant panel created a heat flux distribution along the length of the samples and line burner was used to ignite the sample from one end. The experiment and sample was instrumented with solid phase thermocouples to measure the temperature through the thickness for the thermal penetration. Bidirectional probes along with differential pressure gauges was implemented to gather the velocity data. Video recording was done to extract the flame spread rate from the footages later on.

The experimental scheme consisted of 6 tests conducted, at different representative heat flux distributions to study the effect of heat flux on the ignition times and the flame spread rates. It was found that in this orientation the flame spread is highly sensitive to the geometric changes. The fluid dynamics play a major role in the fire behaviour as well, as no flaming was observed right above the radiant panel due to high turbulence and high gas velocities low residence times. Flame initially spreads on the edges and these two edge flames joined each other downstream from the radiant panel, the pyrolysis gases released from sample right above the radiant panel did not burn right away, rather travelled downstream and burn there. Flames extended far beyond the pyrolysis front and due to buoyancy, flames kept attached to the ceiling, hence no distinction between the flame spread and flame extension could be made.

Critical heat flux for ignition was found to be 14.47kW/m^2 with the ignition/pyrolysis temperature of 378^{0}C. the max flame spread rate was 125mm/s for test 2 with 45kW/m^2.

Table of Contents

Disclaimer ii

Acknowledgement iii

Abstract iv

Table of Contents 1

List of Figures 4

List of Tables 7

Nomenclature 8

Chapter 1: Introduction 10

1.1 Background and Motivation 10

1.1.1 Engineered Timber in Built Environment 11

1.1.2 Open Plan Compartments 12

1.1.3 Flame Spread 13

1.2 Aims and Objectives 13

1.3 Thesis Layout. 14

Chapter 2: Literature Review 15

2.1 Timber in Built Environment and Fire Engineering 15

2.1.1 Compartment Fire Framework and Exposed Timber 16

2.1.2 Open plan compartments and exposed timber 18

2.2 Flame Spread 21

2.2.1 Parameters which affect flame spread 23

2.3 Research gaps 26

Chapter 3: Methodology 28

3.1 Conceptual design and outline 28

3.2 Design of experimental setup 29

3.2.1 Components 29
3.3 Measurements and instrumentation 32
3.3.1 Solid phase temperature 32
3.3.2 Gas phase temperature and velocity 33
3.3.3 Heat flux measurement 33
3.3.4 Visual recording 34
3.4 The instrumentation matrix 34
3.5 Heat flux calibration 37
3.6 Test matrix 38
Chapter 4: Results and Discussion 40
4.1 The fire behaviour 40
4.1.1 Test 1 40
4.1.2 Test 2 41
4.1.3 Tests 3-6 42
4.1.4 Discussion on flame behaviour 47
4.2 Critical heat flux and ignitability 48
4.2.1 Ignition process 48
4.2.2 The ignition model 49
4.2.3 Calculation of CHF, ignition temperature and thermal inertia 50
4.2.4 Discussion 53
4.3 Flame spread investigation 53
4.3.1 Theoretical model of flame spread 53
4.3.2 Experimental results of flame spread 55
4.3.3 Discussion 60
4.4 Pyrolysis front tracking 61
4.4.1 Discussion 69
4.5 Gas velocities 70
4.5.1 Discussion 73
4.6 “Pyrolysis Front Spread Parameter” 73
4.6.1 Discussion 75
Chapter 5: Conclusion and Future Recommendations 76
5.1 Conclusions 76

5.2 Future Work 77
References 79
Appendix A ..... a
Appendix B ..... d
Appendix C ..... j
Appendix D ..... k

List of Figures

Figure 1.1 Flame spread as a sequence of ignition process, reproduced from [20] .. 13
Figure 2.1 Australia's commercial all timber building, copied from [24] 16
Figure 2.2 Physical Schematic of modes of flame spread, reproduced from [52] 22
Figure 2.3 (left) flame spread rate over thin fuel vs angle of inclination from horizontal (data extracted from[56]). (right) flame spread rate from horizontal to 30^0 (data extracted from [57]) 24
Figure 3.1. Flame spread investigation conceptual design. 28
Figure 3.2. Experimental schematic 29
Figure 3.3 Sample placed on the frame 30
Figure 3.4 Radiant panel 31
Figure 3.5 Individual TSC 34
Figure 3.6 Sample and instrumentation view from underside of the sample 34
Figure 3.7 Instrumentation schematic 35
Figure 3.8 Representative heat flux values and their distribution 38
Figure 4.1 Flame stages for test 2. 1) ignition, 2) max extent of flame spread, 3) flames dying out and 4) reignition. Legend -white (no flame) – black (flame).. 42
Figure 4.2 Stages of flame spread for test 3. 1) ignition, 2) flame spreading on the edges, 3) flames joining from the edges and 4) flame spread further after connecting from both edges. Legend -white (no flame) – black (flame) 43
Figure 4.3 Stages of flame spread for test 4. 1) ignition, 2) flame spreading on the edges, 3) flames joining from the edges and 4) flame spread further after connecting from both edges. Legend -white (no flame) – black (flame) 44
Figure 4.4 Stages of flame spread for test 5. 1) ignition, 2) flame spreading on the edges, 3) flames joining from the edges and 4) flame spread further after connecting from both edges. Legend -white (no flame) – black (flame) 45

Figure 4.5 Stages of flame spread for test 6. 1) ignition, 2) flame spreading on the edges, 3) flames joining from the edges and 4) flame spread further after connecting from both edges. Legend -white (no flame) – black (flame) 46
Figure 4.6 Major events during Test 3. 1) Ignition on the edge, 2) Flame spreading on the edges, 3) Edge flames coincide in the middle and 4) Flame spreading further downstream 47
Figure 4.7 Processes leading to piloted ignition of solids, reproduced from [50]..... 49
Figure 4.8 Time to ignition vs heat flux 51
Figure 4.9 Inverse square root of time to ignition vs incident heat flux 52
Figure 4.10 Control volume consideration for the theoretical model development (copied from [52]).....54
Figure 4.11 Centerline flame spread for Test 2..... 55
Figure 4.12 Test 2 inverse square root of flame spread velocity vs heat flux, with linear curve fitting as per equation (4)..... 56
Figure 4.13 Test 3 flame spread rate evaluated as a function of X location. (left) flame spread rate on the edge, (right) flame spread rate on the centreline..... 56
Figure 4.14 Test 4 flame spread rate evaluated as a function of X location. (left) flame spread rate on the edge, (right) flame spread rate on the centreline..... 57
Figure 4.15 Test 3 Inverse square root of flame spread rate vs heat flux. (left) edge, (right) centreline..... 57
Figure 4.16 Test 4 Inverse square root of flame spread rate vs heat flux. (left) edge, (right) centreline..... 58
Figure 4.17 Test 5 flame spread rate evaluated as a function of X location. (left) flame spread rate on the edge, (right) flame spread rate on the centreline..... 58
Figure 4.18 Test 6 flame spread rate evaluated as a function of X location. (left) flame spread rate on the edge, (right) flame spread rate on the centreline..... 59
Figure 4.19 Test 5 Inverse square root of flame spread rate vs heat flux. (left) edge, (right) centreline..... 59
Figure 4.20 Test 6 Inverse square root of flame spread rate vs heat flux. (left) edge, (right) centreline..... 60

Figure 4.21 Test 1 surface temperature at five X locations vs time 62
Figure 4.22 Test 2 surface temperature at five X locations vs time 63
Figure 4.23 Test 3 surface temperature at five X locations vs time 63
Figure 4.24 Test 4 surface temperature at five X locations vs time 64
Figure 4.25 Test 5 surface temperature at five X locations vs time 64
Figure 4.26 Test 6 surface temperature at five X locations vs time 65
Figure 4.27 Test 1 (Left) time to pyrolysis temperature with respect to the X location. (Right) Pyrolysis front movement rate as a function of location. 66
Figure 4.28 Test 2 (Left) time to pyrolysis temperature with respect to the X location. (Right) Pyrolysis front movement rate as a function of location. 66
Figure 4.29 Test 3 (Left) time to pyrolysis temperature with respect to the X location. (Right) Pyrolysis front movement rate as a function of location. 67
Figure 4.30 Test 4 (Left) time to pyrolysis temperature with respect to the X location. (Right) Pyrolysis front movement rate as a function of location. 67
Figure 4.31 Test 5 (Left) time to pyrolysis temperature with respect to the X location. (Right) Pyrolysis front movement rate as a function of location. 68
Figure 4.32 Test 6 (Left) time to pyrolysis temperature with respect to the X location. (Right) Pyrolysis front movement rate as a function of location. 68
Figure 4.33 Test 3 Actual and smoothened gas velocities..... 71
Figure 4.34 Test 4 Actual and smoothened gas velocities..... 72
Figure 4.35 Inverse pyrolysis front speed vs heat flux for Test 3 74

List of Tables

Table 2-1 Summary of fuel load densities in x-ONE and x-TWO (extracted from [45])..... 20
Table 3-1 Instrumentaton matrix..... 35
Table 3-2 The test matrix..... 38
Table 4-1 Time to ignition for Tests 2-6..... 50
Table 4-2 Thermal parameters of CLT*..... 51
Table 4-3 Extent of pyrolysis front as X location with respective heat flux..... 69

Nomenclature

Symbol / Abbreviation	Name	Unit
CLT	Cross Laminated Timber	-
CHF	Critical Heat Flux	kW/m^2
k	Thermal Conductivity	W/mK
ρ	Density of CLT	kg/m^3
c/c_p	Specific Heat of CLT	J/kgK
$k\rho c$	Thermal Inertia	kW^2s/m^4K^2
$\varepsilon_w/\ \varepsilon$	Emissivity of surface	-
T_{ig}	Ignition temperature	^0C
T	Temperature	^0C
t	Time	seconds
t_{ig}	Time to ignition	seconds
t_p	Time to pyrolysis	seconds
$\dot{Q}_R''$	Incident Radiant Heat Flux	kW/m^2
X location (x)	Distance along length of sample from edge above line burner	mm
Y location (y)	Distance along width of sample	mm

Z location (z)	Distance along thickness of sample from fire side	mm
$\emptyset$	Flame Spread Parameter	kW^2/m^3
v	Flame Spread Rate	mm/s
v_e	Edge Flame Spread Rate	mm/s
v_c	Centreline Flame Spread Rate	mm/s
α	Thermal diffusivity	m^2/s
ρ_g	Gas density	kg/m^3
U	Gas velocity	m/s
V	Voltage from BDP and DPT assembly	Voltage
ΔP	Differential pressure from BDP	Pascal
K	Correction factor for BDP	-
T_g	Gas temperature	^0C
ASET	Available Safe Egress Time	
v_p	Pyrolysis front speed	mm/s
σ	Stephen Boltzman Constant	5.67×10^{-8} W/m^2K^4

Chapter 1: Introduction

In the following chapter, the context and motivation are provided that led to my research project. The chapter also outlines the goals, aims and objectives of the research, and the scope of this report which covers the extent of topics to be discussed.

1.1 Background and Motivation

Due to their environmental credentials and societal goals of sustainable development with lower energy demands and less pollution in all sectors, timber structures have undergone a resurgence in recent decades[1–3]. This also includes the construction sector, which represents a significant portion of the overall community economy[4]. In contrast to conventional, usually non-combustible construction forms, timber also satisfies architectural aspirations, can result in lower construction costs, and can speed up construction[5,6]. Recent architectural ideas frequently include tall mass timber structures with spacious open floor plans for use as offices and public spaces[7]. However, as timber is a combustible material and participates in the fire as fuel, hence, the use is restricted by regulatory authorities and building regulations. The restrictions are more strict and severe in case of larger and taller buildings[8–10].

The open plan environments have gained a lot of popularity, they offer many benefits, including a greater sense of space, improved natural light, and greater flexibility in home design[11]. Open-plan offices in contemporary design and modern tall buildings have become increasingly popular in recent decades.

The problem arises when the two concepts of open plan spaces and exposed timber are combined together. Introducing exposed timber into the built environment increases the fire hazard as timber is a combustible material and adds to the overall fuel load.

Gupta presented a framework of open plan compartment fires[12]. He conducted a study of fire dynamics in open plan compartments [12] and the work is still on going. Starting

from 1950s to date detailed research has been conducted for the compartment fire dynamics, the documentations is also readily available and is a part of many building safety regulations. But this work was centred mainly on smaller compartment with respect to the floor area and with restricted ventilation. Open-plan compartments or compartments with a large amount of ventilation cannot be accommodated by this methodology[12–15].

And lastly the spread of flames under the ceilings has been scarcely studied. Flashover can very often be triggered by the flames spreading under the ceilings[16]. The major problem is that it effectively drives flame spread on the fuel load and also increases your burning rate due to large thermal feedback.

After conducting a detailed literature review, Phillion et al[17]. discovered that the parameters pertaining to incident heat flux, flame spread rate, and extinction rate are insufficiently detailed in terms of their expected behaviour when applied to CLT ceilings.

In light of above discussion, the ceiling flame spread is an important aspect of fire dynamics. Additionally, the geometric changes will affect the residence time of combustible gases under ceilings hence changing the fire dynamics significantly. In the compartment fire context it will lead to faster fire growth and result in early flashover. Flame spread under ceiling of carriage was one of the important factor which resulted in Daegu underground railway fire[18,19]. In the context open plan compartment (discussed in Chapter 2:Literature Review) the exposed ceiling will lead to larger heat feedback on the fuel and higher speed of travelling fire in the open compartment. The CHF and ignition temperature affect timeline of the events happening and change the overall ASET value. Hence, this research is focused on the ignition and flame spread of timber, charring combustible material, under ceiling in downward facing orientation. Including the CHF and ignition temperatures along with geometric changes like downstands effect on spread.

1.1.1 Engineered Timber in Built Environment

Engineered timber, is a type of wood product that is made from multiple pieces of wood that have been bonded together using adhesives or other technologies.

Engineered timber is increasingly being used in the built environment due to its unique properties, sustainability, and aesthetic appeal. One of the key advantages of using engineered timber in construction is its high strength-to-weight ratio, which allows for efficient material use and design flexibility. Engineered timber products are also dimensionally stable, meaning they are less likely to warp or shrink than traditional solid wood products.

Cross-laminated timber (CLT) is a type of engineered wood product made from layers of lumber boards stacked crosswise and glued together under pressure, resulting in a solid wood panel with enhanced structural properties. The boards are typically oriented perpendicular to each other, which creates a stable, strong, and rigid panel that can be used for a variety of construction purposes, such as walls, floors, and roofs.

1.1.2 Open Plan Compartments

Open plan compartments refer to interior spaces that are not divided by traditional walls or partitions, but rather have an open and flowing design. This type of design has become increasingly popular in contemporary architecture, particularly in commercial spaces, due to the sense of openness, flexibility, and social interaction it can create[11].

Open plan compartments are often used to create a seamless flow between different areas of a building, such as between the kitchen, dining, and living areas in a residential home. They can also be used in commercial spaces such as offices and coworking spaces to foster collaboration and communication between employees.

In addition to the aesthetic appeal of open plan compartments, this design can also provide practical benefits. It can allow for better natural lighting and ventilation, and it can create the impression of more space, making small areas feel larger.

Overall, open plan compartments can provide a unique and versatile design option for architects and designers, allowing for creative and functional interior spaces that promote social interaction and flow.

1.1.3 Flame Spread

Understanding fire growth is essential to comprehending fire behaviour. The process of fire growth is intrinsically linked to the flame spread through the fuel.

Flame spread can be described as a sequence of ignition processes. This process begins with the ignition of the fuel, which generates heat and a localized flame. As the flame spreads, it heats up the surrounding fuel, causing it to pyrolyze and release combustible gases. These gases mix with the air and ignite, generating additional heat and propagating the flame further. This sequence of ignition processes continues as the flame spreads across the surface, consuming the fuel in its path, as illustrated in the Figure 1.1. Understanding flame spread is necessary to develop design fires and to understand consequence of fire.

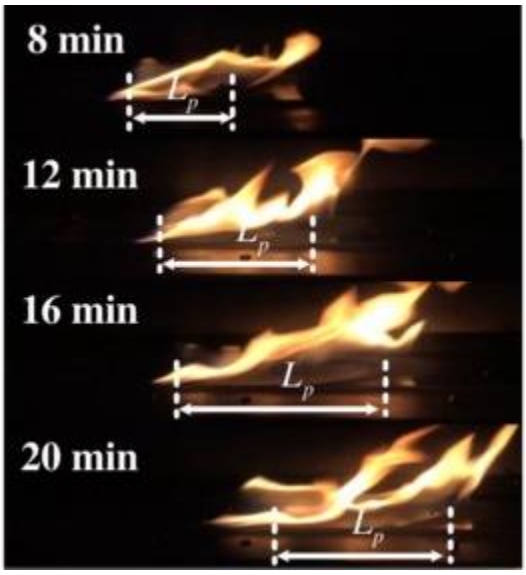

Figure 1.1 Flame spread as a sequence of ignition process, reproduced from [20]

1.2 Aims and Objectives

The aim of this research project is to study the ignition and flame spread of timber (combustible) ceilings (downward oriented surfaces). The objectives are given below,

1. Development of methodology to investigate the flame spread characteristics of combustible ceilings. This includes the experiment setup design along with the associated instrumentation.

2. Study the effects of external heat flux on the ignition characteristics of CLT in downward orientation.
3. Calculate and extract flame spread rate under exposed timber ceilings. And study the effect of heat flux distribution on the flame spread rate.
4. Study the effect of downstands on flame spread and fire behaviour.

1.3 Thesis Layout.

Chapter 1: Introduction

Chapter 1 discusses an introduction to the topic and brief intro to engineered timber in built environment, open plan compartments and flame spread. Motivation and background of the topic is presented along with the aims and objectives of current research.

Chapter 2: Literature Review

Detailed historical literature is presented and discussed in this chapter. Specific focus is kept on the use of timber in built environment and open plan compartments with exposed timber. Along with the aspect of flame spread on the surfaces.

Chapter 3: Methodology

The conception and design of experiment along with the components being used, is presented. Instrumentation and test matrix followed is presented.

Chapter 4: Results and Discussion

The results of fire behaviour, ignition parameters, flame spread and propagation of pyrolysis front is shown, and these results are also discussed. The equations used for calculation are included along with the inferences extracted from the presented results. The discussion also includes error and uncertainty sources where applicable.

Chapter 5: Conclusions and Future recommendations

This chapter concludes the thesis with major outcomes extracted from this research, future recommendations are also provided for further research which will tend to minimize the errors associated with the results.

Chapter 2: Literature Review

The detailed literature review of flame spread and open plan compartment fire is provided in this chapter below this also includes the engineered timber in fire scenarios.

2.1 Timber in Built Environment and Fire Engineering

In the past one to two decades engineered timber has increased in demand in the built environment. This is a result of environmental concerns to reduce the carbon emissions. The Intergovernmental Panel on Climate Change (IPCC) suggests that the built environment sector's operational energy usage is responsible for 40% of primary energy demand and 36% of CO2 emissions in industrialized nations. When the embodied energy and greenhouse gas (GHG) emissions of construction materials are factored in, these percentages become even greater[21]. According to Broun and Menzies (2011), the construction sector globally is linked with 60% of the extractions from the lithosphere[22].

Built environment sector can significantly contribute to reducing climate change by decreasing operational energy usage and selecting construction materials with minimal environmental impact. Increasing the usage of timber in construction has the possibility to reduce the impact of climate change. Timber has a potential for climate change mitigation in two ways - first, by substituting materials that have higher embodied energy and carbon; and second, by storing sequestered atmospheric carbon dioxide in long-life products[23].

Engineered timber is a sustainable building material that has a lower carbon footprint compared to other conventional construction materials like concrete and steel. Additionally, it is a renewable resource that can be sourced from responsibly managed forests, aligning with sustainable building practices.

Engineered timber is being used in a wide range of applications in the built environment, including mid-rise and high-rise buildings, residential homes, schools, and other

commercial structures. Its use in building construction can result in reduced construction time, lower costs, and improved environmental performance.

Furthermore, engineered timber's aesthetic appeal is driving its use in building design, where it is used to create warm and inviting spaces, provide natural texture and warmth, and create unique and expressive architectural features. Overall, the use of engineered timber in the built environment is increasing due to its many advantages, and it is likely to continue to grow in popularity in the future

With the increase in the use of timber in construction the fire safety engineering concerns have surfaces because of its combustible nature. Also, architects aspire to have an exposed timber for more artistic look but fire safety is being a biggest hurdle in its way. Figure 2.1 shows Australia's commercial timber building.

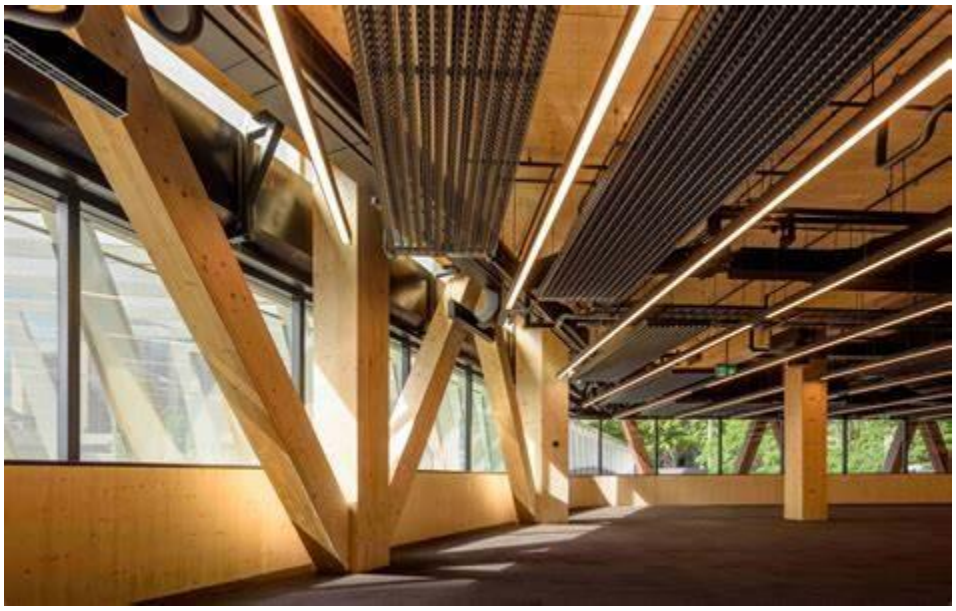

Figure 2.1 Australia's commercial all timber building, copied from [24]

2.1.1 Compartment Fire Framework and Exposed Timber

A detailed research has been conducted in the past of the compartment fire dynamics to understand the various concepts of the fire inside the compartment. This detailed research has led to simplified correlations which can be used to a certain degree of acceptance in the fire scenarios. This leads to a compartment fire framework, that provides correlations for the fire design of the compartment fire. The compartment fire framework refers to a

systematic approach or framework used to analyse and understand the behaviour, dynamics, and effects of fires that occur within confined spaces or compartments. It involves the study of various factors such as fire growth, flame spread, heat transfer, smoke production, and structural response within the compartment[25].

Adding, timber (CLT) into the compartment as exposed structural element not only increases the fire load inside the compartment but also changes the fire dynamics of the compartment[26]. This has been shown in the recent researches over the year.

Two significant assumptions have been identified by Gorska et al[27] that are not sufficient for compartments built with Engineered Wood Products (EWP):

1. The methodology proposed for predicting maximum temperatures assumes heat loss through all compartment boundaries except for the floor covered in burning fuel. However, this assumption may not hold true for timber surfaces, as timber is prone to igniting and contributing additional heat to the compartment instead of acting as a heat sink. The exposed CLT walls might act as thermal source rather than heat sink.
2. Transition from fuel controlled to ventilation controlled fire and the velocity field is attributed to the geometric dimensions. But for the exposed timber these velocity field will be altered.

Hadden et al[28] found that there was no significant difference on the compartment temperatures with exposed timber as compared to those predicted by existing correlations for compartment fire. This was also found by Frangi and Fontana[29]. However, the rate at which heat was released was greater than what the correlations predicted. The most significant finding of the research was that in compartments with two exposed timber surfaces, it has been observed that auto-extinction, occurs if the char layer remains attached without delamination during the fuel load combustion or decay period. Auto-extinction in timber refers to the phenomenon where the combustion of a timber sample ceases to produce flames once the net heat flux to the sample falls below a critical threshold[30–32]. Compartments with three exposed timber surfaces did not exhibit this phenomenon since heat transfer between the surfaces prevented the critical heat flux required for extinction

from being achieved. This implies that the occurrence of auto-extinction in timber compartments depends on the count of exposed surfaces as well as the characteristics of the char layer throughout combustion and decay.

Bartlett et al [8] provide some literature review for fire dynamics with exposed timber. Compared to light timber frames, large solid timber panels such as CLT are less likely to have fire spread through void cavities[33]. However, the use of large solid timber panels may lead to an increase in the effective fire load, which is caused by the increased surface area of timber due to the possibility of delamination during heating [34]. Frangi and Fontana also concluded that for the compartment with combustible lining the flashover is reached 30-55% earlier and with severe external flaming[29].Mcgregor [35] found that during the growth phase of the fire in the unprotected tests, the CLT panels were quickly involved, leading to an escalated fire growth rate . Also, the ceiling panels were the first to ignite, and in just 20 seconds, all exposed surfaces of the CLT were on fire, causing rapid flashover[35]. Secondary flashover is also one of the concepts for the exposed timber compartment, this can happen due to delamination[36].

In the research focused on the compartment fire dynamics with CLT ceilings, Mcnamee et al [37], found that by addition of a timber ceiling made of flammable material increases the temperatures inside the compartment, regardless of whether the fire is fuel-controlled or ventilation-controlled.

2.1.2 Open plan compartments and exposed timber

Fire dynamics in an open plan compartment is the current topic of interest of researchers and efforts are being made to better understand the phenomenon[12]. In the open plan compartments the flow dynamics are different and are not primarily hydrostatically driven, hence, cannot be explained by the compartment fire dynamics[12].

The complexity of large compartment fires stems from the possibility that post-flashover may not always occur during their evolution. This can result in various "modes of fire spread" that affects and controls the fire dynamics[38]. It has been observed that there are three modes of fire spread in open floor plans, which are determined by the ratio between the velocity of the flame front (V_S) and the burnout front (V_{BO})[39]. Although experiments

have shown the existence of these modes[40], comprehending the fundamental physical mechanisms governing each mode and their unique behaviour is essential to establish a scientific framework for evaluating the thermal exposure of structures in real fires within large open-plan compartments.

Gupta et al studied the ventilation effects in the open compartments. The thermal properties resulting from the various modes of fire spread and the influence of the ventilation applied were examined[41]. Spatial heat distributions with distinct and significant characteristics are induced by each fire spread mode. The results showed that even with lower gas temperatures and irradiation, fires in open-plan compartments with large opening areas and dominant plume flows imposed equivalent or possibly severe thermal loading on structural systems. This suggests that the current design fire methodologies do not fully capture the unique and potentially more severe thermal loading of fires in open-plan compartments.

Nothard et al studied the influence of a timber ceiling and intrusions on the ceiling on the rate at which flames spread across the fuel-bed located on the floor[42]. The conclusion drawn from this research are important consideration in the context of current dissertation.

It was found that upon ignition of a Cross Laminated Timber (CLT) ceiling, there is a notable escalation in the rate of fire spread within the compartment. The compartment rapidly progresses to a fully developed fire state. It is observed that the transition to a fully developed fire state is significantly quicker in the case of CLT ceilings[42]. Moreover, the results suggested that the ceiling orientation is a critical variable in predicting the ignition of CLT ceiling as the residence time is changed due to the change in orientation. Ceiling intrusions led to a significant increase in spread rates. The fuel-bed spread rates are slower initially when a timber ceiling is present, but once the ceiling ignites, flames spread rapidly across it. Flames and smoke layer tends to accelerate the flame spread[42]. HRR was found to be increased by 45% by the inclusion of the exposed CLT as secondary fuel load. The presence of CLT was observed to have a substantial impact on the flame spread rate, increasing it by as much as 40%. This is attributed to the flaming ceiling emitting radiation downwards, which affects the remaining fuel load and accelerates the spread of the fire[43]. During the postprocessing the CHF was evaluated to be 30kW/m^2[43], which is much

larger than 11-14kW/m^2 presented in the literature. This asks for a more refined research and approach to the ignition problem.

In 2017 x-ONE fire experiment was conducted in the attempt to study the fire dynamics of open large compartment[44], with the floor area of 380m^2. The results showed a travelling fire along the span of the compartment. A changing flame spread from 3mm/s to 167mm/s was observed as the rate accelerated. This experiment was with non-combustible lining having no exposed timber on ceiling or walls or columns. The installation of thermocouples and cameras along the fire path revealed distinct near-field and far-field regions, indicating significant non-uniform spatial temperatures and burning within the compartment and no evidence of occurrence of flashover was observed. In 2019 same enclosure was used to perform x-TWO experiment with a different fuel load[45]. Table 2-1 below shows a summary of x-ONE and x-TWO experiment fuel load. The objective of the study was to investigate how altering the fuel load affects the dynamics of travelling fires and to minimize other factors that may influence the behaviour of fires, given that the compartment and ventilation were kept constant. The experiment allowed the fire to grow naturally and effectively recorded a 32-minute fast and accelerating fire spread during Part 1, and a 180-minute steady-state traveling fire spread during Part 2. Flashover was not observed which was consistent with the result from x-ONE. In Part 1 of the experiment, the fire spread rate was not consistent, and it was gradually increasing instead of being assumed as constant in the traveling fire methodology. The same was true to some extent in Part 2 as well[45].

Table 2-1 Summary of fuel load densities in x-ONE and x-TWO (extracted from [45])

Experiment/Code	**x-ONE [15]**	**x-TWO Part 1**	**x-TWO Part 2**
Fuel load MJ/m^2	370	355	249
Wood crib layers	11,5	11,5	8,5
Fibreboard layers	2 covered 6m x 29m	2 covered 6m x 1m	2 covered 6m x 1m

To further the research of the open-plan compartment, especially with exposed timber, new set of experiments were designed named CodeRed experiments. CodeRed#1 experiments, with floor area of 352m^2, found that involvement of timber structure (CLT ceiling and

Glulam columns) in the fire increased the HRR nearly two times as was expected by the burning of wood crib only[46]. It was found that flames spread rapidly across the ceiling and within almost 5 minutes whole of the crib was flaming as well. Kotsovinos et al found in the CodeRed #2 experiment, that ventilation has an effect on the fire dynamics of a large compartment. The research suggested that reduction in ventilation slowed down the fire spread along with the burning rate. However, it increased the duration of fire[47]. CodeRed #4 was aimed at studying the effect of encapsulation (partial) on the fire dynamics of open plan compartment[48]. Around 50% of the CLT ceiling was encapsulated, which resulted in delayed ignition of ceiling. Once the ceiling ignited the fire spread rapidly throughout the compartment. The max HRR was approximately 17% less than the fully exposed CLT ceiling. The charring depth was found to be around 25mm which was not significantly different, suggesting that the severity of fire is not affected by the encapsulation and also ceiling went on to smoulder even with encapsulation.

Comparing between x-ONE, x-TWO and CodeRed experiments it can be said that exposed timber increases the fire spread rate. Also with combustible ceiling faster and increase heat feedback is provided by burning ceiling.

2.2 Flame Spread

Surface flame spread refers to the movement of a flame in the vicinity of a region on the surface of a solid or liquid where pyrolysis or vaporization is occurring respectively, acting as a fuel source[49]. Flame spread is an important parameter to study in the domain of fire safety engineering. Fire growth is dependent on flame spread rate[50]. Flame spread is complex and complicated problem as this is not only a gas phase problem but also a solid phase problem as the pyrolysis gases are being released from the combustible surface[51]. This can be defined by a cycle process described below,

- The fuel is vaporized to give combustible gases.
- Pyrolyzing gases mix with oxygen.
- The pyrolyzed gases burn and form a diffusion flame.

- Heat feedback from this flame heat the virgin material to the ignition temperature and the flame spreads further on the surface.

This scope of this literature review will include solid flat surfaces for simplicity. Based upon the flow and direction of the free stream oxidizer, the spread can be categorized in two types of flame spreads, opposed flow (counter current) and concurrent flame spread. Opposed flow flame spread can be defined as a type of flame spread when the flow direction of air (oxidizer) is opposite to the direction of spread[50]. Some authors refer it as opposed flow flame spread[52]. The concurrent flame spread is when the direction of flow of free stream air is same as that of spread direction. The two modes are illustrated in the Figure 2.2.

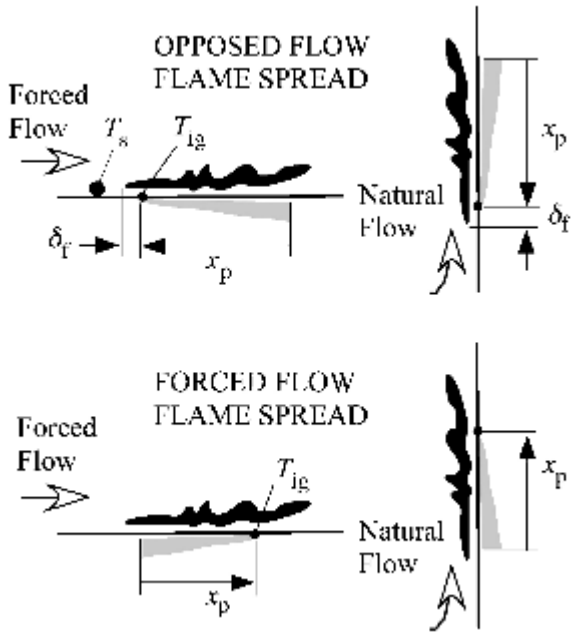

Figure 2.2 Physical Schematic of modes of flame spread, reproduced from [52]

De Ris [53] in 1969 presented a mathematical model for the counter current flame spread taking the heat transfer and mass transfer problem under consideration but assuming laminar flow and most of today's theoretical models build on this model. A detailed review of the theoretical models is presented I. S. Wichman [51] which states chronological developments in the topic of counter current (opposed flow) flame spread.

2.2.1 Parameters which affect flame spread

Flame spread can be influenced by several factors, such as the direction in which the surface is oriented, thickness of fuel, geometry of sample, the presence of wind and gravity, the flow of air or other materials, the physical state of the material being burned (solid or liquid), the size of the flame and amount of radiation, as well as the shape and geometry of the space in which the fire is occurring, such as corners, channels, or ducts[52]. Density, specific heat and thermal conductivity also affects the rate of spread significantly. Environmental factors such as oxygen concentration, ambient temperature or temperature of fuel, imposed external heat flux and atmospheric pressure affect the flame spread rate [50].

Few of these factors which are important and relevant in the scope of this research are discussed in the following sections

2.2.1.1 Effect of surface orientation

Solid surfaces are generally capable of burning in any orientation; however, when a flame is directed upwards on a vertical surface, flame spread occurs more rapidly. This has been shown by Magee and McAlevy[54,55].

The downward flame spread in vertical orientation was found to be less affected by the change in orientation. From -90^0 (vertically downwards) to -30^0 the spread rate was estimated to be almost constant but it increased approximately 3 times as the angle was changed from -30^0 to 0^0 (completely horizontal facing upwards)[56]. Here the angles are measured from the horizontal as 0^0. If we combine the above two results it can be fair to say that the increase from downward flame spread is approximately 50 times less than that in the upwards direction. This is shown in the Figure 2.3 extracted from data provided by Drysdale and Macmillan[57] and Hirani et al[56].

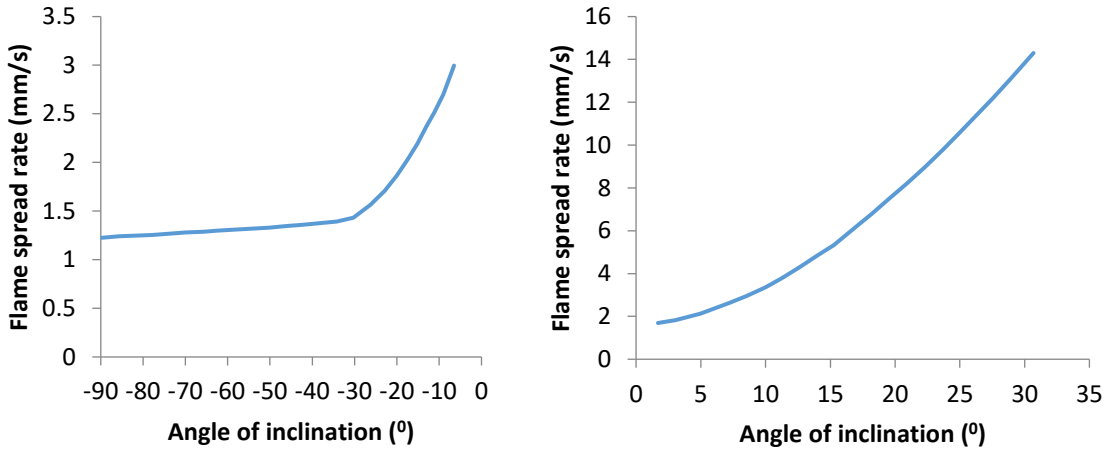

Figure 2.3 (left) flame spread rate over thin fuel vs angle of inclination from horizontal (data extracted from[56]**). (right) flame spread rate from horizontal to 30^0 (data extracted from** [57]**).**

Downward flame spread on the vertical orientation is termed as counter current spread as the pyrolysis front is moving downward and the air is entrained from below the flame into the fire. Whereas the upward flame spread is termed as concurrent flame spread as the air is entrained in the upward direction same as the spread direction[50,58]. The fast upward flame spread can be attributed to preheat zone ahead of the flame that helps heat the virgin fuel ahead[59,60].

Drysdale and Macmillan [57] discovered that a noticeable increase in the upward spread of fire occurs only when the inclination of the surface exceeds +15◦. The effect is particularly evident when the flame is spreading up a plane incline. However, the effect is considerably more pronounced when sidewalls prevent air entrainment from the side. This was observed during an investigation of a fire that spread rapidly on a wooden escalator at the King's Cross Underground Station in London[61,62]. The air entrainment was hindered by the escalator sides. This phenomenon was first identified by Markstien and deRis [63] which was later termed as the "Trench Effect". Detailed experimental and CFD simulation was later taken up to better understand and characterize this phenomenon[64–69].

Ceiling flame spread

The rate of upward spread on the underside of an incline has not been thoroughly researched, although there is a suggestion, that the phenomenon of upward spread may manifest at a faster rate on the lower surface of a fuel of substantial thickness as compared to its upper surface. This is attributed to the flame's buoyancy which keeps it in close proximity to the surface, leading to heightened efficiency of flame to surface heat transfer and thus an accelerated rate of spread. This is discussed below in context of flames under ceilings.

While a combustible ceiling can burn and disseminate flames, in order for this to happen, a "ceiling jet" must first be produced by a fire on the floor or a fire on a wall[50] or even the flames themselves under the ceiling. Without this forced flow, the flame spread rate will be slowed down. It can be said that for effective spread of flames under the ceilings we require an imposed co-current flow. This was shown by researches in wind tunnel studies with PMMA slab on the ceiling[70]. The factors responsible for upward flame spread are also responsible for the flame spread under the ceilings as confirmed by studies[16,71–76]. One interesting effect int this configuration is the buoyancy as it pushes the flame closer to the ceiling surface, hence if we assume everything else as same, the horizontal flame spread under the surface will be effectively more than the spread above the surface. However, if we discuss the spread below the surface in the inclined orientation it will not require an imposed flow as the flow will be induced by the flames themselves, creating a flow field below the surface.

2.2.1.2 Effect of imposed heat flux

If we have an imposed radiant heat flux, it will preheat the material ahead of the flame and will cause increase in the rate of flame spread[77–79]. As the rate of burning behind the flame front increases, the strength of the flames also intensifies, resulting in a greater amount of forward heat transfer and ultimately accelarating the process. The effects mentioned above are applicable in a broad sense, however, their significance varies depending on the orientation of the flame spread. Specifically, when the spread occurs in an upward vertical direction, the impact is significantly more pronounced than horizontal spread[[80,81].

Transient heating effects should be taken into account while examining the response of a surface to the applied flux, as the surface's reaction is not immediate[82,83]. According to Kashiwagi's findings [82], the flame spread rate on the surface of a material with high thermal thickness increases as the duration of exposure to constant heat flux increases. The way a material responds to thermal radiation initially is contingent on its thermal inertia, represented by the product of its thermal conductivity, density, and specific heat capacity ($k\rho c$). On the other hand, the surface temperature achieved at equilibrium determines the steady-state velocity, which corresponds to a long preheating time[82].

2.2.1.3 Effect of thickness of sample

For a thin sample of fuel lumped thermal capacity model can be applicable. For this kind of system with small thickness the flame spread rate is found to be inversely proportional to the thickness. The lesser the thickness is the faster the flame spread across the surface[55,84]. The lumped thermal capacity models suggests that whole thickness of the sample is at the same temperature and there is no temperature gradient across the thickness. Suzuki found that this relation holds for thickness up to 1.5mm[84]. As the thickness is increased the material starts to behave as thermally thick and starts to deviate from lumped thermal capacity model. Hence the flame spread rate starts to be independent of the thickness, so for semi-infinite material flame spread it can be said that change in thickness has no effect on the flame spread[52].

2.3 Research gaps

The issue of flame spread beneath ceilings has not been studied extensively, which is concerning given the increasing use of exposed timber in open plan compartments within the built environment. This problem is particularly important to address in order to ensure the safety of building occupants and to minimize damage to property. Therefore, it is crucial to identify and understand the variables that affect flame spread in a downward orientation. By doing so, these variables can be optimized during the design stage of buildings with exposed timber, ultimately leading to safer and more resilient structures.

Therefore, the objective of this research is to investigate and identify the various parameters and conditions that impact flame spread, with the aim of extracting and analysing key variables that contribute to this phenomenon. By doing so, this study will contribute to a better understanding of the factors that govern flame spread in exposed timber constructions.

Chapter 3: Methodology

An experimental methodology was designed to investigate the behaviour combustible ceiling, the ignition and flame spread and effect of incident heat flux on these parameters. This chapter discusses the experimental setup, instrumentation, target input and output variables.

3.1 Conceptual design and outline

To study the flame spread on the surface, a heat flux distribution is imposed in the surface and then the spread rate is measured against the imposed distribution of heat flux. Leung et al. [85] provides a detailed review of the various standard test procedures used for Lateral Ignition and Flame spread Test (LIFT). Usually, a decreasing heat flux is imposed on sample and is ignited at the end with highest flux measurement. Similar concept is adopted from these LIFT experiments for this experimental design. The conceptual outline is shown in Figure 3.1.

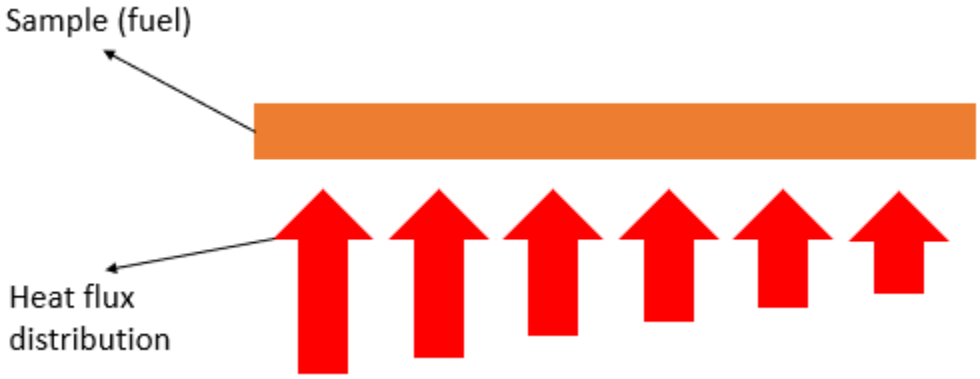

Figure 3.1. Flame spread investigation conceptual design.

3.2 Design of experimental setup

An experiment was designed to be conducted under the extraction hood. The schematic is presented in the Figure 3.2, showing the sample and various other components under the extraction hood.

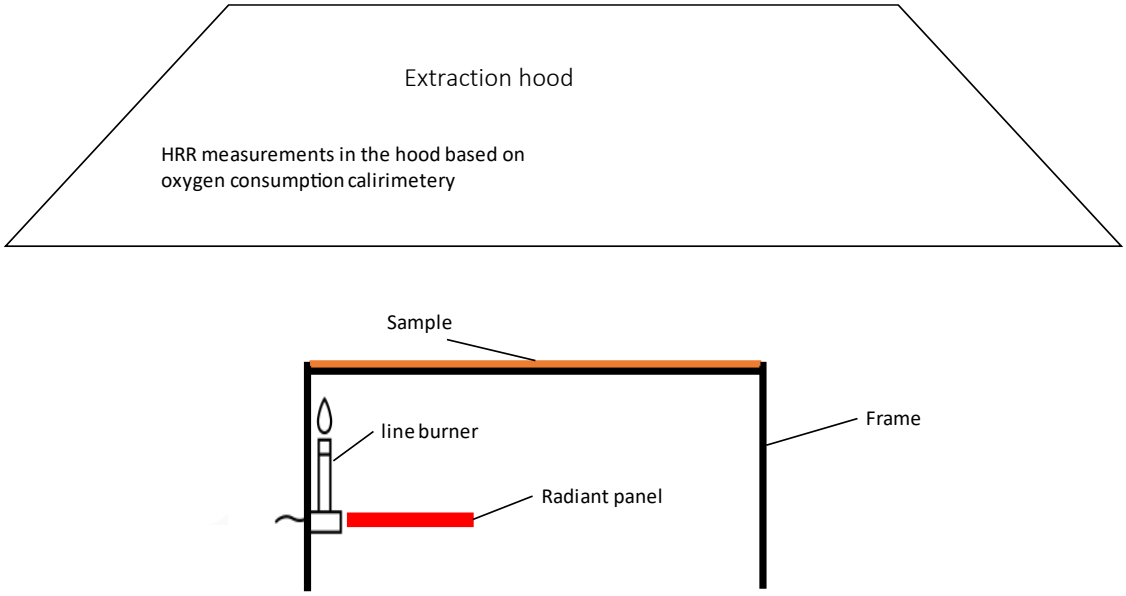

Figure 3.2. Experimental schematic

3.2.1 Components

Various components are used in the design and development of the setup that can be used to investigate the target parameters such as flame spread rate, flame spread parameter and ignition characteristics.

3.2.1.1 Frame/sample holder

In the context of flame spread testing, it is often necessary to lift the sample off of the ground. This requirement typically arises when the sample is in a downward-facing configuration or orientation. The reason for this is that in such cases, heat flux distribution needs to be applied from below the sample. By lifting the sample off of the ground, it becomes possible to achieve the desired heat flux distribution and accurately measure flame spread characteristics. To fulfil this requirement, a metallic frame with four legs is

utilized. This frame provides a sturdy base for the sample to be placed above the heat source. The frame also provides a fixture for gas phase instrumentation which will be discussed in this chapter later on, which is fixed to the metallic frame providing a stable fixture. This fixture helps in accurate measurements of gas parameters during the experiment. The frame's stability ensures the instruments remain in place and provide reliable data. Additionally, the instruments mounted on the frame can be positioned at specific distances from the sample, allowing for precise measurements. Figure 3.3 shows the sample holder/frame used.

Figure 3.3 Sample placed on the frame

3.2.1.2 Sample

CLT sample of 500mm width and 1500mm length. The samples had thickness of 150mm. The side exposed to fire is referred as fire side, had 40mm holes with depth of 40mm. These holes were drilled to install the TSCs for the heat flux measurement. The unexposed side had 5 holes at 5 different locations for the solid phase temperature measurement through thermocouple. The details of the instrumentation is provided in section 3.2.2 and section 3.2.3. Drilling template or drawing for the sample preparation is provided in appendix.

3.2.1.3 Ignition source

In this experiment, the line burner is employed as an ignition source. The purpose of using a line burner is to facilitate the distribution of the pilot flame uniformly across the width of the sample. This results in more simultaneous and even ignition along the entire width of

the sample, which is essential for achieving consistent and accurate experimental results. The line burner is designed to produce a thin, linear flame that can be easily controlled and manipulated to suit the specific requirements of the experiment. By using the line burner as an ignition source, it can be ensured that the combustion process is initiated in a controlled and uniform manner

3.2.1.4 Radiant panel for heat flux distribution

The use of propane gas radiant panels to create a heat flux distribution provides a controlled method of heat transfer to the sample being tested. The fuel and oxidizer are premixed and fed through the nozzles, allowing for consistent and even combustion on the surface of the panel. By adjusting the distance between the panel and the surface of the sample, the desired heat flux can be obtained. This method is widely used in fire science experiments to simulate the heat flux that a material or structure may be exposed to in a real fire scenario.

Figure 3.4 shows the radiant panels used to create the heat flux distribution.

Figure 3.4 Radiant panel

3.2.1.5 Smoke extraction hood

Typically for most of the fire science experiments the extraction hoods are used. The purpose of an extraction hood in fire science experiments is to capture and remove smoke and other combustion by-products generated during the experiment. The complete experimental setup is typically placed under the hood to ensure that any smoke or fumes generated are captured and removed from the surrounding environment. This helps to minimize the amount of smoke and other combustion by-products that may be released into the laboratory or testing facility, which can pose health and safety risks to people present and conducting the experiment. Additionally, the extraction hood helps to maintain a clear field of view, which is important to monitor the progress of the experiment and collect data. The extraction hood is also instrumented with the gas analysis probes, so HRR can be calculated based on Oxygen Consumption Calorimetry[86].

3.2.1.6 Blue light

A UV light was used during the experiment. The purpose of this light was to attempt to track the pyrolysis front using camera with the blue filter. The blue filter removes all the other possible wavelengths from the video and only keeps the blue wavelengths, this helps in visualizing the pyrolysis gases being released and tracking the pyrolysis front. This filters out the flame and effectively can see through the flame[87].

3.3 Measurements and instrumentation

This section provides a description of all the measurements and instrumentation used for the experiment.

3.3.1 Solid phase temperature

The thermal penetration through the sample thickness was monitored by utilizing 1.5mm K-type thermocouples, during the experiment. The placement of these thermocouples involved a total of 5 locations spanning the length of the sample. These 5 locations are 125mm, 375mm, 625mm, 875mm and 1125mm. Within each location, temperature readings were collected from 5 different thicknesses, specifically at 2mm, 4mm, 8mm,

15mm, and 25mm. The data collected by these thermocouples allowed for a time history analysis of the temperature evolution through the sample thickness throughout the entire duration of the experiment.

3.3.2 Gas phase temperature and velocity

5mm K type TCs are used to obtain the gas phase temperatures near the surface of the panel at 5 different locations. The location are 250mm, 500mm, 750mm, 1000mm and 1250mm from edge of the sample. Temperature readings of these TCs are also used for the density correction calculation for the velocity gases.

In order to measure the gas phase velocity, bidirectional probes are employed along with differential pressure transducers (DPT) to determine the differential pressure. The resulting measurements are then converted to velocity using Bernoulli's principle and temperature-corrected density values, the mathematical equations (12)-(14) are provided in results and discussion session. In this thesis, the combined assembly of bidirectional probe and pressure transducer is referred to as BDP for simplicity. The location at which velocity is measured coincides with the gas phase temperature, allowing the use of temperature values for density correction. The velocity measurements are crucial for understanding the behaviour of the gas flow and its interaction with the sample during the experiment.

3.3.3 Heat flux measurement

One of the instruments utilized in measuring heat transfer rates during a fire test is the Thin Skin Calorimeter (TSC). This instrument enables the quantification of incident radiant heat flux on the exposed surface of solid elements such as structural elements, by gauging the total heat flux[88,89]. 5 TSCs are used here in this experiment at locations coincident with those of the gas phase instrumentation. Figure 3.5 shows individual TSC and Figure 3.6 shows a view from underside of the sample.

$$\dot{Q}''_{inc} = \frac{1}{\alpha_{disc}(1-C)}\left(\frac{m_{disc}}{S_{disc}} c_{p\,disc} \frac{dT_{disc}}{dt} + \varepsilon_{disc}\sigma T_{disc}^4 + h_c(T_{disc} - T_g)\right)$$

Here, $\dot{Q}''_{inc}$ is incident heat flux, α_{disc} is absorptivity of TSC disc. m_{disc}, S_{disc} and $c_{p\,disc}$ is the mass, surface area and specific heat of TSC disc. ε_{disc} is emissivity and T_{disc} is temperature of disc.

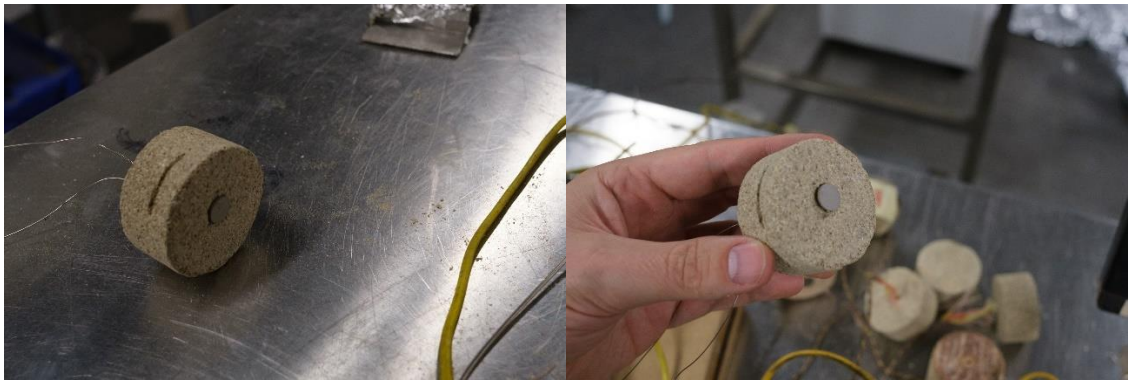

Figure 3.5 Individual TSC

3.3.4 Visual recording

Two cameras were implemented for video recording, these recordings were later used to track the flame front and consequently the flame spread rate under the CLT sample. One of the camera included blue light filter in attempt to track the movement of pyrolysis front.

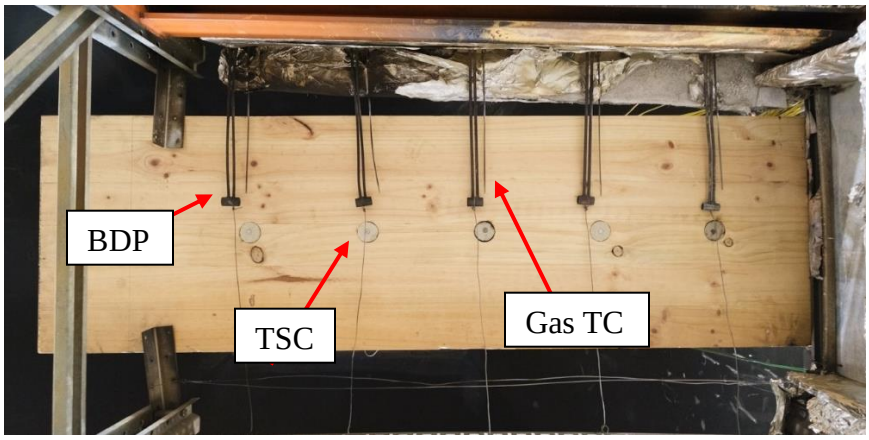

Figure 3.6 Sample and instrumentation view from underside of the sample

3.4 The instrumentation matrix

Table 3-1 provides the instrumentation matrix and nomenclature for the experimentation. Figure 3.7 shows the schematic of instrumentation for the experimentation.

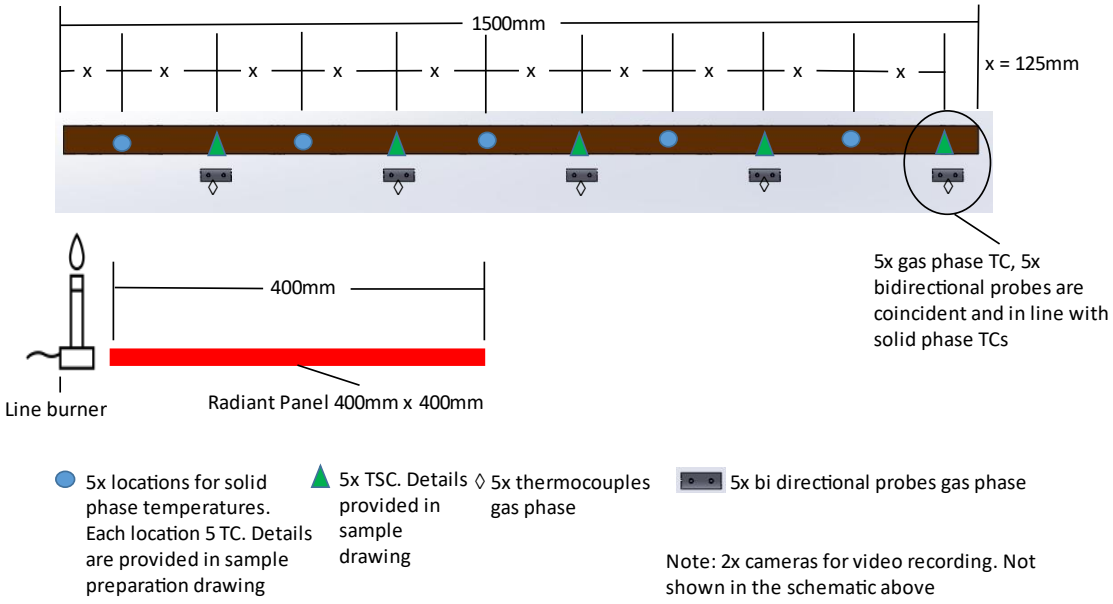

Figure 3.7 Instrumentation schematic

Table 3-1 Instrumentaton matrix

Instrument Name/ Type	Instrument Tag	X location *	Z location	Category
K type Thermocouple	TC11	125mm	2mm	Solid Phase
K type Thermocouple	TC12		4mm	
K type Thermocouple	TC13		8mm	
K type Thermocouple	TC14		15mm	
K type Thermocouple	TC15		25mm	
K type Thermocouple	TC21	375mm	2mm	
K type Thermocouple	TC22		4mm	
K type Thermocouple	TC23		8mm	
K type Thermocouple	TC24		15mm	
K type Thermocouple	TC25		25mm	

K type Thermocouple	TC31	625mm	2mm	
K type Thermocouple	TC32		4mm	
K type Thermocouple	TC33		8mm	
K type Thermocouple	TC34		15mm	
K type Thermocouple	TC35		25mm	
K type Thermocouple	TC41	875mm	2mm	
K type Thermocouple	TC42		4mm	
K type Thermocouple	TC43		8mm	
K type Thermocouple	TC44		15mm	
K type Thermocouple	TC45		25mm	
K type Thermocouple	TC51	1125mm	2mm	
K type Thermocouple	TC52		4mm	
K type Thermocouple	TC53		8mm	
K type Thermocouple	TC54		15mm	
K type Thermocouple	TC55		25mm	
K type Thermocouple	GTC1	250mm	-25mm	Gas Phase
K type Thermocouple	GTC2	500mm		
K type Thermocouple	GTC3	750mm		
K type Thermocouple	GTC4	1000mm		
K type Thermocouple	GTC5	1250mm		
Bi Directional Probe	BDP1	250mm	-25mm	
Bi Directional Probe	BDP2	500mm		
Bi Directional Probe	BDP3	750mm		

Bi Directional Probe	BDP4	1000mm		
Bi Directional Probe	BDP5	1250mm		
Thin Skin Calorimeter	TSC1	250mm	0mm	Surface heat Flux
Thin Skin Calorimeter	TSC2	500mm		
Thin Skin Calorimeter	TSC3	750mm		
Thin Skin Calorimeter	TSC4	1000mm		
Thin Skin Calorimeter	TSC5	1250mm		

*It is to be noted that all the X location values are measured from the edge of sample present right above the line burner as an ignition source.

All the instrumentation was installed on the centreline of the sample, at y=250mm.

3.5 Heat flux calibration

Before starting the experimentation, the heat flux values to be used were calibrated to find the height below the sample where that flux is obtained. This was done using a Boelter-Schmidt [90] water cooled heat flux gauge that was free of any convective influence therefore it measured the radiative heat flux. So, radiant panel are just placed at that location before starting the experiment rather than calibrating it every time. The three representative heat flux values are 45, 30 and 20 kW/m^2. The results of calibration is shown in Figure 3.8.

The representative heat flux values are the maximum values of the distribution right above the centre of radiant panel. The point on sample , right above the centre of radiant panel has largest view factor, hence the largest the heat flux values is coincident with x=375mm. The value drops on either side of this location as the view factor starts to drop.

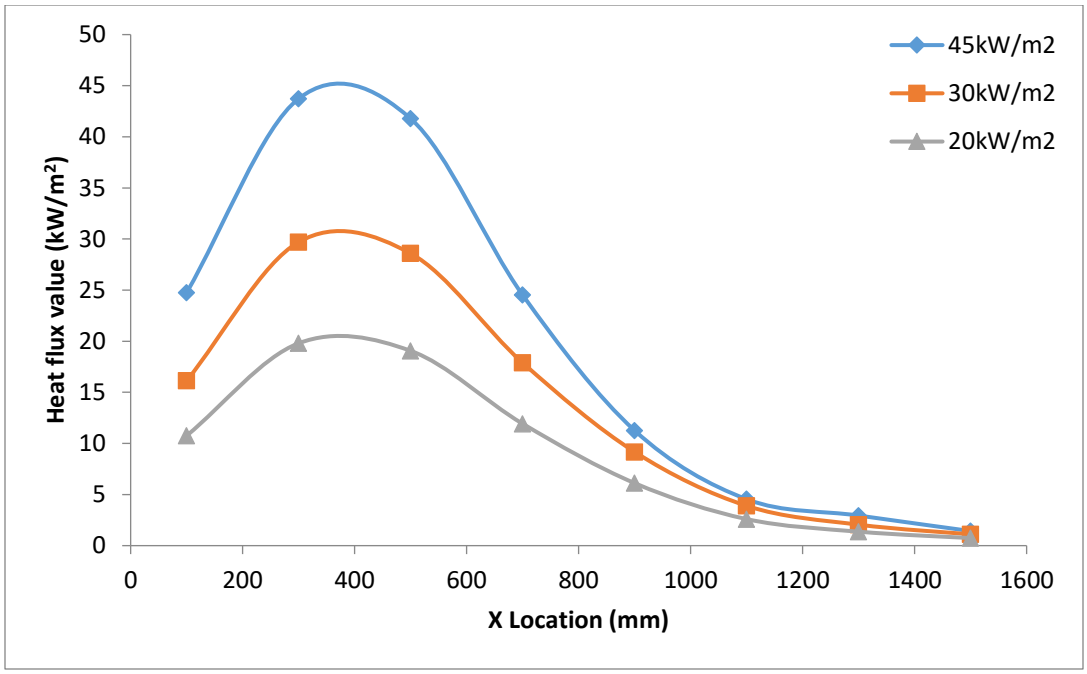

Figure 3.8 Representative heat flux values and their distribution

3.6 Test matrix

The testing scheme was developed for the investigation. Test 1 was conducted to verify and validate the working of the proposed methodology and was used as the basis for developing the matrix further based on the observations. The detailed view of Test 1 is provided in section 4.1.1 and also the changes made to the setup based on the findings from this test. Table 3-2 shows the final test matrix used. The purpose of downstands was to study effect of geometrical changes on flame spread, as it affects the residence of combustible gases.

Table 3-2 The test matrix

Test Number	Representative Heat Flux	Downstands	Preheating
1	30kW/m^2	No	Yes
2	45kW/m^2	No	No
3	30kW/m^2	No	No

4	20kW/m^2	No	No
5	20kW/m^2	Yes	No
6	20kW/m^2	Yes	No

Preheating was done for only Test 1, such that the measurement of TC21 reached 200^0C. Subsequently this preheat was omitted from later experiments as the pyrolysis gases released during preheat time did not ignite and majority of these gases were lost into the exhaust stream without igniting.

Chapter 4: Results and Discussion

This chapter contains the all the results obtained from the experimentation and also the post processing that has been conducted to obtain the values of desired output variables.

4.1 The fire behaviour

The general fire behaviour of various tests is presented and discussed here. The time (t) is presented here in this section is presented as minutes (m) and seconds (s) in the form mm:ss.

4.1.1 Test 1

Test 1 was the heat flux corresponding to the 30kW/m^2. This test was performed with the preheating. Sample was placed and radiant panels were ignited at t=0sec. It was let to preheat for 6min and 14 seconds, till TC21 reaches 200^0C The line burner was ignited at t=6:14, and the CLT sample ignited within 6 seconds at t=6:20.

No flame spread was observed here and only the edge of CLT right above the line burner (x=0mm) was ignited. The flame went on till t=8:00 and then self-extinguished. The radiant panel and the line burner were kept on to see if reignition happens but no reignition was observed till t=18:00. The radiant panel and line burner were turned off at this time.

4.1.1.1 Observations from Test 1

- In this configuration, a large proportion of the pyrolysis gases released from the sample did not undergo combustion and instead escaped/spilled through the sample's edges into the exhaust stream. As a result, any alterations to the experimental setup's geometry can have a significant impact on flame spread in this orientation.

- Few of the instrumentation cables got damaged due to hot gases spilling from the edges so a slight change in the experimental setup was suggested for future experiments. To keep the cables from burning, a plasterboard sheet was put on the edges, flush with the bottom surface of the sample, to prevent the hot gases from spilling over the edges and damage the instrument cables running above the sample. Also, more insulation was provided for the cables to keep them from getting damaged during the test.
- For the next tests preheat was eliminated as an input variable and all further testing was done with no preheat time. This was done as it was observed from Test 1 that most of the generated pyrolysis gases were spilled over and did not burn.

4.1.2 Test 2

This test was performed with the representative heat flux of 45 kW/m^2. As there was no preheat time to radiant panels and the line burner both were ignited at the same time t=0. The sample ignited at t=0:49. The sample ignited throughout the whole width of the sample (y=0-500) simultaneously.

The ignition happened right above the centre of the radiant panel at x=375mm (location of highest heat flux) and the flame spread both ways (towards x=0mm and also towards x=1500mm). The flame spread till x=1000mma at t=1:41. Afterwards, flames started to die down and extinguished at t=5:01.

The test was allowed to continue further and the sample reignited at t=6:00 and x=625mm. Flaming continues till t=7:58 and completely self-extinguishes. The test was stopped at t=20:00 and no further reignition was observed. This complete ignition and flame development is shown in Figure 4.1 in form of contour plots extracted from the video data using MATLAB R2021b, the sample of code is presented in the appendix. The data extracted manually from the video data. Value of 1 was assigned to the location where there was flame and 0 where there was no flame, this was repeated for various time steps. Plotting 0 and 1 in black and white contours provide such images. Black for flame and white for no flame.

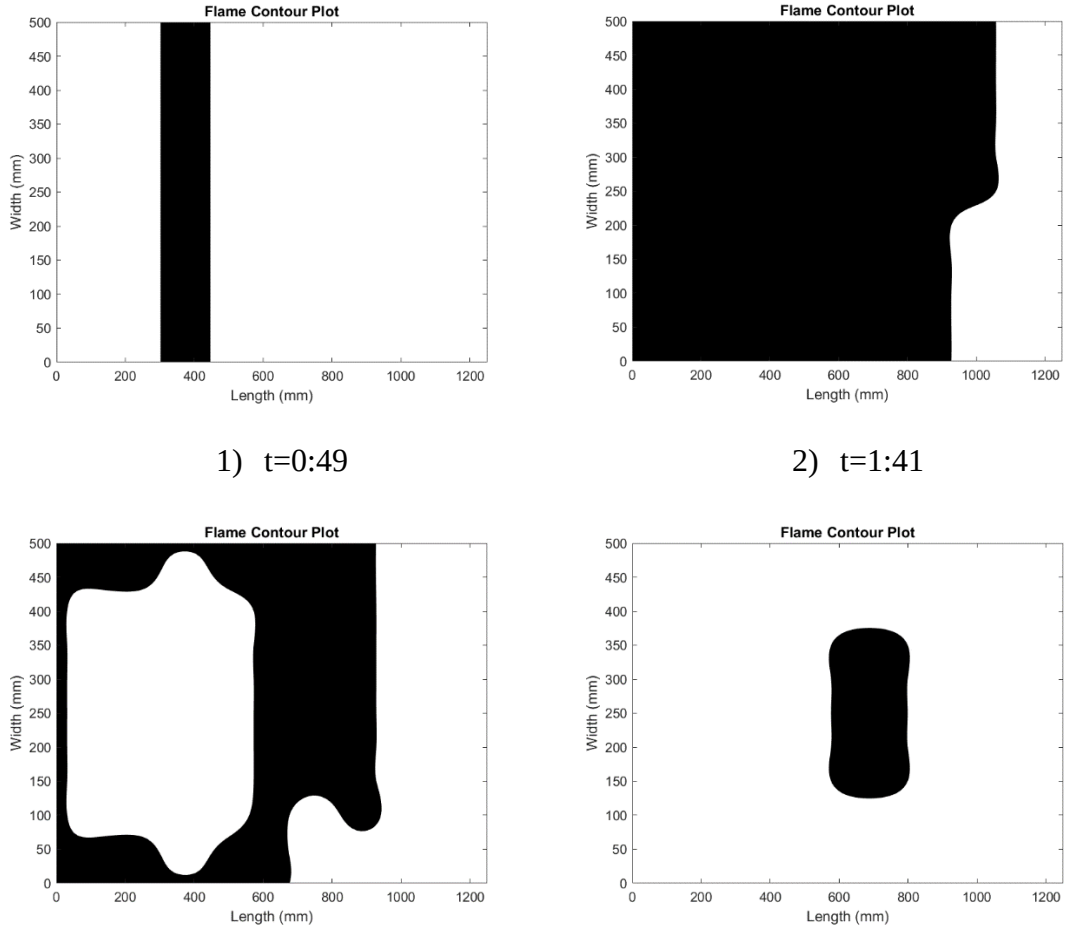

Figure 4.1 Flame stages for test 2. 1) ignition, 2) max extent of flame spread, 3) flames dying out and 4) reignition. Legend -white (no flame) – black (flame)

4.1.3 Tests 3-6

Test 3 to Test 6 are presented together as the fire behaviour was consistent within all these experiments and similar to each other. However, individual values of parameters like time to ignition, flame spread rate and the extent of flame spread was different within these individual tests.

The radiant panel and the line burner were ignited together. At time of ignition, the CLT sample ignited on the edge above the line burner. The difference from test 2 is that the ignition occurred above the radiant panel in test 2 but here the ignition occurred at the edge above the line burner (x=0mm). Once the edge ignited, the flame started to spread along

the longitudinal edges (along x direction). No or very little flame spread was observed along the centreline or any point apart from the edges. The two flames on each edge of the sample started to spread inwards laterally (y direction), towards each other and then connected between 750-1000mm. The actual point of contact between the two flames is different for each test but the same trend for the flame behaviour was observed in all these tests.

After these two streams of flames connect, the flame spreads further along x axis and slowly starts to die out. In the end, the flames were extinguished using water spray. These various stages of flame spread is shown from Figure 4.2 to Figure 4.5.

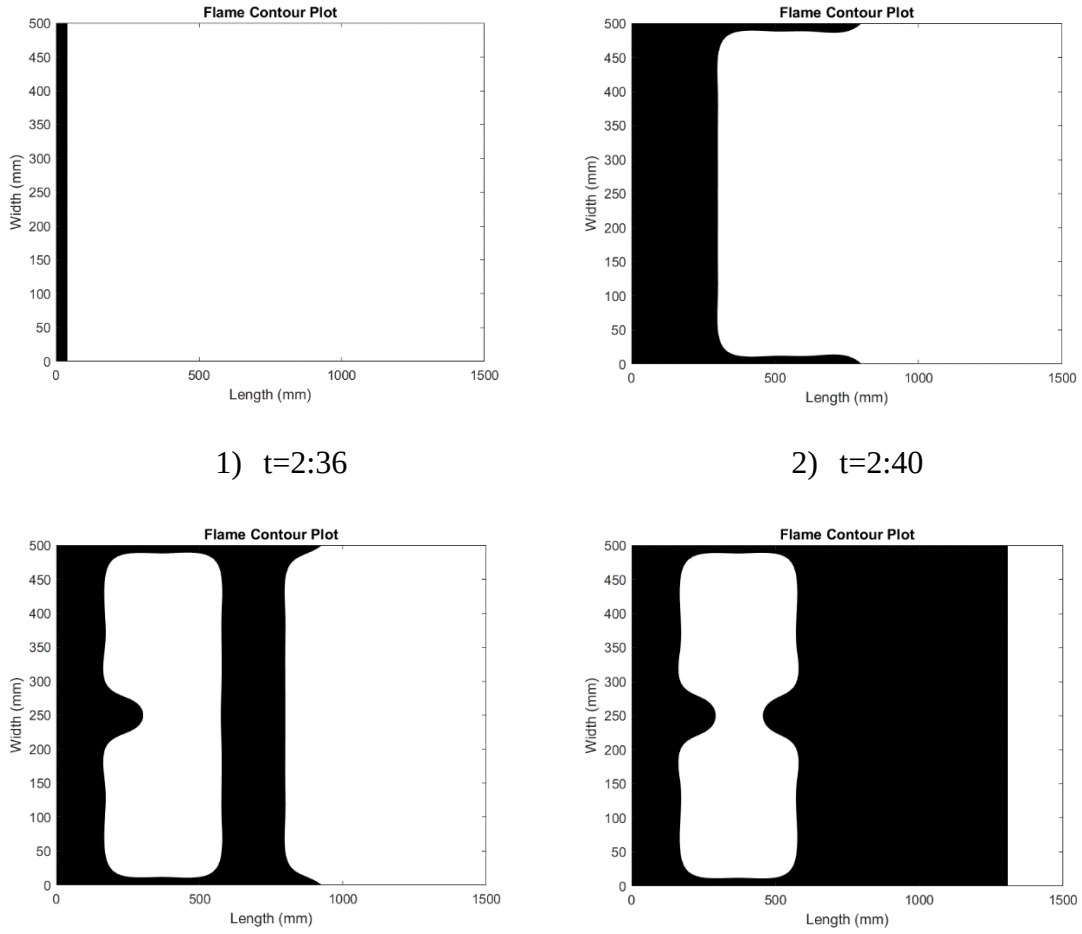

1) t=2:36 2) t=2:40

3) t=2:45 4) t=3:35

Figure 4.2 Stages of flame spread for test 3. 1) ignition, 2) flame spreading on the edges, 3) flames joining from the edges and 4) flame spread further after connecting from both edges. Legend -white (no flame) – black (flame)

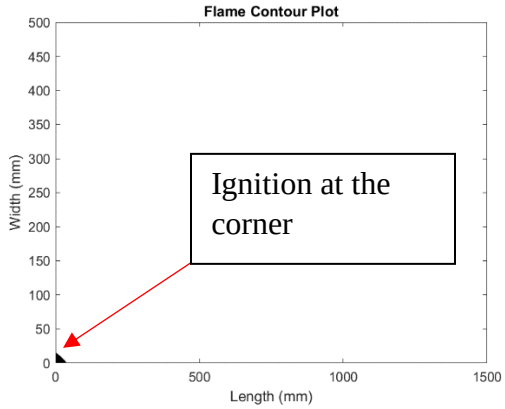

1) t=5:37

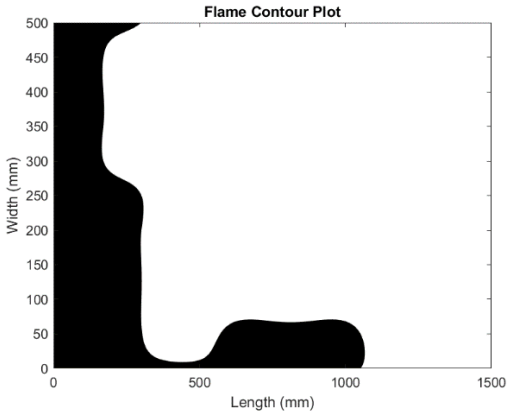

2) t=7:17

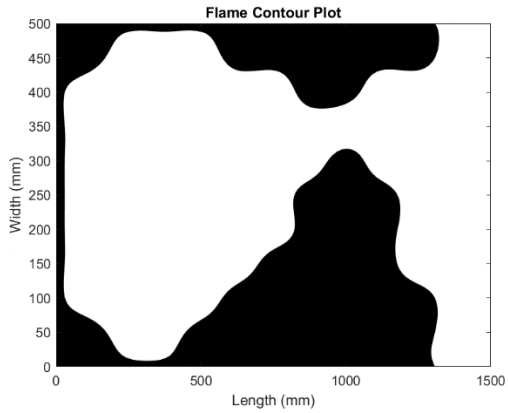

3) t=8:02

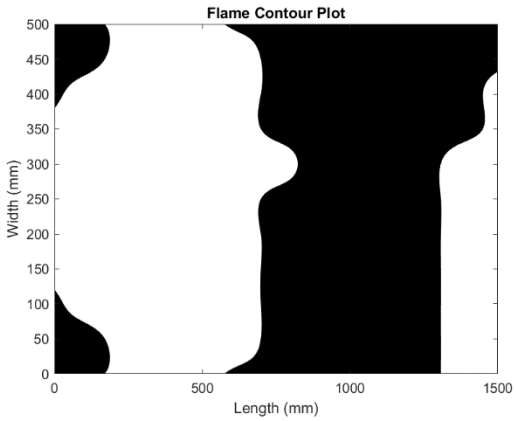

4) t=9:02

Figure 4.3 Stages of flame spread for test 4. 1) ignition, 2) flame spreading on the edges, 3) flames joining from the edges and 4) flame spread further after connecting from both edges. Legend -white (no flame) – black (flame)

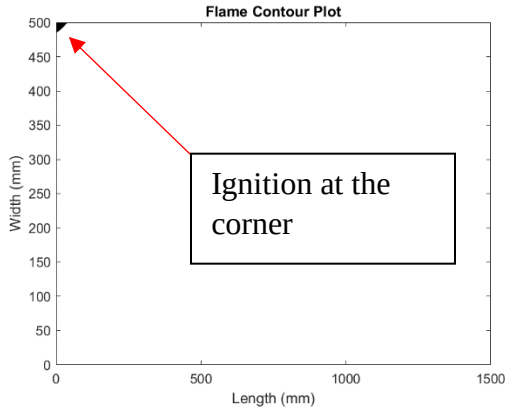

1) t=7:36

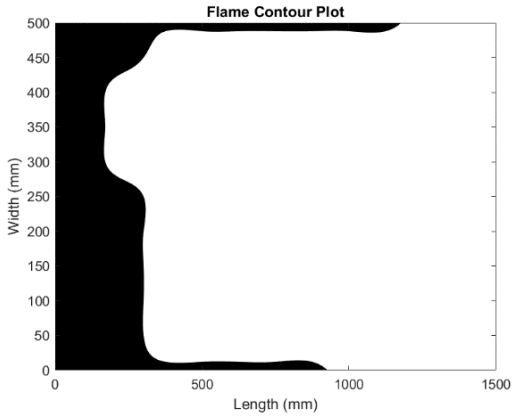

2) t=8:05

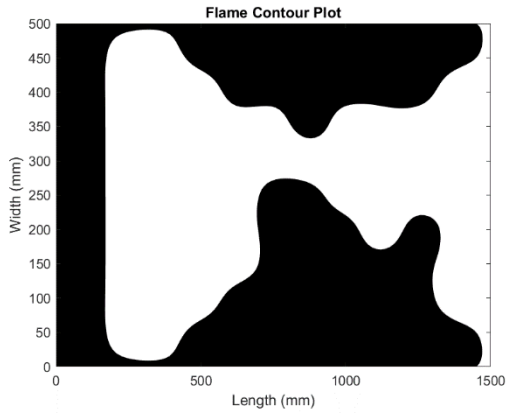

3) t=8:35

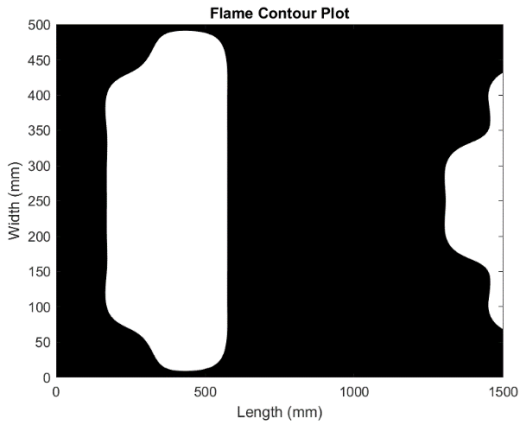

4) t=9:05

Figure 4.4 Stages of flame spread for test 5. 1) ignition, 2) flame spreading on the edges, 3) flames joining from the edges and 4) flame spread further after connecting from both edges. Legend -white (no flame) – black (flame)

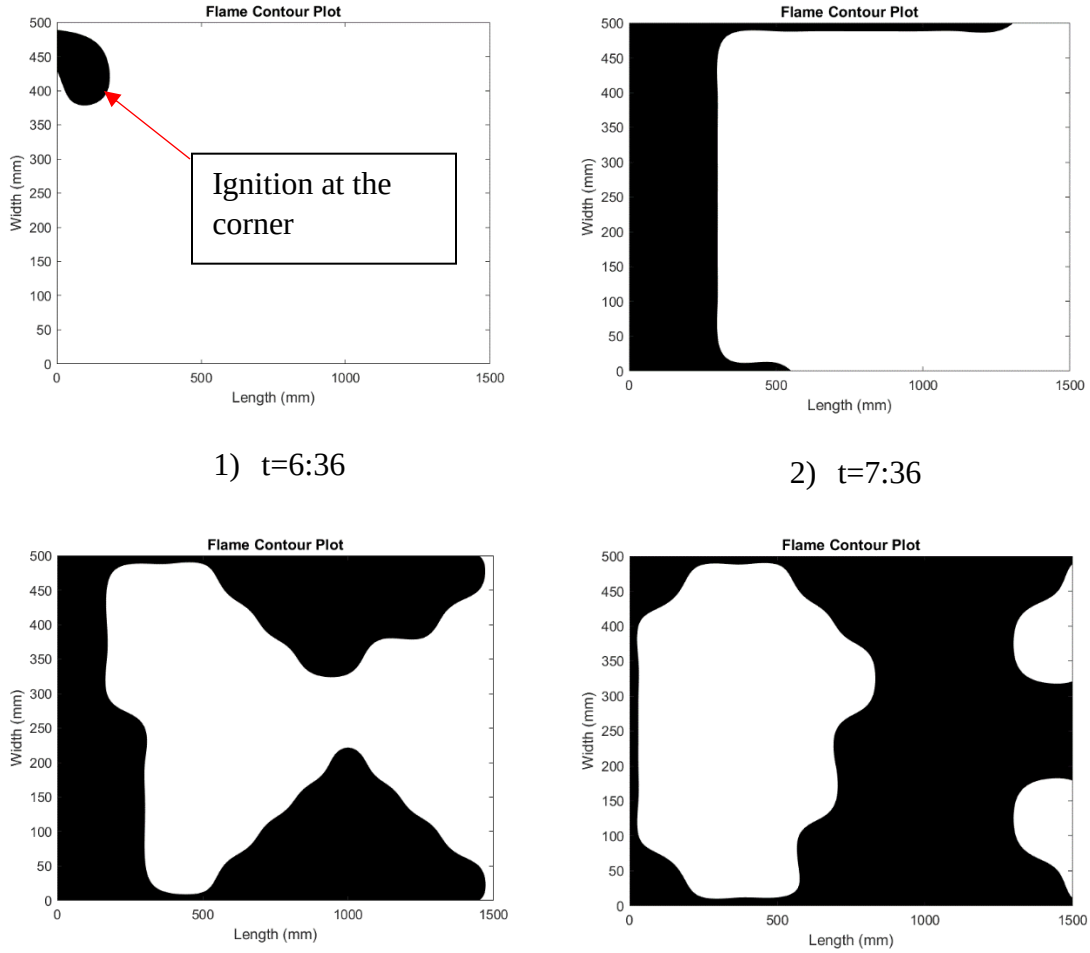

Figure 4.5 Stages of flame spread for test 6. 1) ignition, 2) flame spreading on the edges, 3) flames joining from the edges and 4) flame spread further after connecting from both edges. Legend -white (no flame) – black (flame)

One difference can be noted between Test 3 and Test 4-6, is that test3 ignited over the complete edge and test4-6 ignited only at the corner and then the flame spread around the edges.

The actual snapshots from experiments for test 3 is shown in Figure 4.6.

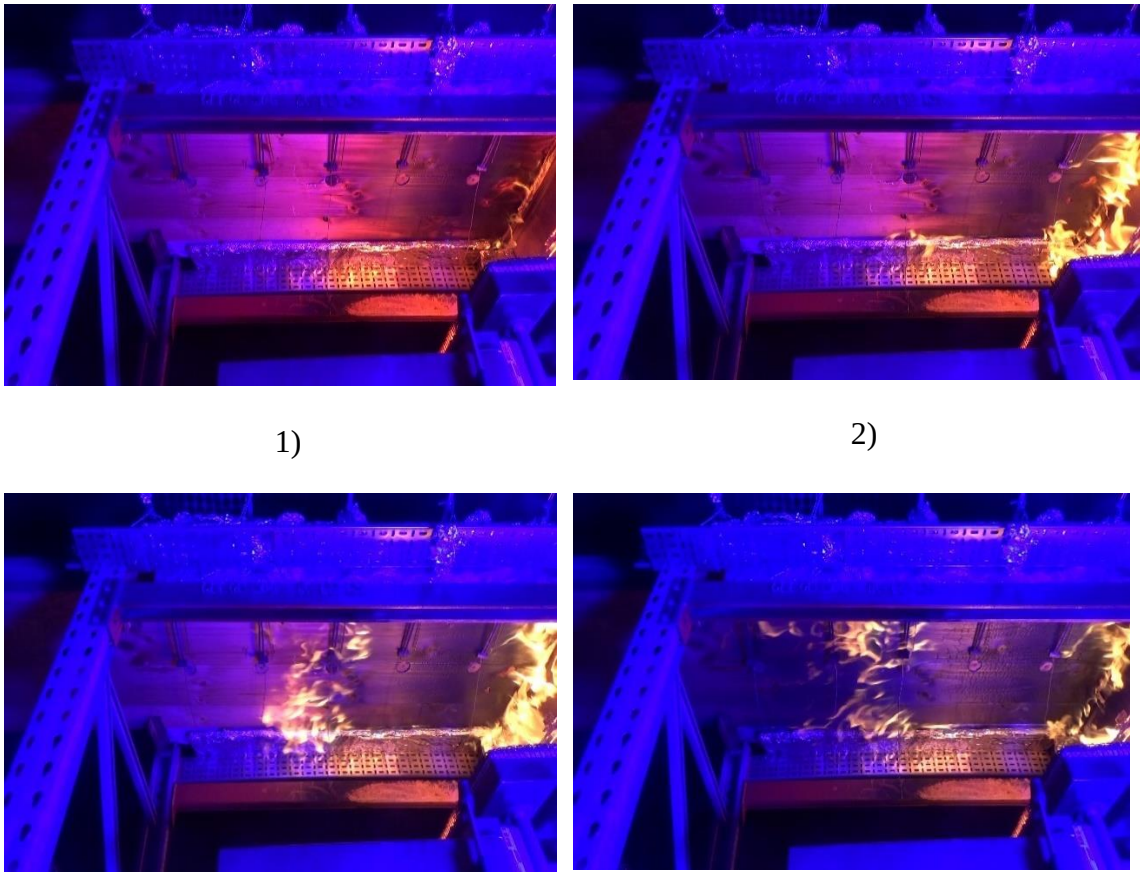

1) 2)

3) 4)

Figure 4.6 Major events during Test 3. 1) Ignition on the edge, 2) Flame spreading on the edges, 3) Edge flames coincide in the middle and 4) Flame spreading further downstream

4.1.4 Discussion on flame behaviour

It can be deduced from the results presented for Tests 3-6, that once it ignited at the end the flame spread on the edges and did not spread in the middle part of the sample from the range x=250mm-600mm. This phenomenon can be explained by 3 reasons as stated below.

- Important consideration of the experimental setup is that the centre of radiant panel is right below the location x=375mm and y=250mm. So the buoyant gases from the panel rise up and hit the sample at around x=375mm and spread radially. As a result, the fluid flow is from x=375mm to x=0mm, the sample ignited at x=0mm, this

results in counter current flame spread because the flame has to spread against the flow of the gases. This counter current flow suppresses the flame spread.

- Another reason is the high velocities and high turbulence, as the buoyant gases hit the sample. High velocity at this point allows the combustible gases to be carried away quickly without burning. These gases burn further downstream where the flow is much more stable. This is presented and discussed in detail in section 4.5.
- A hypothesis can be drawn here, that play a role is the thermochemistry aspect of combustion. The gases released from the radiant panel are basically the combustion products from the propane fired radiant panel, predominantly carbon dioxide and water vapours. This mixture is very dilute in oxygen. As the hot gases rise under buoyancy, air is entrained but this air might not be enough to form a combustible mixture right above the panel. As the gases move further downstream more air is entrained to produce combustible mixture that burns.

The test 2 follows a different pattern, as the incident heat flux is so high that the rate of production of pyrolysis gas is too high and hence the above mentioned points are not valid for that test. Also, the ignition happened at x=375mm, as opposed to the edge in all the other experiments.

4.2 Critical heat flux and ignitability

4.2.1 Ignition process

When a combustible material is exposed to a heat flux, the temperature of surface starts to rise. If there is moisture content in the sample, the temperature will rise to a 100^{o}C and will stay there until either all the moisture is evaporated or migrated into the thickness of the sample. The temperature starts to rise again after the removal of moisture and reaches such a level that the material starts to disintegrate (pyrolyze). This temperature is usually termed as the pyrolysis temperature. This can also be referred as the ignition temperature, because at this temperature the pyrolysis gases also burn in oxidizer in presence of a pilot flame. The processes leading to formation of vapours for combustion from solid is presented in Figure 4.7.

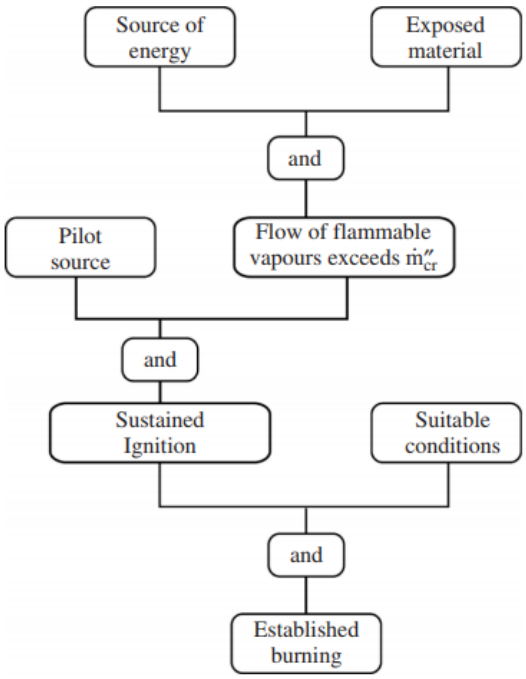

Figure 4.7 Processes leading to piloted ignition of solids, reproduced from [50]

4.2.2 The ignition model

Ignition model is presented by Quintiere and Drysdale [50,52]is provided below for thermally thick material. The model derives from the basic one dimensional conduction heat transfer problem from Fourier law.

$$\frac{\partial^2 T}{\partial z^2} = \frac{1}{\alpha}\frac{\partial T}{\partial t} \tag{1}$$

For the solution condition radiation heat flux which is incident at the surface is considered. Also a thermally thick material is considered for this derivation i.e. semi-infinite solid. Following solution can be obtained.

$$T(z,t) = T_0 + \frac{2\varepsilon_w \dot{Q}''_R}{k}\left[\left(\frac{\alpha t}{\pi}\right)^{1/2}\exp\left(-\frac{z^2}{4\alpha t}\right) - \frac{z}{2}erfc\left(\frac{z}{2\sqrt{\alpha t}}\right)\right] \tag{2}$$

Solving for z=0 (at the surface) the solution becomes,

$$t_{ig} = \frac{\pi}{4}k\rho c\frac{\left(T_{ig}-T_0\right)^2}{\dot{Q}''^2_R} \tag{3}$$

Linearizing the above equation we get,

$$\frac{1}{\sqrt{t_{ig}}} = \frac{2}{\sqrt{\pi}} \frac{1}{\sqrt{k\rho c}} \frac{\dot{Q}_R''}{(T_{ig} - T_0)} \tag{4}$$

The equation (4) is plotted for $\frac{1}{\sqrt{t_{ig}}}$ vs $\dot{Q}_R''$ we get a straight line and slope is $\frac{2}{\sqrt{\pi}} \frac{1}{\sqrt{k\rho c}(T_{ig} - T_0)}$.

Equation (3) when plotted for t_{ig} vs heat flux, has the asymptote at 0 value of heat flux. This implies that critical heat flux of any case is always zero and even small heat fluxes with eventually ignite the material if left for enough time. But this observation is contrary to what has been observed from the experiments. From experimental evidence, it is concluded that there is a definite CHF which depends of fuel but there exists a threshold below which ignition is not observed[91,92]. Equation three is derived based on purely thermal stand point and no other argument is taken in consideration for derivation.

Hence, using the experimental proof this equation is corrected by incorporating CHF, provided below as equation (5).

$$t_{ig} = \frac{\pi}{4} k\rho c \frac{(T_{ig} - T_0)^2}{(\dot{Q}_R'' - CHF)^2} \tag{5}$$

4.2.3 Calculation of CHF, ignition temperature and thermal inertia

From the videos obtained from the tests, time to ignition was obtained against the representative heat flux values as presented in Table 4-1.

Table 4-1 Time to ignition for Tests 2-6

Test Number	Heat Flux Value (kW/m^2)	Time to ignition (s)
2	45	51
3	30	146
4	20	337
5	20	406
6	20	396

Figure 4.8 shows graphical representation of this data along with an asymptotic curve fit.

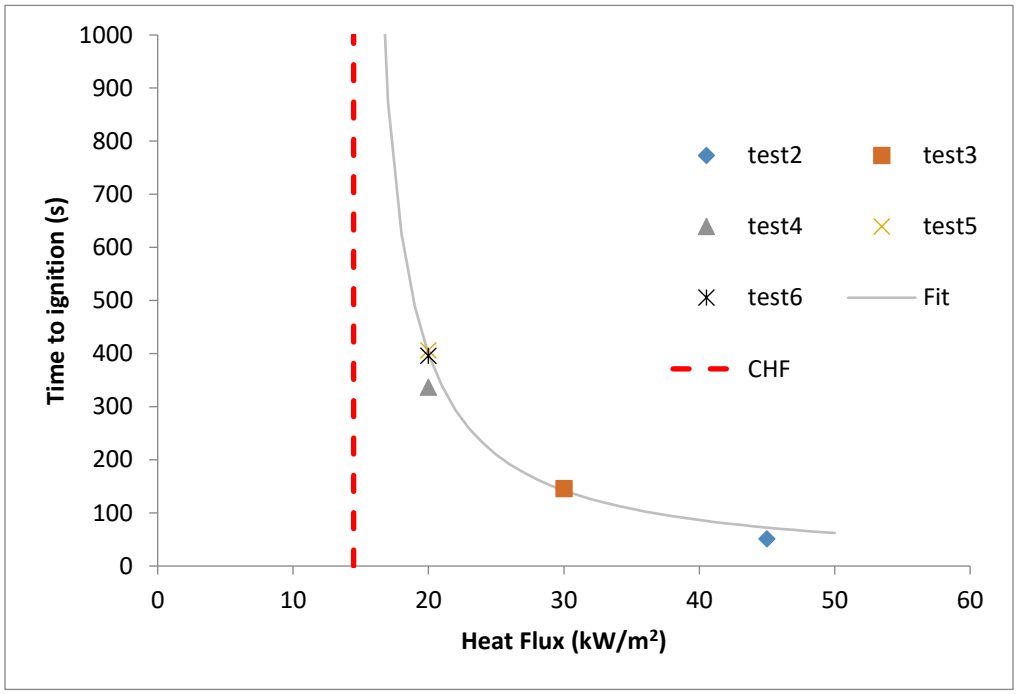

Figure 4.8 Time to ignition vs heat flux

The theoretical value for the thermal parameters of CLT obtained from literature are mentioned in Table 4-2

Table 4-2 Thermal parameters of CLT*

Parameter	Value
Thermal conductivity (k)	0.265 W/m.K [93]
Density (ρ)	972 kg/m^3 [93].
Heat capacity (c)	2.5 kJ/kg.K [94]
Thermal inertia ($k\rho c$)	0.65 kW^{2}s/m^{4}K^2

*The values are representative, taken from various sources. Actually the values are presented as large range with a lot of uncertainty due to many factors.

The asymptotic curve fit equation used in Figure 4.8 is of the form y=a/(x-b). The value of 'b' in this equation is the value of asymptote hence the b=CHF. Using curve fitting and solving simultaneous equation the constant values are calculated,

b=CHF=14.47 (kW/m^2) a=2210.21

For the calculation of the ignition temperature a simple heat balance equation at the surface is considered,

$$\varepsilon \dot{Q}''_{cr} = h_c(T_{ig} - T_0) + \varepsilon\sigma(T_{ig}^4 - T_0^4) \quad (6)$$

Here,

$\dot{Q}''_{cr}$=CHF=14.47kW/m^2, h_c=12 W/m^{2}K [95] and Ɛ=emmisivity=0.9 (assumed).

Solving equation iteratively for evaluating the ignition temperature, the result comes out to be T_{ig}=378^{0}C.

For calculation of thermal inertia ($k\rho c$) the inverse square root of time to ignition vs heat flux was plotted, this graph of the form of equation (4) is presented in Figure 4.9.

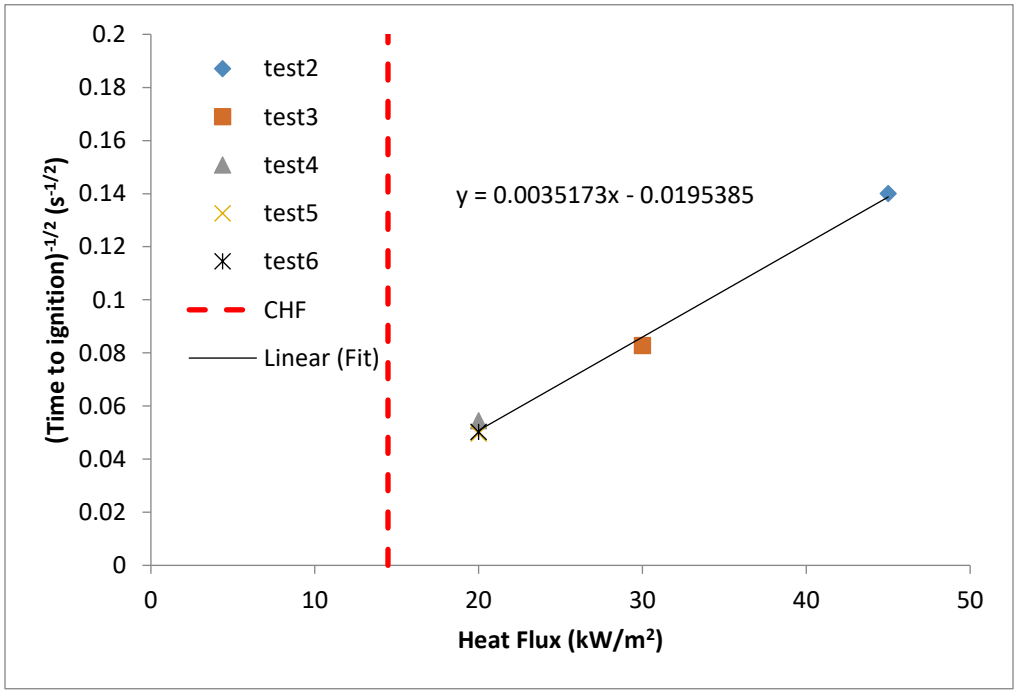

Figure 4.9 Inverse square root of time to ignition vs incident heat flux

The slope of this graph represents $\sqrt{\frac{2}{\pi k\rho c}}\frac{1}{Tig-To}$ = 0.0036, and using the value of ignition temperature from above the thermal inertial is calculated to be $k\rho c$ = 0.78 kW^2s/m^4K^2.

4.2.4 Discussion

The CHF and ignition temperature is not a constant value, it varies depending on the type of wood, orientation, moisture content and also the flow conditions [96–100]. But all the values provided in literature sources are either for upward facing, horizontal or vertical. Range of 13-17 kW/m2 is usually found in the literature sources. And the ignition temperature is also a wide range of 330^0C-480^0C.

As cone calorimeter cannot be used for ignitability investigation in this orientation, hence a different kind of testing setup needs to designed to investigate the critical heat flux, ignition temperature and other ignition parameters. This experiment was not designed for the purpose of testing of ignitability of CLT in downward facing orientation, but the results provided above can be used as a basis for the expected outcomes. The critical heat flux in this testing is calculated to be 14.47kW/m^2. This falls within the range provided above.

A heat balance is considered for the analysis of the ignition temperature, which gives the value that is fairly accurate within the range mentioned above.

Test 1 is excluded from this calculation, as it included the preheat part and line burner was ignited later-on after preheat.

4.3 Flame spread investigation

4.3.1 Theoretical model of flame spread

Quintiere [52] formulated a theoretical model for the flame spread with few base assumptions to arrive at a rather simple solution to a complex problem. During the formulation he neglected the phase change process of the burning fuel, thermal deformations were also neglected along with heat loses. A thermally thick solid is considered which is assumed to be homogeneous and continuous.

A control volume consideration is shown in the Figure 4.10.

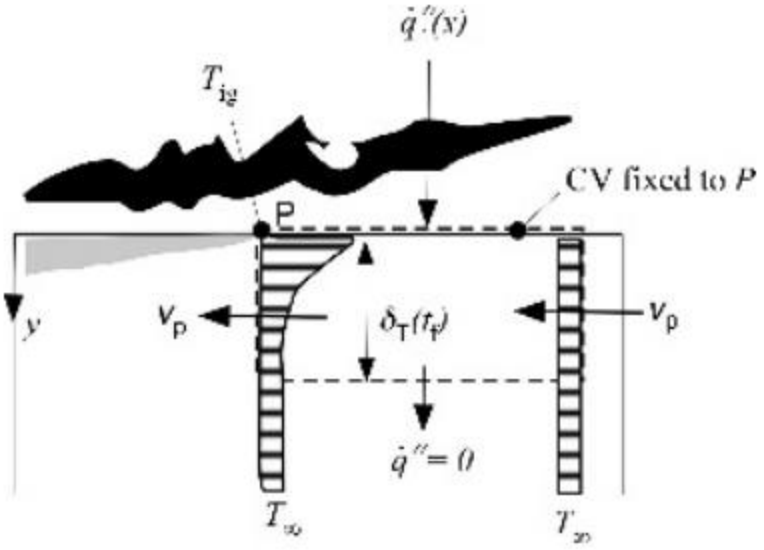

Figure 4.10 Control volume consideration for the theoretical model development (copied from [52]**).**

Solving the heat transfer problem for the control volume consideration we can get

$$v \approx \frac{4\dot{Q}_R^{"}\delta_f}{\pi(k\rho c_p)(T_{ig} - T_s)^2} \tag{7}$$

Here a flame spread parameter can be introduced as $\emptyset = \frac{4\dot{Q}_R^{"}\delta_f}{\pi}$ so we get the following equation

$$v \approx \frac{\emptyset}{(k\rho c_p)(T_{ig} - T_s)^2} \tag{8}$$

Considering that heating Ts is obtained by external heating flux, this can be rewritten as,

$$v \approx \frac{h_t^2\emptyset}{(k\rho c_p)(\dot{Q_{ig}^{"}} - \dot{Q}_R^{"})^2} \tag{9}$$

Writing the above equation in terms of straight line y=-mx+c

$$\frac{1}{\sqrt{v}} = -\sqrt{\frac{k\rho c_p}{h_t^2\emptyset}}\,\dot{Q}_R^{"} + \sqrt{\frac{k\rho c_p}{h_t^2\emptyset}}\,\dot{Q}_{ig}^{"} \tag{10}$$

Hence plotting using slope and intercept the flame spread parameter can be estimated.

4.3.2 Experimental results of flame spread

Two different flame spread rates were calculated. One for edge flame spread and one for centreline flame spread, v_e and v_c respectively. Both these rates are calculated manually from the videos obtained from the testing, by timing flame location (leading edge) based on markers. These are mean flame spread rates with the time steps used as the averaging window. The results are provided below and discussed in this section.

4.3.2.1 Test 2

Test 2 results are presented separately because the flame spread behaviour was different for this test as compared to all the other tests. Flame spread rate is shown in Figure 4.11.

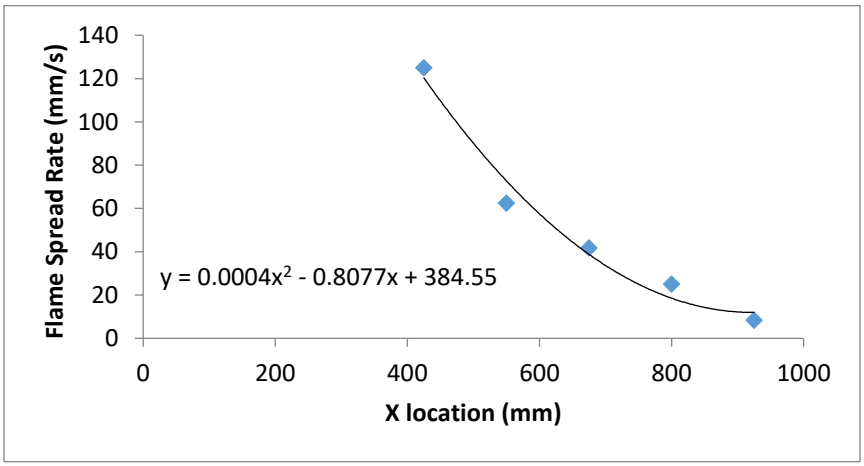

Figure 4.11 Centerline flame spread for Test 2

As the flame spread occurred on the entire width, edge flame spread is not evaluated separately for this test. Plotting the data in the form of equation (10) to calculate the flame spread parameter in Figure 4.12.

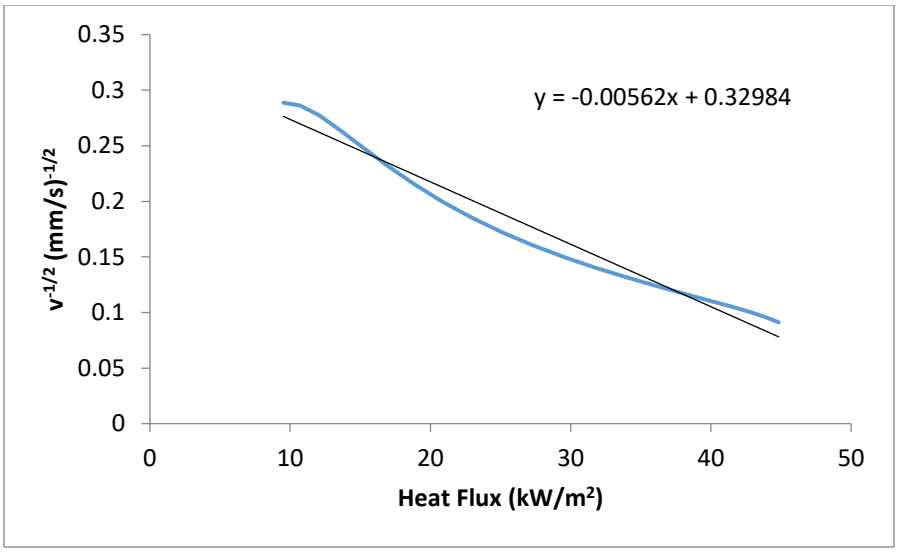

Figure 4.12 Test 2 inverse square root of flame spread velocity vs heat flux, with linear curve fitting as per equation (4)

4.3.2.2 Test 3 and Test 4

As the flame spread first started at the edge of the samples and then coincided with each other downstream from the ignition. Hence, two distinct flame spread rates are evaluated from the video data of the experiments. This is presented in Figure 4.13 and Figure 4.14

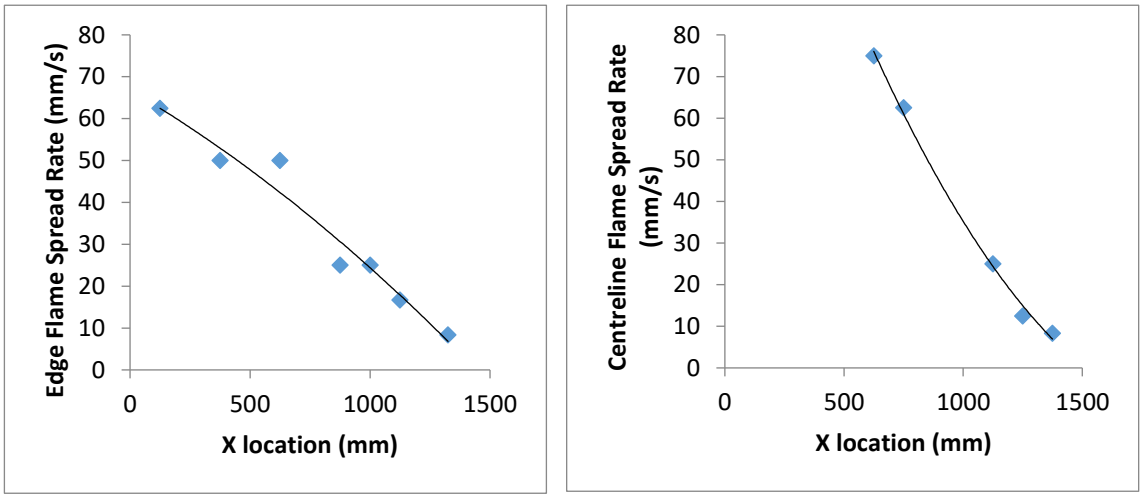

Figure 4.13 Test 3 flame spread rate evaluated as a function of X location. (left) flame spread rate on the edge, (right) flame spread rate on the centreline.

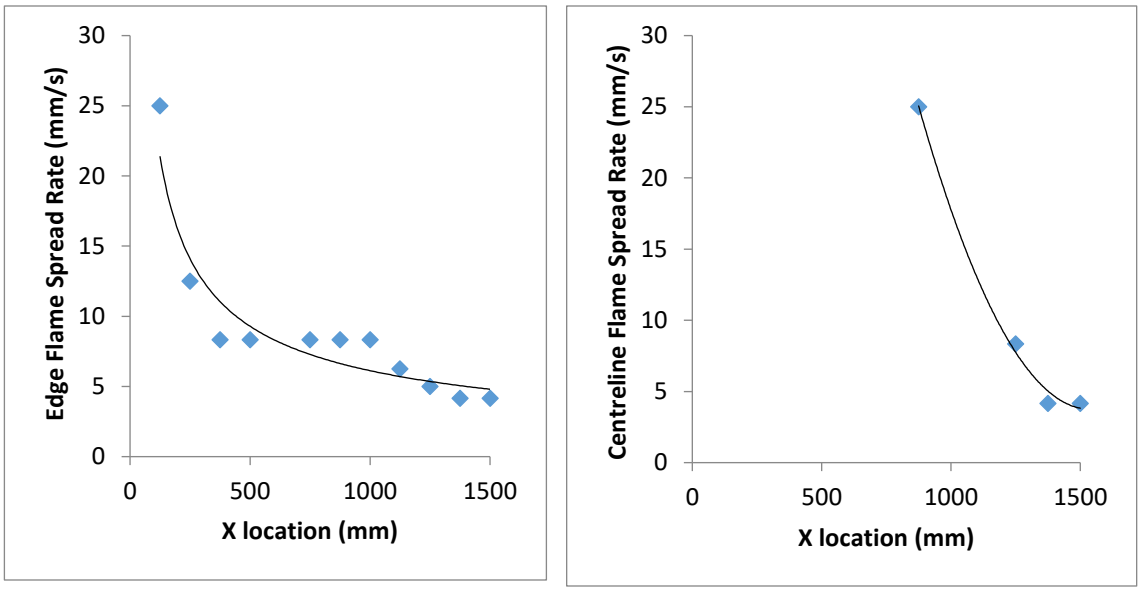

Figure 4.14 Test 4 flame spread rate evaluated as a function of X location. (left) flame spread rate on the edge, (right) flame spread rate on the centreline

The linearized form of equation (10), the inverse square root of flame spread rate vs the heat flux is presented in Figure 4.15 and Figure 4.16.

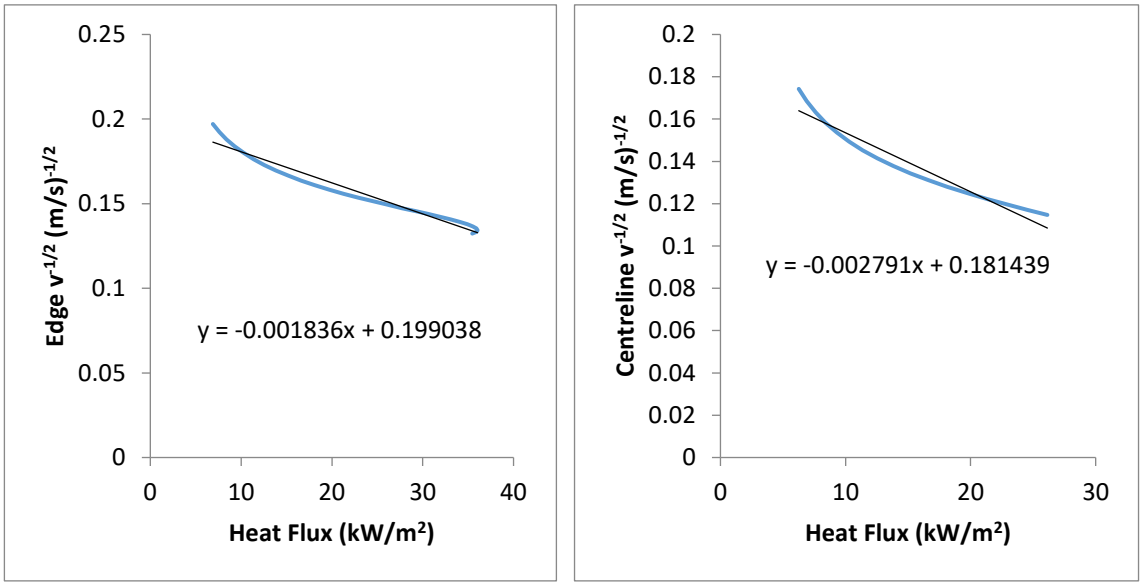

Figure 4.15 Test 3 Inverse square root of flame spread rate vs heat flux. (left) edge, (right) centreline

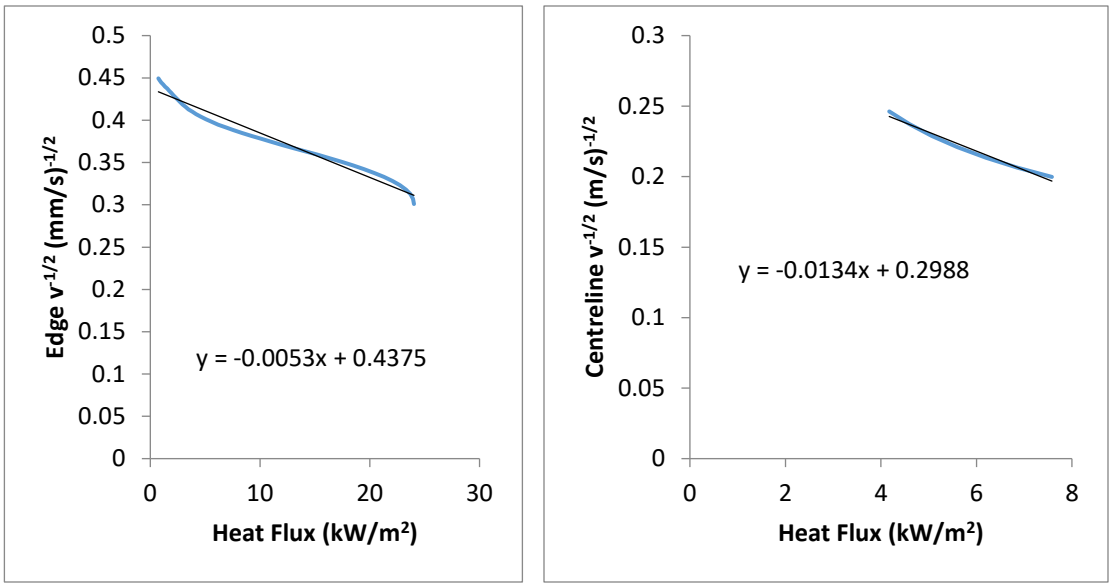

Figure 4.16 Test 4 Inverse square root of flame spread rate vs heat flux. (left) edge, (right) centreline

4.3.2.3 Test 5 and Test 6

These two tests were both conducted with the downstands and the results are presented below from Figure 4.17 to Figure 4.20.

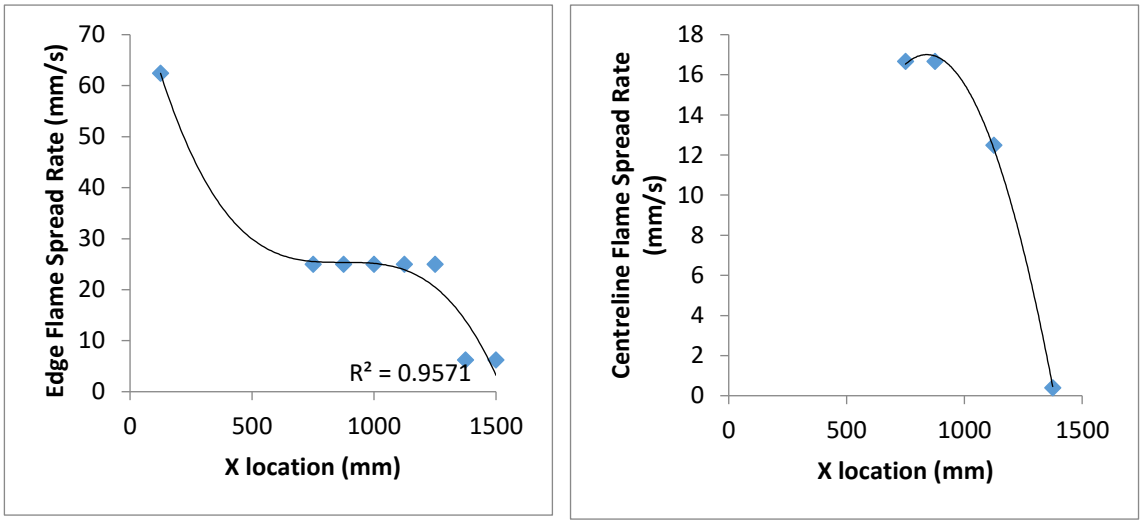

Figure 4.17 Test 5 flame spread rate evaluated as a function of X location. (left) flame spread rate on the edge, (right) flame spread rate on the centreline

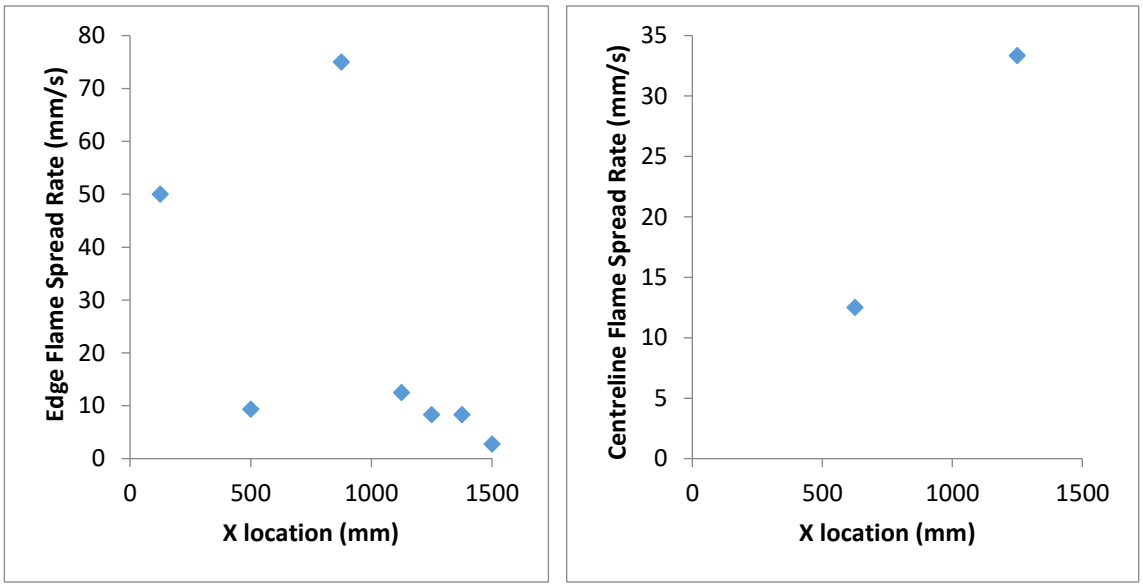

Figure 4.18 Test 6 flame spread rate evaluated as a function of X location. (left) flame spread rate on the edge, (right) flame spread rate on the centreline

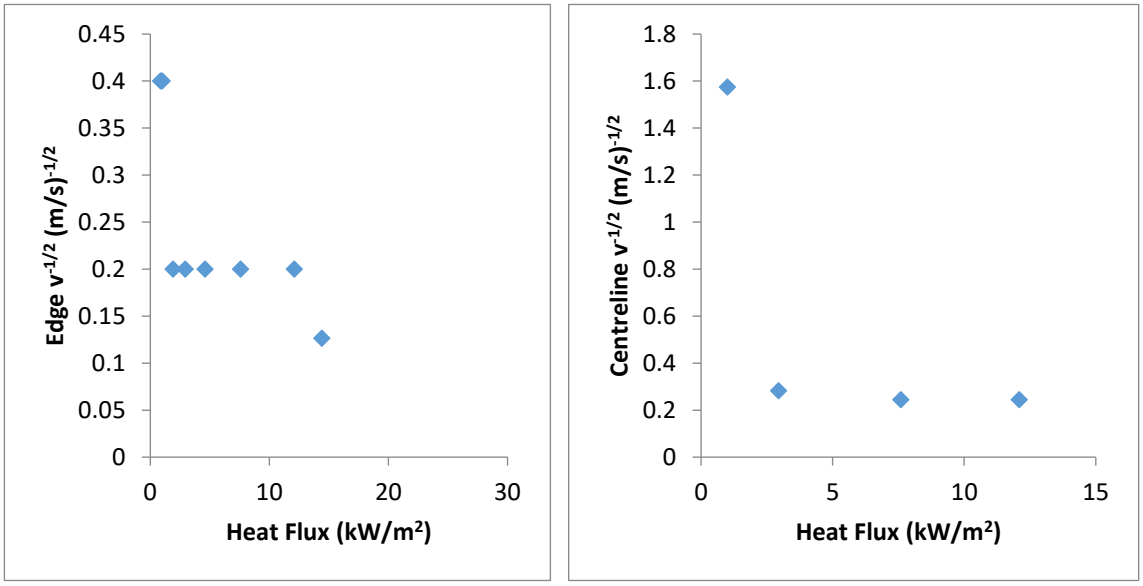

Figure 4.19 Test 5 Inverse square root of flame spread rate vs heat flux. (left) edge, (right) centreline

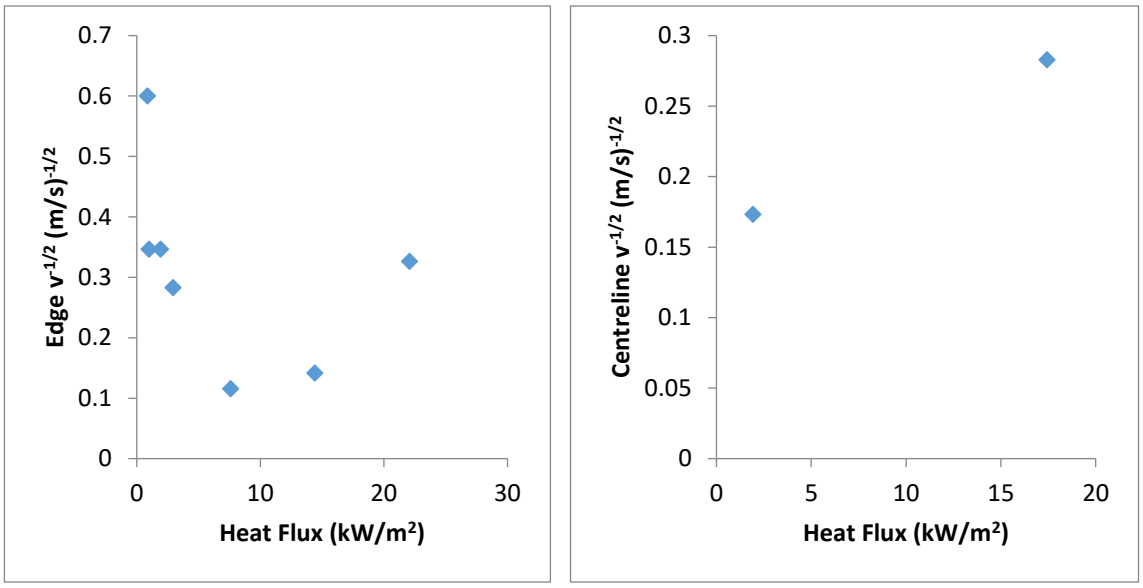

Figure 4.20 Test 6 Inverse square root of flame spread rate vs heat flux. (left) edge, (right) centreline

4.3.3 Discussion

Test 2 ignited, and flame spread happened throughout the width of the sample so it has the most smooth and accurate evaluation. The flame spread evaluated for test 3 and 4 also showed similar trend. A trend of decreasing flame spread rate with respect to decreasing heat flux while doing downstream in X direction. This can be seen for both edge flame spread and centreline flame spread.

The slope of Figure 4.12, Figure 4.15 and Figure 4.16 is $\sqrt{\frac{k\rho c}{h_t^2 \emptyset}}$ where $h_t = 36.88$ W/m^{2}K is the total heat transfer coefficient calculated according to equation (11). This slope is expected to be linear but the results do not follow linear pattern.

$$h_t(T_{ig} - T_0) = h_c(T_{ig} - T_0) + \varepsilon\sigma(T_{ig}^4 - T_0^4) \qquad (11)$$

The value of this slope is in the range of 0.0028-0.134 $m^2 s^{1/2}/kW mm^{1/2}$ for the centreline flame spread and the range for edge flame spread is 0.00184-0.0053 $m^2 s^{1/2}/kW mm^{1/2}$. Non-linear slope suggests that the flame spread model is not valid in this orientation because the underlying assumption is of, preheat to a time till we have

approximately dT/dz=constant (thermal equilibrium) this thermal equilibrium is not achieved during the testing due to flame movement.

There is large inaccuracies and uncertainty in the calculation of flame spread rates which are discussed here. The main source of uncertainty is the difficulty to distinguish between the flame spread and flame extension. Flame under the ceiling tends to extend for longer lengths, mainly due to lack of entrainment of air[50,52,101–104]. So the flame can be identified at a location due to flame extension but that part sample might not be actually burning or taking part in combustion. This creates an error in judgement and calculation of flame spread rate because it will also include the flame extension even though the sample is not burning at that location. Consequently, a pyrolysis front tracking is done in the following section to see the extent of sample pyrolyzing and giving combustible gases.

For Test 5 and Test 6, the main difference was that down stands were included in these tests. These downstands have an effect on the residence time and also on the collection of gases under sample. The downstands attempt to gather and collect the combustible gases near the edges and consequently it can be seen that the flames spreads longer on the edges and starts to join in the middle, throughout the flame length rather than connecting at one location and then spreading further downstream this is shown in Figure 4.4 and Figure 4.7. This effect is much more pronounced in test 6 with longer (6cm downstands).

4.4 Pyrolysis front tracking

The temperature values taken through the thickness were used to extrapolate the temperature value at the surface. MATLAB script was used to extrapolate the temperature values at the surface. 2mm, 4mm and 8mm values are used and using spline interpolation algorithm, a curve fitting is done and finally extrapolated for 0mm values. This surface temperature evolution, is presented in Figure 4.21 to Figure 4.26 for all the tests. The temperature evolution of in the thickness of the samples is presented on all 5 X locations for all tests in the Appendix this is the base value for extrapolating the surface temperature.

These figures show very well set trend. The temperature rises to 100^0C and stays there for a while for dehydration. The temperature starts to rise again and reaches the pyrolysis

temperature of 378^{0}C as calculated in section 4.2.3. It can be said that after some time the rate of temperature rise starts to decrease and tends towards a plateau value before the ignition. After ignition the temperature starts to rise again to reach the max value. Plots for test 5 and test 6 show a different trend lot of error as during the experimentation, some of the thermocouple cables got damaged after some time so could not log the temperature for the whole duration.

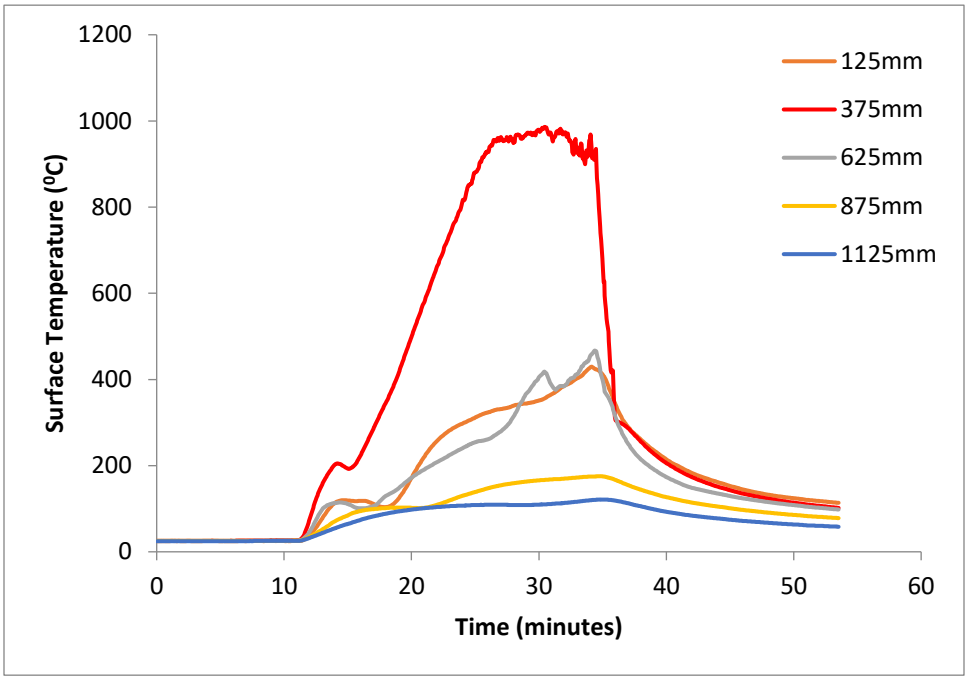

Figure 4.21 Test 1 surface temperature at five X locations vs time

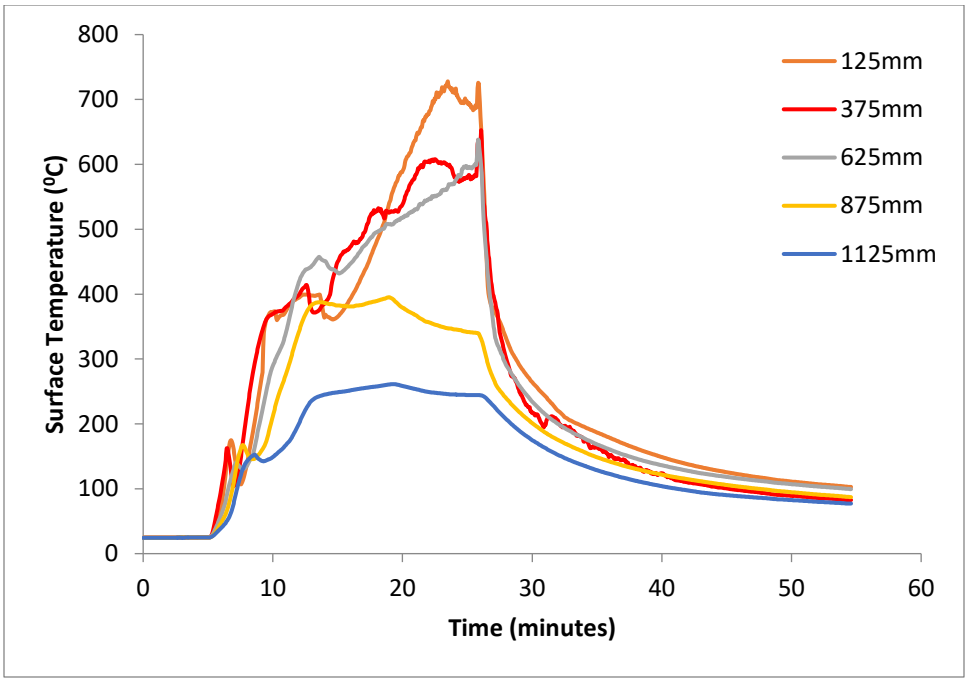

Figure 4.22 Test 2 surface temperature at five X locations vs time

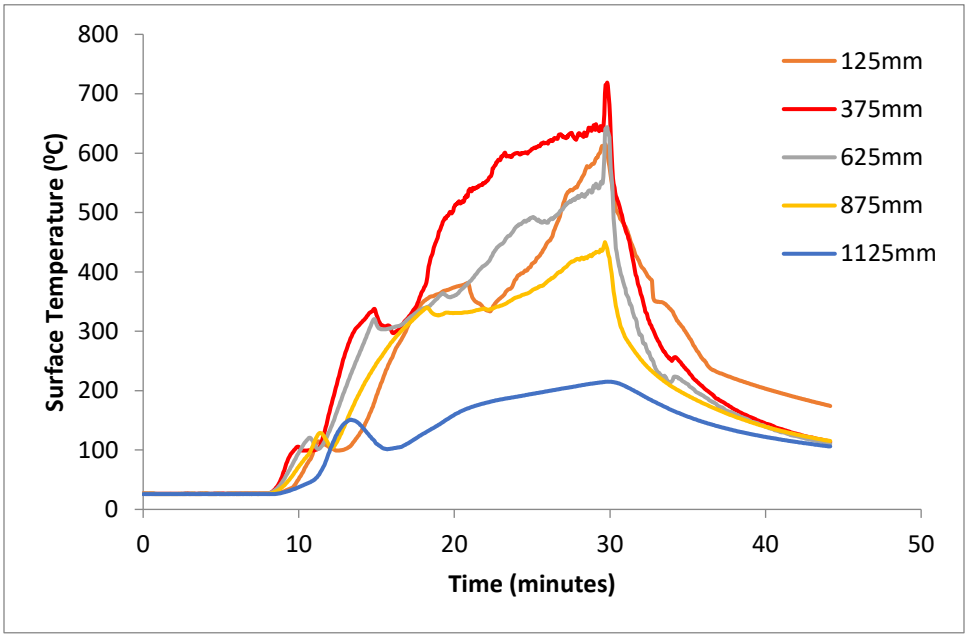

Figure 4.23 Test 3 surface temperature at five X locations vs time

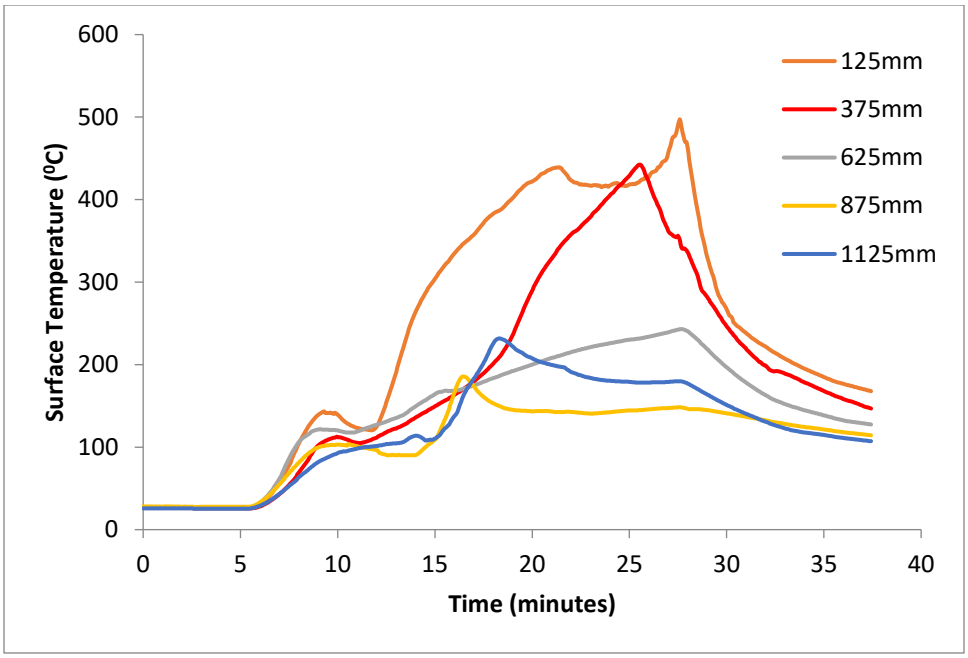

Figure 4.24 Test 4 surface temperature at five X locations vs time

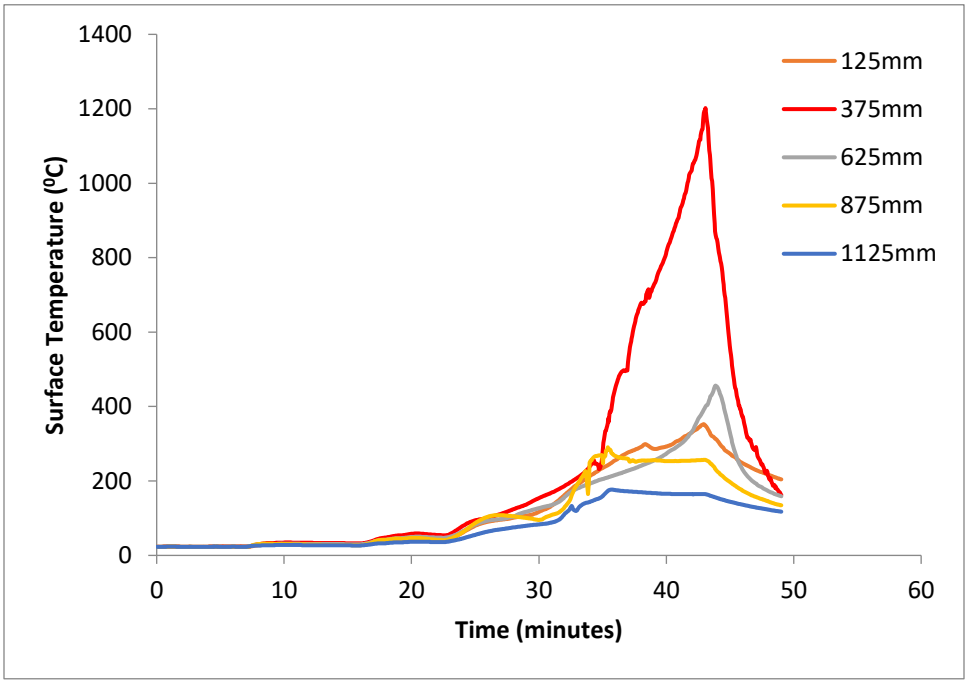

Figure 4.25 Test 5 surface temperature at five X locations vs time

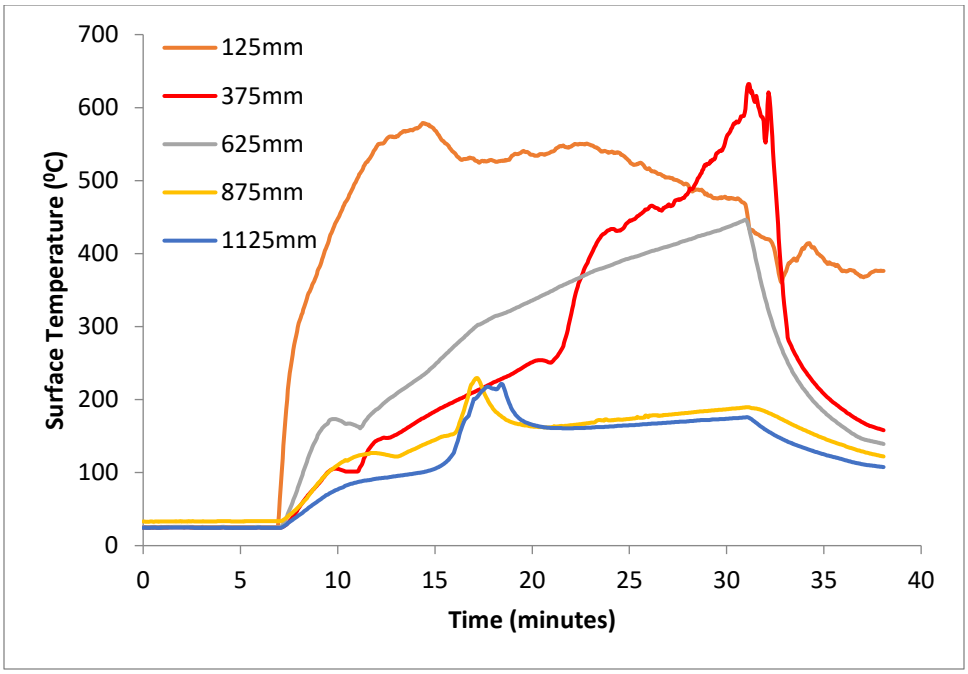

Figure 4.26 Test 6 surface temperature at five X locations vs time

The time for the surface temperature curve to reach the pyrolysis is evaluated using the same MATLAB code and that is the time when the pyrolysis starts at that particular location. A plot was created for time to pyrolysis temperature with respect to X location. The location where the pyrolysis front can be identified is donated as x_p. Plot provides t vs x_p so the inverse slope is $v_p = \frac{dx_p}{dt}$. This inverse slope is also plotted for each test with respect to the location. Show in Figure 4.27 to Figure 4.32.

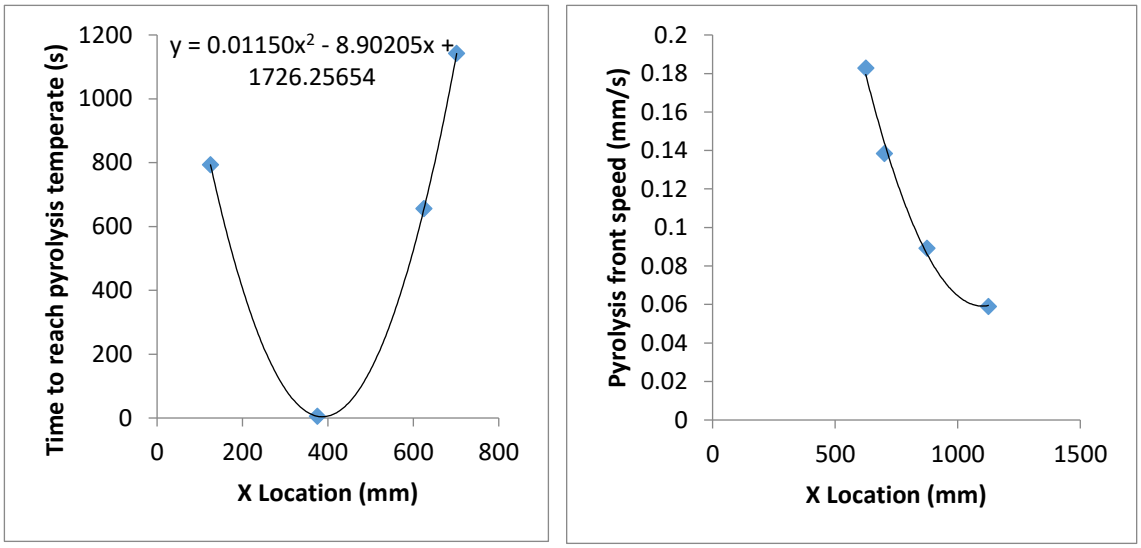

Figure 4.27 Test 1 (Left) time to pyrolysis temperature with respect to the X location. (Right) Pyrolysis front movement rate as a function of location.

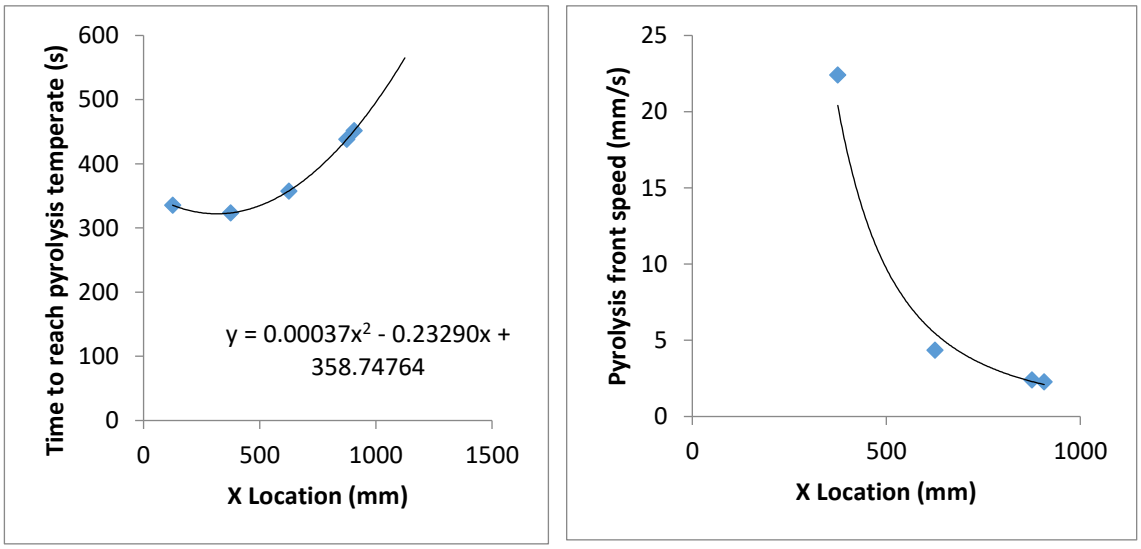

Figure 4.28 Test 2 (Left) time to pyrolysis temperature with respect to the X location. (Right) Pyrolysis front movement rate as a function of location.

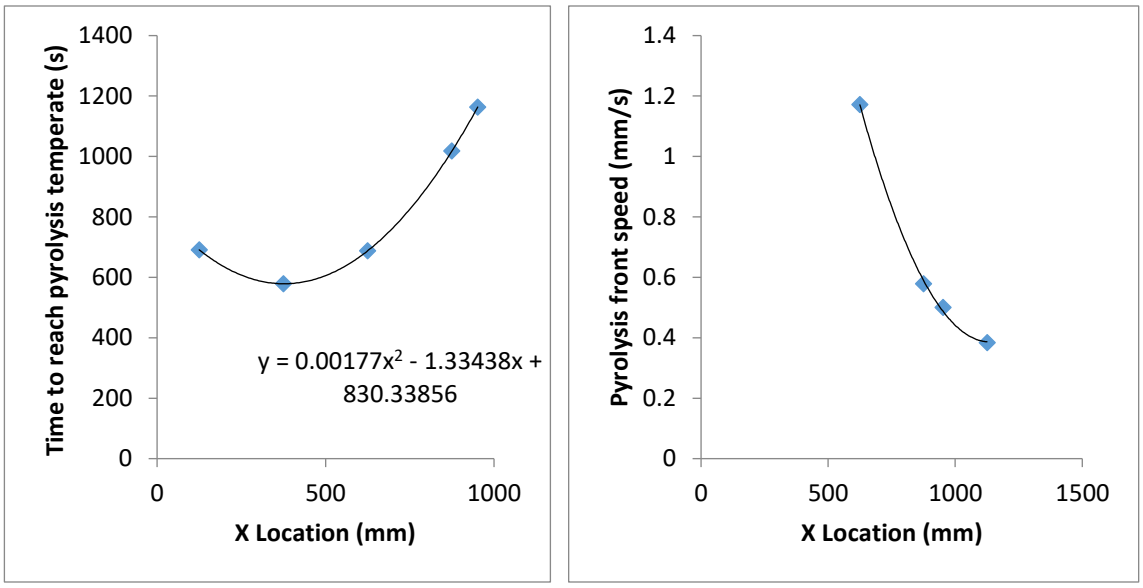

Figure 4.29 Test 3 (Left) time to pyrolysis temperature with respect to the X location. (Right) Pyrolysis front movement rate as a function of location.

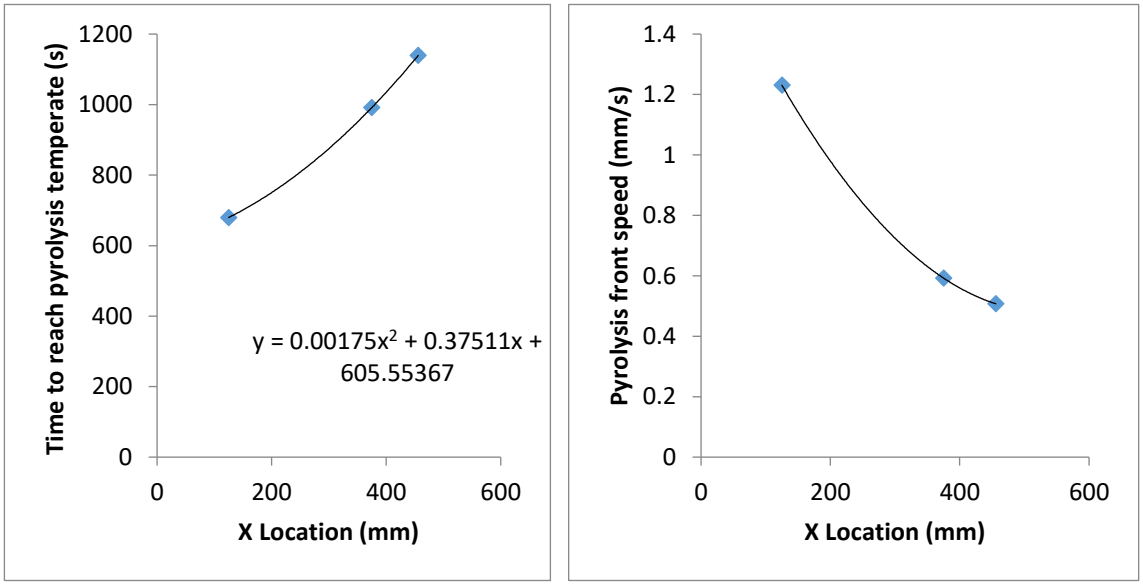

Figure 4.30 Test 4 (Left) time to pyrolysis temperature with respect to the X location. (Right) Pyrolysis front movement rate as a function of location.

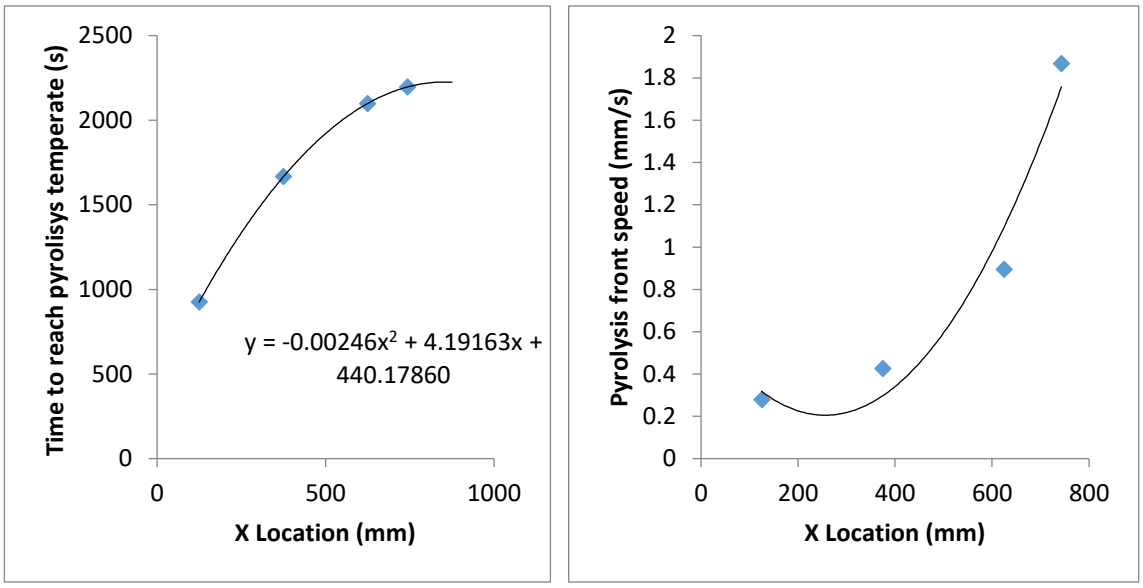

Figure 4.31 Test 5 (Left) time to pyrolysis temperature with respect to the X location. (Right) Pyrolysis front movement rate as a function of location.

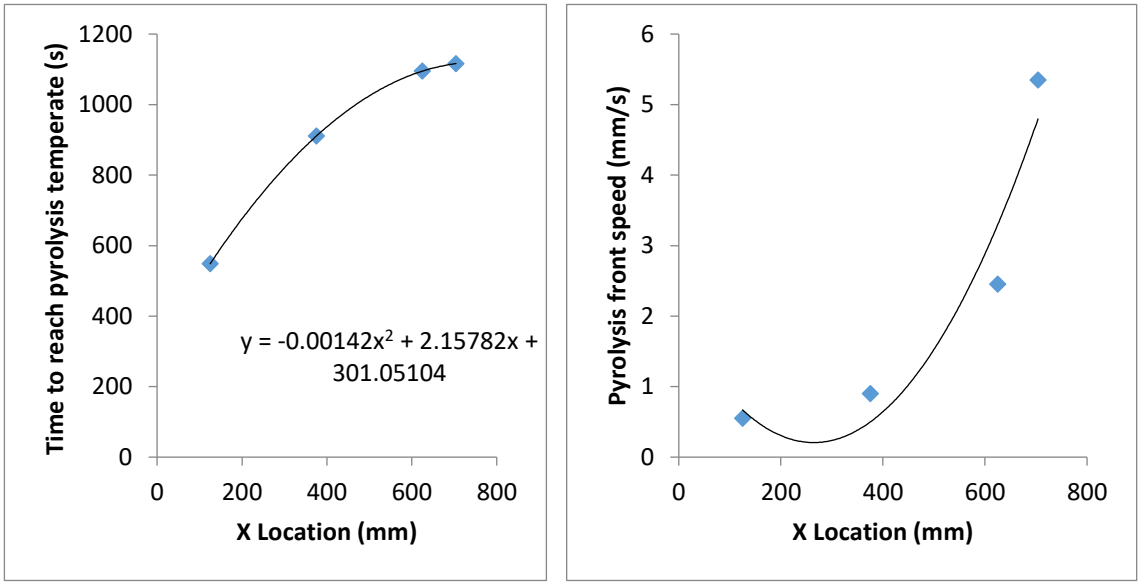

Figure 4.32 Test 6 (Left) time to pyrolysis temperature with respect to the X location. (Right) Pyrolysis front movement rate as a function of location.

Table 4-3 gives the extent of pyrolysis in the tabular form against X location as well as the heat flux value at that location. The heat flux is interpolated from that obtained from calibration before the starts of experimental investigation as mentioned in the chapter 3 previously.

Table 4-3 Extent of pyrolysis front as X location with respective heat flux

Test Number	X location (mm)	Heat Flux value (kW/m^2)
1	701	18.2
2	907	10.3
3	952	7.1
4	456	19.9
5	743	12.2
6	704	14.1

4.4.1 Discussion

Figure 4.27 to Figure 4.30, reveal that the initiation of the pyrolysis front occurs at x=375mm, which is just above the centre of the radiant panel where the highest heat flux value is present, and propagates in both directions. The figures also present the rate of forward propagation of the pyrolysis front, which follows a steady quadratic decline trend.

Figure 4.31 and Figure 4.32, show a completely different trend for Test 5 and 6. Seems like the pyrolysis propagation is accelerating. One of the explanation that can be provided here is that due to the downstands used in these tests the hot gases tend to get collected underneath the ceiling, forming a kind of hot layer. This increase the heat feedback and might in turn also enhance the movement of pyrolysis front. But this is not an very accurate or quantitative evidence based explanation rather just an observation from the experiments. Further detailed investigation and quantitative evidence is required to back this hypothesis.

The values of heat flux in the Table 4-3 contain a number of error sources, one of the major error source is that the heat flux values are given by calibration prior to the experiment. Hence, it does not incorporate the actual heat flux at that location during the experiment. This error can be minimized by using the TSC values for the heat flux which will provide the actual value at that location during the experiment, this will include the contribution by the flames as well as the hot layer created right below the sample.

4.5 Gas velocities

Test 3 and Test 4 results of gas velocities is presented in this section. These two tests are chosen as the representative as the trend and behaviour is similar in all the tests. Moreover, for other Tests either the some or all of the GTCs got damaged which are required for the density correction of the velocity values.

The voltages (V) from the DPTs are first converted into pressure values using calibration constant, P=10V. The differential pressure is calculated $\Delta P=P-P_0$. Where P_0 is the time average of 1st minute for the pressure values. This differential pressure ins converted into velocity using equation (12).

$$U = K\sqrt{\frac{2\Delta P}{\rho_g}} \tag{12}$$

Here ρ_g is the gas velocity given by equation (13) [50],

$$\rho_g = \frac{352.14}{T_g + 273.15} \tag{13}$$

The correction factor K is given by

$$K = 0.0649\ln(V) + 0.8486 \tag{14}$$

The calculation of the velocity 'U' and the correction factor, denoted as 'K', was performed using the model for the differential pressure transducers, with an adapted version of the proposed model by Gupta et al [88]. This is presented by Julian et al [105].

For the data smoothing, exponential smoothing was done which is presented in equation (15) [106],

$$S_t = \beta A_{t-1} + (1-\beta)S_{t-1} \tag{15}$$

Here 'S' is the smoothed value and 'A' is the actual value. Subscript 't' is for the current time step and 't-1' is for previous time step. The results are shown in Figure 4.33 and Figure 4.34.

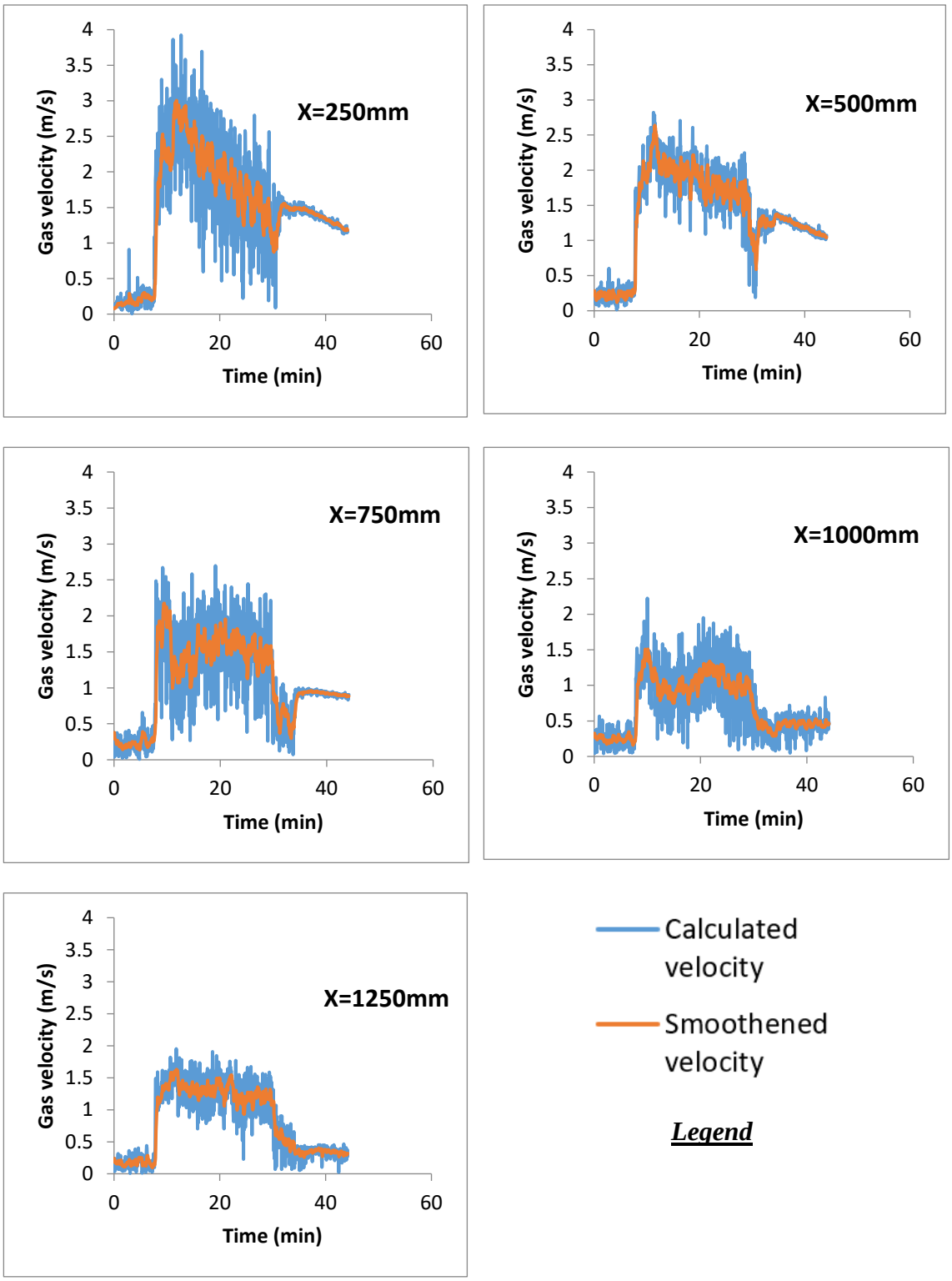

Figure 4.33 Test 3 Actual and smoothened gas velocities

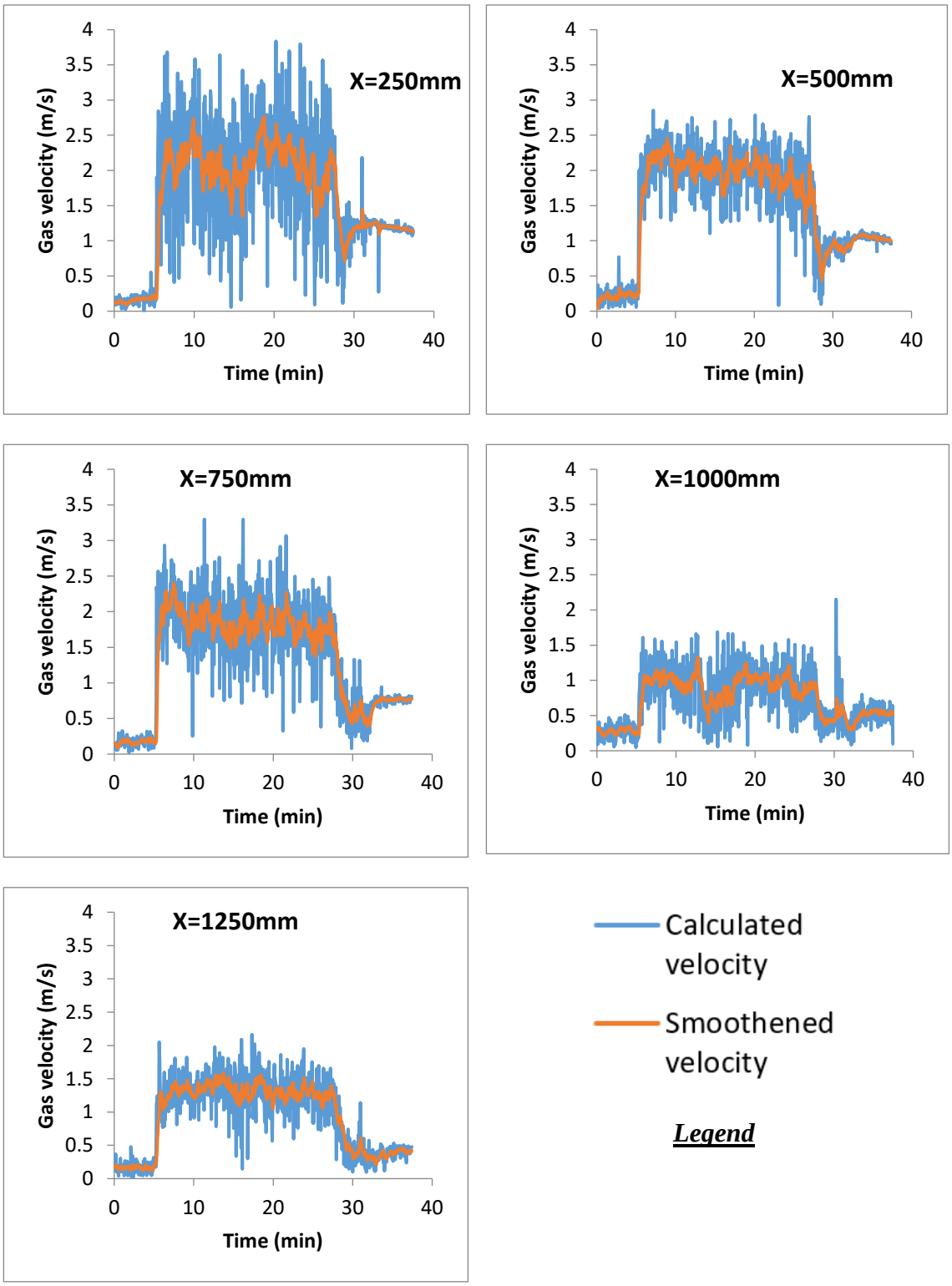

Figure 4.34 Test 4 Actual and smoothened gas velocities

4.5.1 Discussion

The smoothing factor 'β', in equation (15) is optimized for different locations based on the fluctuations. Using a guess value for 'β', say 0.5, a smoothened curve is obtained. Error between these two is calculated, $E_t = A_t - S_t$. The root mean squared error is evaluated using equation (16),

$$E_{rms} = \sqrt{\frac{\sum_1^n E_t^2}{n}} \tag{16}$$

This E_{rms} varies with 'β', so Erms is minimized and corresponding 'β' is selected. The values of 'β' are in the range of 0.71-0.85.

From Figure 4.33 and Figure 4.34 it can be observed that the highest velocity is observed at x=250mm and this value decreases downstream. High turbulence is also observed in the form of fluctuations at x=250mm, which yields high smoothing factors. This supports the previous conclusion of no flame spread on top of radiant panel due high gas velocities and high turbulence. The fluctuations tend to increase again around 750mm, this is due to flaming at this location. The edge flames tends to join each other near this location hence high fluctuations.

4.6 "Pyrolysis Front Spread Parameter"

Time to ignition is a different variable than time to pyrolysis, as pyrolysis time only include the time required to reach a temperature where the volatile are released form the surface, whereas the time ignition includes the pyrolysis time as well as the mixing time. Usually, the mixing time scale are small enough to neglect as compared to the time to pyrolyze.

An effort to develop an analogy between the time to ignition and time to pyrolysis is made to replace the t_{ig} with t_p in equation (4), (5), (9) and (10). The resulting equations are given below,

$$t_p = \frac{\pi}{4} k\rho c \frac{\left(T_p - T_0\right)^2}{\left(\dot{Q}_R^{''} - CHF\right)^2} \tag{12}$$

$$\frac{1}{\sqrt{t_p}} = \frac{2}{\sqrt{\pi}} \frac{1}{\sqrt{k\rho c}} \frac{\dot{Q}_R''}{(T_p - T_0)} \tag{13}$$

$$v_p \approx \frac{h_t^2 \emptyset_p}{(k\rho c)(\dot{Q}_{ig}^{"} - \dot{Q}_R^{"})^2} \tag{14}$$

$$\frac{1}{\sqrt{v_p}} = -\sqrt{\frac{k\rho c}{h_t^2 \emptyset_p}} \dot{Q}_R^{"} + \sqrt{\frac{k\rho c}{h_t^2 \emptyset_p}} \dot{Q}_{ig}^{"} \tag{15}$$

Here, it can be seen the by replacing time to ignition with time to pyrolysis, a new parameter analogous to the flame spread parameter has emerged as $\emptyset_p$. This can be termed as the "Pyrolysis front spread parameter". It has the same units as the flame spread parameter. The only difference is that in flame spread parameter, movement of flame front is considered, whereas $\emptyset_p$ considers movement of pyrolysis front.

Test 3 is used a representative test as it has the best data from the tests such that little or no cable damages were observed and having a definitive trends in the measurement.

Figure 4.35 is plotted for the linearized form provided in equation (15). For inverse pyrolysis front speed obtained from Figure 4.29 vs heat flux obtained from Figure 3.8.

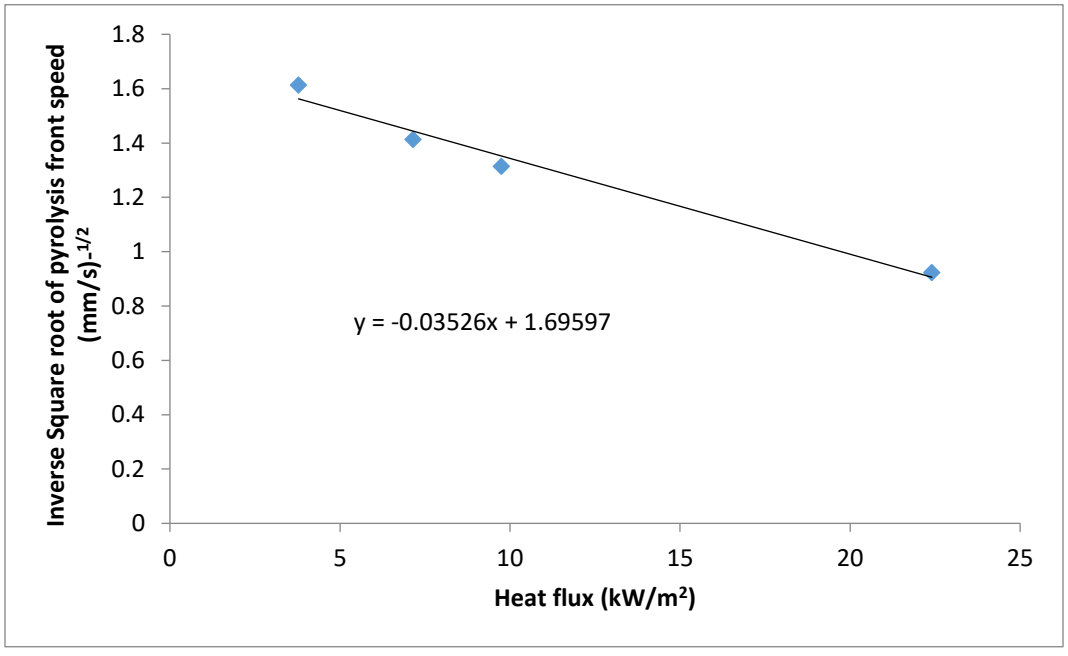

Figure 4.35 Inverse pyrolysis front speed vs heat flux for Test 3

Here the slope = $\sqrt{\frac{k\rho c}{h_t^2 \emptyset_p}}$ =0.03526 $m^2 s^{1/2}/kW mm^{1/2}$. After rearranging and separating the $\emptyset_p$ is evaluated to be 365 kW^2/m^3. This is an attempt to estimate the pyrolysis front spread parameter as analogous to the flame spread parameter. This attempt is made because the flame is attached to ceiling due to buoyancy and flame extension and flame spread are hard tell apart so pyrolysis front is considered. The value obtained for $\emptyset_p$ is almost 2 orders of magnitude larger than the flame spread parameter obtained for LIFT tests form literature for wooden products. The range of values obtained from Quintiere[52] is 9-13 kW^2/m^3 for wood based materials. This huge variation suggests that the theoretical model might not be valid in this orientation which is further discussed in the final discussion provided below.

4.6.1 Discussion

The ignition model and also the flame spread model, as flame spread is considered to be sequence of ignition processes, has the same assumptions. A major assumption here is that tine scale of mixing is neglected as it is considered to be small enough as compared to the time to release combustibles. But this assumption tends to break down in this orientation as we have seen that combustible released don't burn and tend to go downstream, mix with air and then combust downstream from the ignition.

Considering Test 3, X location 750mm the time to pyrolysis is found to be t_p=825s. And the time for flame to reach this location is t=200s. This shows that there is flaming at this location even before the pyrolysis has started. Flame has reached this location because the combustibles released from the surface upstream of this location, reach this location and burn. So actually the flame is due to upstream combustibles because this location has not yet reached the pyrolysis temperature.

Chapter 5: Conclusion and Future Recommendations

5.1 Conclusions

The conclusions that can be drawn from this experimental research and from the results and discussion are provided in this section below,

- The flame problem is highly sensitive to the geometric design. Small changes in the experimental setup changes the fire behaviour. This is due to fact that geometric changes affect the residence time of combustible gases below the sample and higher the residence time more the probability of combustion we can get. This is evident from the results of Test 1 and Test 3. Even though the heat flux distribution is identical but no flame spread was observed in Test 1 but there was flame spread in Test 3.
- The fluid dynamics plays a very important role in the flaming. As seen that the part right above the radiant panel did not burn with flames, but the pyrolysis was going on. This is the evidence of being depend heavily on the fluid dynamics. The velocity of gases and high turbulence right above do not allow the combustibles being released from the surface to ignite. Rather these combustible are ignited and burnt downstream from the radiant panel.
- The above points are also evident from the addition of the downstands in Test 5 and Test 6. This had a huge impact on the flame spread and fire behaviour. Even the propagation of pyrolysis was effected, which seemed to accelerate downstream.
- The ignition temperature is found to be 378^0C, which is inside the wide range obtained from different sources of literature.

- The critical heat flux value obtained is 14.47 kW/m^2. This value is also conservative and the actual value might even be lower than this. This is mainly due to the fact that actual heat flux value at the ignition location is not equal to representative heat flux being used. Rather due to change in view factors, a drop of heat flux is always present when we move in any direction away from the centre of radiant panel.
- Highest flame spread rate of 125mm/s was observed in Test 2 with highest heat flux.

5.2 Future Work

Further recommendations for the future is provided here in this section. These will be instrumental in any future investigation of this problem and complement current research effectively.

- Better experimental techniques to be used to characterize the flow field under the ceiling. Particle Image Velocimetry (PIV) [107] can be used to better understand the flow properties and turbulence created due to radiant panel buoyant flow. This will help quantify the pressures and velocities created due to buoyant flow. This will also provide insight into residence time of the gases under the samples before they spill from edges and go to exhaust.
- Use of electrical radiant panel instead of gas powered radiant panel is recommended by the author. This will remove any influence of the thermochemistry as the gases released by gas radiant panel is rich in content of CO_2 and H_2O vapour, which might have the suppression effect on the flame. Electrical radiant panel will remove this effect and the buoyant flow created by the panel will only have the ambient air.
- As the buoyant gases from radiant panel hit the sample from below, they tend to spread and flow radially. So a slight change in the experimental design, using square sample instead of rectangular samples, will be beneficial in understanding the fire behaviour and flame spread. The heating source placed at the centre, below the square sample and pilot flame will create a radial spread. In the cartesian coordinate system it will be 2D flame spread problem in x and y axis. But can be

simplified using cylindrical coordinate system, radial flame spread will be 1D flame spread problem in this coordinate system.

- Thin Skin Calorimeter (TSCs) cables got damaged during the testing, hence, for future TSC data should be used to identify any increase in the heat flux feedback due to the downstands, to quantify the possible trench effect. Also, to quantify the heat flux from the flame.

References

[1] Renewability and wood - decisions you can make to be kinder to the environment - Make It Wood, (n.d.). https://makeitwood.org/articles/renewability-and-wood (accessed March 18, 2023).

[2] I. Ferguson, B. La Fontaine, P. Vinden, L. Bren, R. Hateley, B. Hermesec, Environmental properties of timber, School of Forestry and Resource Conservation, University of Melbourne, Australia. (1996).

[3] M. Aboulnaga, M. Elsharkawy, Timber as a Sustainable Building Material from Old to Contemporary Experiences: Review and Assessment of Global and Egypt's Examples, The Importance of Wood and Timber in Sustainable Buildings. (2022) 89–129.

[4] B. Östman, D. Brandon, H. Frantzich, Fire safety engineering in timber buildings, Fire Saf J. 91 (2017) 11–20. https://doi.org/10.1016/j.firesaf.2017.05.002.

[5] C. Sposito, F. Scalisi, High-rise timber architecture: An opportunity for the sustainability of the built environment, Project: Essays & Researches. 2 (2019) 93–122.

[6] G. Concu, Introductory Chapter: Timber and Sustainability in Construction, in: G. Concu (Ed.), IntechOpen, Rijeka, 2019: p. Ch. 1. https://doi.org/10.5772/intechopen.90079.

[7] R. Emberley, C.G. Putynska, A. Bolanos, A. Lucherini, A. Solarte, D. Soriguer, M.G. Gonzalez, K. Humphreys, J.P. Hidalgo, C. Maluk, A. Law, J.L. Torero, Description of small and large-scale cross laminated timber fire tests, Fire Saf J. 91 (2017) 327–335. https://doi.org/10.1016/j.firesaf.2017.03.024.

[8] A. Bartlett, F. Wiesner, R. Hadden, L. Bisby, B. Lane, A. Lawrence, P. Palma, A. Frangi, Needs for total fire engineering of mass timber buildings, WCTE 2016 - World Conference on Timber Engineering. (2016).

[9] D. Barber, Tall Timber Buildings: What's Next in Fire Safety ?, Fire Technol. 51 (2015) 1279–1284. https://doi.org/10.1007/s10694-015-0497-7.

[10] B. Östman, E. Mikkola, R. Stein, A. Frangi, J. König, D. Dhima, T. Hakkarainen, J. Bregulla, Fire safety in timber buildings: technical guideline for Europe, 2010.

[11] C. Candido, P. Chakraborty, D. Tjondronegoro, The rise of office design in high-performance, open-plan environments, Buildings. 9 (2019) 100.

[12] V. Gupta, Open-plan compartment fire dynamics, (2021).

[13] J.L. Torero, A.H. Majdalani, C. Abecassis-Empis, A. Cowlard, Revisiting the compartment fire, Fire Safety Science. 11 (2014) 28–45.

[14] A.H. Majdalani, Compartment fire analysis for contemporary architecture, (2015).

[15] X. Dai, S. Welch, A. Usmani, A critical review of "travelling fire" scenarios for performance-based structural engineering, Fire Saf J. 91 (2017) 568–578.

[16] Y. Hasemi, M. Yoshida, Y. Yokobayashi, T. Wakamatsu, Flame Heat Transfer And Concurrent Flame Spread In A Ceiling Fire, Fire Safety Science. 5 (1997) 379–390. https://doi.org/10.3801/iafss.fss.5-379.

[17] E. Philion, B. Chorlton, J. Gales, P. Kotsovinos, Structural Fire Modeling Strategies for Exposed Mass Timber Compartments and Experimental Gaps for Model Validation, Journal of Performance of Constructed Facilities. 36 (2022) 1–14. https://doi.org/10.1061/(asce)cf.1943-5509.0001761.

[18] H.J. Park, An investigation into mysterious questions arising from the Dargue underground railway arson case through fire simulation and small-scale fire test, in: Proceedings of the 6th Asia-Oceania Symposium on Fire Science and Technology, 2004: pp. 16–27.

[19] W.G. Weng, Y. Hasemi, A numerical model for flame spread along combustible flat solid with charring material with experimental validation of ceiling flame spread and upward flame spread, Fire and Materials: An International Journal. 32 (2008) 87–102.

[20] N. Zhu, X. Huang, J. Fang, L. Yang, L. Hu, Transitional flame-spread and fuel-regression behaviors under the change of concurrent wind, Fire Saf J. 120 (2021) 103015.

[21] C.A.S. Hill, The environmental consequences concerning the use of timber in the built environment, Front Built Environ. 5 (2019) 129.

[22] R. Broun, G.F. Menzies, Life cycle energy and environmental analysis of partition wall systems in the UK, Procedia Eng. 21 (2011) 864–873.

[23] J. Hart, F. Pomponi, More timber in construction: Unanswered questions and future challenges, Sustainability (Switzerland). 12 (2020). https://doi.org/10.3390/SU12083473.

[24] Australia's largest commercial timber building rises in Sydney, (n.d.). https://inhabitat.com/australias-largest-commercial-timber-building-rises-in-sydney/ (accessed May 11, 2023).

[25] J.L. Torero, A.H. Majdalani, A.E. Cecilia, A. Cowlard, Revisiting the compartment fire, in: Fire Safety Science, International Association for Fire Safety Science, 2014: pp. 28–45. https://doi.org/10.3801/IAFSS.FSS.11-28.

[26] A.H. Buchanan, Fire performance of timber construction, Progress in Structural Engineering and Materials. 2 (2000) 278–289. https://doi.org/10.1002/1528-2716(200007/09)2:3<278::aid-pse33>3.3.co;2-g.

[27] C. Gorska, J.P. Hidalgo, J.L. Torero, Fire dynamics in mass timber compartments, Fire Saf J. 120 (2021) 103098. https://doi.org/10.1016/j.firesaf.2020.103098.

[28] R.M. Hadden, A.I. Bartlett, J.P. Hidalgo, S. Santamaria, F. Wiesner, L.A. Bisby, S. Deeny, B. Lane, Effects of exposed cross laminated timber on compartment fire dynamics, Fire Saf J. 91 (2017) 480–489. https://doi.org/10.1016/j.firesaf.2017.03.074.

[29] A. Frangi, M. Fontana, Fire performance of timber structures under natural fire conditions, Fire Safety Science. 8 (2005) 279–290.

[30] A. Bartlett, R. Hadden, L. Bisby, B. Lane, Auto-extinction of engineered timber as a design methodology, WCTE 2016 - World Conference on Timber Engineering. (2016).

[31] A.I. Bartlett, R.M. Hadden, J.P. Hidalgo, S. Santamaria, F. Wiesner, L.A. Bisby, S. Deeny, B. Lane, Auto-extinction of engineered timber: Application to compartment fires with exposed timber surfaces, Fire Saf J. 91 (2017) 407–413. https://doi.org/10.1016/j.firesaf.2017.03.050.

[32] A.I. Bartlett, Auto-Extinction of Engineered Timber, (2018) 190. https://pdfs.semanticscholar.org/c5a4/dbdf9a6e139f46cde0ea33a2d4e71a625ef7.pdf.

[33] A. Frangi, G. Bochicchio, A. Ceccotti, M.P. Lauriola, Natural full-scale fire test on a 3 storey XLam timber building, in: Proceedings of the 10th World Conference on Timber Engineering, 2008: pp. 2–5.

[34] D. Barber, R. Gerard, High-rise timber buildings, Fire Protection Engineering. 63 (2014) 10–20.

[35] C. McGregor, Contribution of cross laminated timber panels to room fires, (2013).

[36] R. Crielaard, J.-W. van de Kuilen, K. Terwel, G. Ravenshorst, P. Steenbakkers, Self-extinguishment of cross-laminated timber, Fire Saf J. 105 (2019) 244–260.

[37] R. McNamee, J. Zehfuss, A.I. Bartlett, M. Heidari, F. Robert, L.A. Bisby, Enclosure fire dynamics with a cross-laminated timber ceiling, Fire Mater. 45 (2021) 847–857.

[38] G.M.E. Cooke, Tests to determine the behaviour of fully developed natural fires in a large compartment, CRC, 1998.

[39] J.P. Hidalgo, A. Cowlard, C. Abecassis-Empis, C. Maluk, A.H. Majdalani, S. Kahrmann, R. Hilditch, M. Krajcovic, J.L. Torero, An experimental study of full-scale open floor plan enclosure fires, Fire Saf J. 89 (2017) 22–40. https://doi.org/10.1016/j.firesaf.2017.02.002.

[40] J.P. Hidalgo, T. Goode, V. Gupta, A. Cowlard, C. Abecassis-Empis, J. Maclean, A.I. Bartlett, C. Maluk, J.M. Montalvá, A.F. Osorio, J.L. Torero, The Malveira fire test: Full-scale demonstration of fire modes in open-plan compartments, Fire Saf J. 108 (2019) 102827. https://doi.org/10.1016/j.firesaf.2019.102827.

[41] V. Gupta, J.P. Hidalgo, A. Cowlard, C. Abecassis-Empis, A.H. Majdalani, C. Maluk, J.L. Torero, Ventilation effects on the thermal characteristics of fire spread modes in open-plan compartment fires, Fire Saf J. 120 (2021). https://doi.org/10.1016/j.firesaf.2020.103072.

[42] S. Nothard, D. Lange, J.P. Hidalgo, V. Gupta, M.S. McLaggan, The response of exposed timber in open plan compartment fires and its impact on the fire dynamics, (2020) 911–922. https://doi.org/10.14264/5d97785.

[43] S. Nothard, Traveling Fires in Open Plan Compartments with Mass Timber Lining, n.d.

[44] E. Rackauskaite, M. Bonner, F. Restuccia, N. Fernandez Anez, E.G. Christensen, N. Roenner, W. Wegrzynski, P. Turkowski, P. Tofilo, M. Heidari, P. Kotsovinos, I. Vermesi, F. Richter, Y. Hu, C. Jeanneret, R. Wadhwani, G. Rein, Fire Experiment Inside a Very Large and Open-Plan Compartment: x-ONE, Fire Technol. 58 (2022) 905–939. https://doi.org/10.1007/s10694-021-01162-6.

[45] M. Heidari, E. Rackauskaite, M. Bonner, E. Christensen, S. Morat, H. Mitchell, P. Kotsovinos, P. Turkowski, W. Wegrzynski, P. Tofilo, G. Rein, Fire experiments inside a very large and open-plan compartment: x-TWO, (2020). https://doi.org/10.14264/b666dc1.

[46] P. Kotsovinos, E. Rackauskaite, E. Christensen, A. Glew, E. O'Loughlin, H. Mitchell, R. Amin, F. Robert, M. Heidari, D. Barber, G. Rein, J. Schulz, Fire dynamics inside a large and open-plan compartment with exposed timber ceiling and columns: CodeRed #01, Fire Mater. (2022) 1–27. https://doi.org/10.1002/fam.3049.

[47] P. Kotsovinos, E.G. Christensen, E. Rackauskaite, A. Glew, E. O'Loughlin, H. Mitchell, R. Amin, F. Robert, M. Heidari, D. Barber, Impact of ventilation on the fire dynamics of an open-plan compartment with exposed timber ceiling and columns: CodeRed# 02, Fire Mater. (2022).

[48] P. Kotsovinos, E.G. Christensen, A. Glew, E. O'Loughlin, H. Mitchell, R. Amin, F. Robert, M. Heidari, D. Barber, G. Rein, J. Schulz, Impact of partial encapsulation on the fire dynamics of an open-plan compartment with exposed timber ceiling and columns: CodeRed #04 , Fire Mater. (2023) 1–30. https://doi.org/10.1002/fam.3112.

[49] M.J. Hurley, D.T. Gottuk, J.R. Hall Jr, K. Harada, E.D. Kuligowski, M. Puchovsky, J.M. Watts Jr, C.J. WIECZOREK, SFPE handbook of fire protection engineering, Springer, 2015.

[50] D. Drysdale, An introduction to fire dynamics, third edition, 3rd ed., Wiley, Chichester, West Sussex, U.K, 2011. https://doi.org/10.1002/9781119975465.

[51] I.S. Wichman, Theory of opposed-flow flame spread, Prog Energy Combust Sci. 18 (1992) 553–593. https://doi.org/10.1016/0360-1285(92)90039-4.

[52] J.G. Quintiere, Fundamentals of Fire Phenomena, 2006. https://doi.org/10.1002/0470091150.

[53] J.N. De Ris, Spread of a laminar diffusion flame, Symposium (International) on Combustion. 12 (1969) 241–252. https://doi.org/10.1016/S0082-0784(69)80407-8.

[54] R.F. McAlevy III, R.S. Magee, The mechanism of flame spreading over the surface of igniting condensed-phase materials, in: Symposium (International) on Combustion, Elsevier, 1969: pp. 215–227.

[55] F.A. Lastrina, R.S. Magee, R.F. McAlevy III, Flame spread over fuel beds: solid-phase energy considerations, in: Symposium (International) on Combustion, Elsevier, 1971: pp. 935–948.

[56] T. Hirano, S.E. Noreikis, T.E. Waterman, Postulations of flame spread mechanisms, Combust Flame. 22 (1974) 353–363.

[57] D.D. Drysdale, A.J.R. Macmillan, Flame spread on inclined surfaces, Fire Saf J. 18 (1992) 245–254.

[58] J.-W. Kwon, N.A. Dembsey, C.W. Lautenberger, Evaluation of FDS V. 4: upward flame spread, Fire Technol. 43 (2007) 255–284.

[59] M.J. Gollner, C.H. Miller, W. Tang, A. V. Singh, The effect of flow and geometry on concurrent flame spread, Fire Saf J. 91 (2017) 68–78. https://doi.org/10.1016/j.firesaf.2017.05.007.

[60] M.J. Gollner, X. Huang, J. Cobian, A.S. Rangwala, F.A. Williams, Experimental study of upward flame spread of an inclined fuel surface, Proceedings of the Combustion Institute. 34 (2013) 2531–2538. https://doi.org/10.1016/j.proci.2012.06.063.

[61] D. Fennell, Investigation into the King's Cross underground fire, (1988).

[62] D.D. Drysdale, A.J.R. Macmillan, D. Shilitto, The King's Cross fire: Experimental verification of the 'Trench effect,' Fire Saf J. 18 (1992) 75–82.

[63] G.H. Markstein, J. De Ris, Dynamics of Textile Fires: A Study of the Mechanisms--theory and Experiment, Factory Mutual Research, 1972.

[64] G.T. Atkinson, D.D. Drysdale, Y. Wu, Fire driven flow in an inclined trench, Fire Saf J. 25 (1995) 141–158.

[65] P.J. Woodburn, D.D. Drysdale, Fires in inclined trenches: the dependence of the critical angle on the trench and burner geometry, Fire Saf J. 31 (1998) 143–164.

[66] D.A. Smith, Measurements of flame length and flame angle in an inclined trench, Fire Saf J. 18 (1992) 231–244.

[67] P.J. Woodburn, D.D. Drysdale, Fires in inclined trenches: the effects of trench and burner geometry on the critical angle, Fire Safety Science. 5 (1997) 225–236.

[68] S. Simcox, N.S. Wilkes, I.P. Jones, Computer simulation of the flows of hot gases from the fire at King's Cross underground station, Fire Saf J. 18 (1992) 49–73.

[69] G. Cox, Letter to the Editor, Fire Modelling and the King's Cross Fire Investigation, Fire Safety J. 15 (1989) 103–106.

[70] L. Zhou, A.C. Fernandez-Pello, Turbulent, concurrent, ceiling flame spread: The effect of buoyancy, Combust Flame. 92 (1993) 45–59.

[71] W. Weng, Y. Hasemi, A numerical model for ceiling flame spread beneath a combustible board with charring material, Fire Safety Science. (2005) 385–396. https://doi.org/10.3801/IAFSS.FSS.8-385.

[72] W.G. Weng, Y. Hasemi, A Model for Ceiling Flame Spread, Fire Science and Technology. 24 (2005) 1–15. https://doi.org/10.3210/fst.24.1.

[73] W.G. Weng, Y. Hasemi, Theoretical analysis on flame dimension in turbulent ceiling fires, Int J Heat Mass Transf. 49 (2006) 154–158. https://doi.org/10.1016/j.ijheatmasstransfer.2005.06.036.

[74] W.G. Weng, Y. Hasemi, Heat transfer to an unconfined ceiling from an impinging buoyant diffusion flame, Heat and Mass Transfer/Waerme- Und Stoffuebertragung. 42 (2006) 652–659. https://doi.org/10.1007/s00231-005-0043-0.

[75] Y. Hasemi, D. Nam, M. Yoshida, Experimental flame correlations and dimensional relations in turbulent ceiling fires, in: Proceedings of the Fifth Asia-Oceania Symposium on Fire Science and Technology, Newcastle, Australia, Paper, 2001: pp. 1–11.

[76] Y. Hasemi, D. Nam, M. Yoshida, Experimental flame correlations and dimensional relations in turbulent ceiling fires, Proceedings of the Fifth Asia-Oceania Symposium on Fire Science and Technology, Newcastle, Australia, Paper. 25 (2001) 1–11.

[77] A.C. Fernandez-Pello, T. Hirano, Controlling Mechanisms of Flame Spread, Fire Science and Technology. 2 (1982) 17–54. https://doi.org/10.3210/fst.2.17.

[78] A.C. Fernandez-Pello, Upward laminar flame spread under the influence of externally applied thermal radiation, Combustion Science and Technology. 17 (1977) 87–98.

[79] A.C. Fernandez-Pello, Downward flame spread under the influence of externally applied thermal radiation, Combustion Science and Technology. 17 (1977) 1–9.

[80] K. Saito, F.A. Williams, I.S. Wichman, J.G. Quintiere, Upward turbulent flame spread on wood under external radiation, (1989).

[81] Y. Hasemi, M. Yoshida, A. Nohara, T. Nakabayashi, Unsteady-state upward flame spreading velocity along vertical combustible solid and influence of external radiation on the flame spread, in: Fire Safety Science—Proceedings of the Third International Symposium, Routledge, 2006: pp. 197–206.

[82] T. Kashiwagi, A study of flame spread over a porous material under external radiation fluxes, in: Symposium (International) on Combustion, Elsevier, 1975: pp. 255–265.

[83] K. Saito, F.A. Williams, I.S. Wichman, J. Quintiere, Experimental Study of Upward Turbulent Flame Spread on Wood Under External Radiation., Chemical and Physical Processes in Combustion, Fall Technical Meeting, The Eastern States Section. (1985).

[84] M. Suzuki, R. Dobashi, T. Hirano, Behavior of fires spreading downward over thick paper, in: Symposium (International) on Combustion, Elsevier, 1994: pp. 1439–1446.

[85] C.W. Leung, W.K. Chow, H. Kong, Review on four standard tests on flame spreading, International Journal on Engineering Performance-Based Fire Codes. 3 (2001) 67–86.

[86] M.L. Janssens, Measuring rate of heat release by oxygen consumption, Fire Technol. 27 (1991) 234–249. https://doi.org/10.1007/BF01038449.

[87] C.M. Smith, M.S. Hoehler, Imaging Through Fire Using Narrow-Spectrum Illumination, Fire Technol. 54 (2018) 1705–1723. https://doi.org/10.1007/s10694-018-0756-5.

[88] Gupta V, Maluk C, Torero JL, Hidalgo JP, Analysis of Convective Heat Losses in a Full-scale Compartment Fire Experiment, n.d.

[89] J.P. Hidalgo, C. Maluk, A. Cowlard, C. Abecassis-Empis, M. Krajcovic, J.L. Torero, A Thin Skin Calorimeter (TSC) for quantifying irradiation during large-scale fire testing, International Journal of Thermal Sciences. 112 (2017) 383–394. https://doi.org/10.1016/j.ijthermalsci.2016.10.013.

[90] C.M. Wolff, A versatile instrument for thermal radiation measurement, NASA. Goddard Space Flight Center Space Simulation, 7th. (1973).

[91] ASTM E1321, Standard Test Method for Determining Material Ignition and Flame Spread Properties, An American National Standard. 04 (2002) 1–16. https://doi.org/10.1520/E1321-18.1.

[92] BSI Standards Publication Reaction-to-fire tests — Heat release , smoke production and mass loss rate Part 1 : Heat release rate (cone calorimeter method) and smoke production rate, (2015).

[93] S. Srivaro, Z. Pásztory, H.A. Le Duong, H. Lim, S. Jantawee, J. Tomad, Physical, mechanical and thermal properties of cross laminated timber made with coconut wood, European Journal of Wood and Wood Products. 79 (2021) 1519–1529. https://doi.org/10.1007/s00107-021-01741-y.

[94] M.J. Hurley, D. Gottuk, J.R. Hall, K. Harada, E. Kuligowski, M. Puchovsky, J. Torero, Jj.M. Watts, C. Wieczorek, SFPE handbook of fire protection engineering, fifth edition, 2016. https://doi.org/10.1007/978-1-4939-2565-0.

[95] J. Shinoda, O.B. Kazanci, S.I. Tanabe, B.W. Olesen, Review on the surface heat transfer coefficients of radiant systems, E3S Web of Conferences. 111 (2019). https://doi.org/10.1051/e3sconf/201911101075.

[96] V. Babrauskas, Ignition of wood: A review of the state of the art, Journal of Fire Protection Engineering. 12 (2002) 163–189. https://doi.org/10.1177/10423910260620482.

[97] M. Janssens, Fundamental thermophysical characteristics of wood and their role in enclosure fire growth, (1991).

[98] Q. Xu, L. Chen, K.A. Harries, F. Zhang, Q. Liu, J. Feng, Combustion and charring properties of five common constructional wood species from cone calorimeter tests, Constr Build Mater. 96 (2015) 416–427. https://doi.org/10.1016/j.conbuildmat.2015.08.062.

[99] L. Shi, M.Y.L. Chew, A review of thermal properties of timber and char at elevated temperatures, Indoor and Built Environment. 32 (2023) 9–24. https://doi.org/10.1177/1420326X211035557.

[100] L. Yudong, D. Drysdale, Measurement of the Ignition Temperature of Wood, Fire Safety Science. 1 (1992) 25–30.

[101] F. Tang, P. Hu, Q. He, J. Zhang, J. Wen, Effect of sidewall on the flame extension characteristics beneath a ceiling induced by carriage fire in a channel, Combust Flame. 223 (2021) 202–215.

[102] M. Heidari, P. Kotsovinos, G. Rein, Flame extension and the near field under the ceiling for travelling fires inside large compartments, Fire Mater. 44 (2020) 423–436.

[103] Z. Gao, J. Ji, H. Wan, K. Li, J. Sun, An investigation of the detailed flame shape and flame length under the ceiling of a channel, Proceedings of the Combustion Institute. 35 (2015) 2657–2664.

[104] X. Zhang, H. Tao, W. Xu, X. Liu, X. Li, X. Zhang, L. Hu, Flame extension lengths beneath an inclined ceiling induced by rectangular-source fires, Combust Flame. 176 (2017) 349–357.

[105] V.K. Lach, A.W. Bradley, D. Lundberg, The Proceedings of the Tenth International Seminar on Fire and Explosion Hazards (ISFEH), n.d.

[106] W. Stallings, Exponential smoothing, Dr. Dobb's Journal. 23 (1997) 127–130. https://doi.org/10.1007/978-1-4419-6247-8_15241.

[107] R.J. Adrian, J. Westerweel, Particle image velocimetry, Cambridge university press, 2011.

Appendix A

Thermal penetration into the thickness

The temperature penetrated and travelled into the thickness of the sample. The rate of this thermal penetration was dependent on the incident heat flux. Higher the heat flux value higher the penetration rate into the thickness. The contour plots for the temperature isotherms travelling into the thickness are presented below for all the tests.

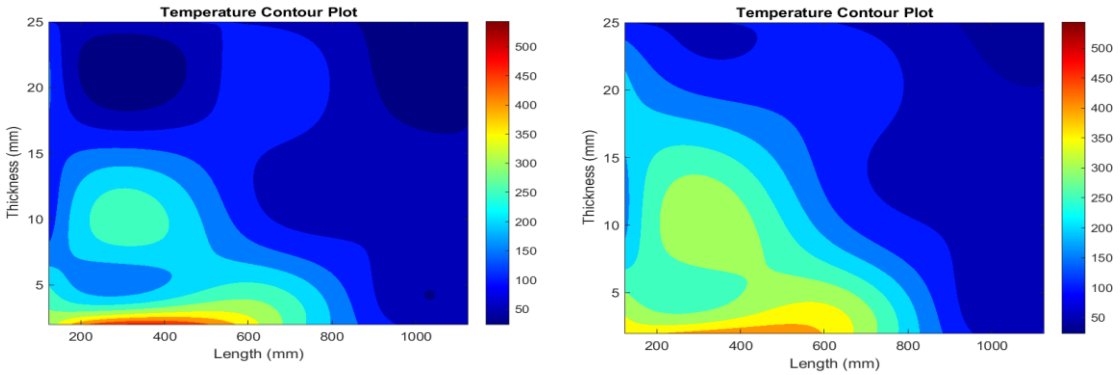

t=30min t=35min

Figure A-1 Temperature penetration contour plots for Test 1

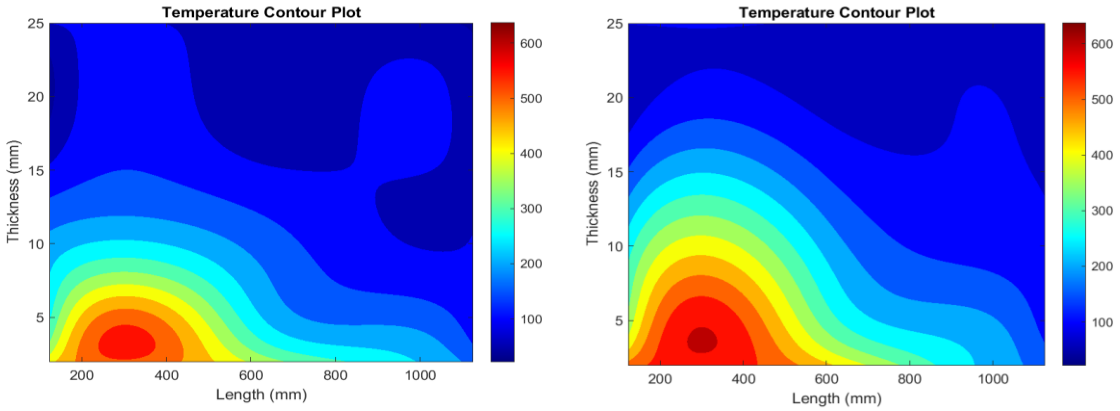

t=20min t=25min

Figure A-2 Temperature penetration contour plots for Test 2

a

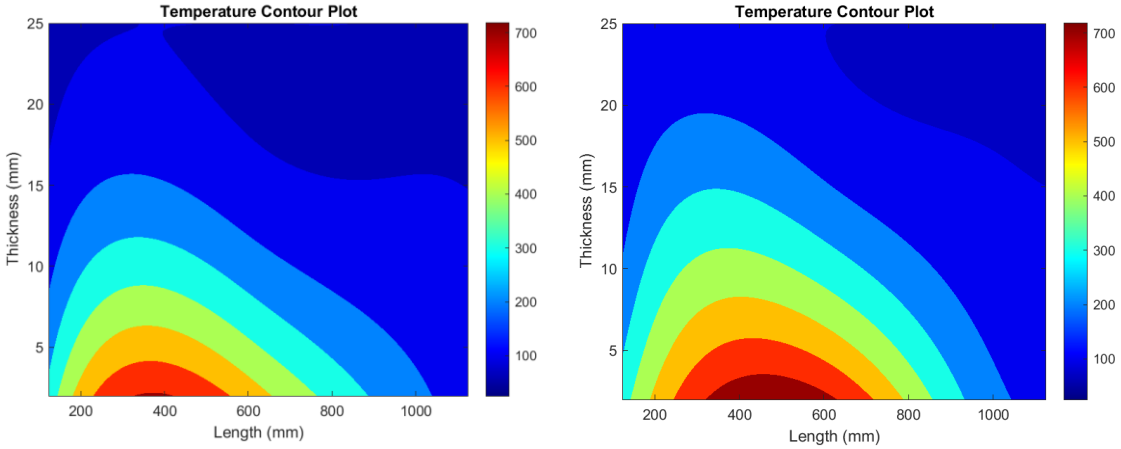

t=25min t=30min

Figure A-3 Temperature penetration contour plots for Test 3

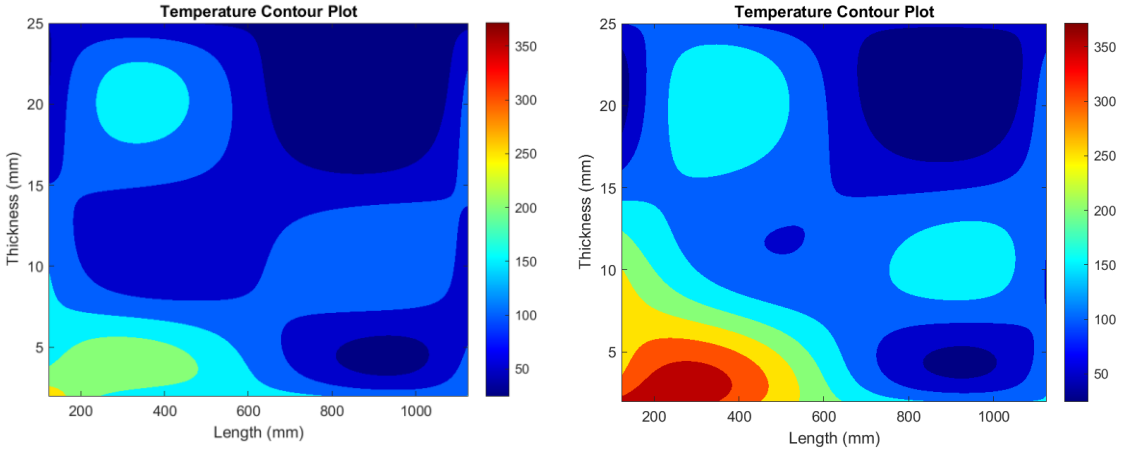

t=20min t=27min

Figure A-4 Temperature penetration contour plots for Test 4

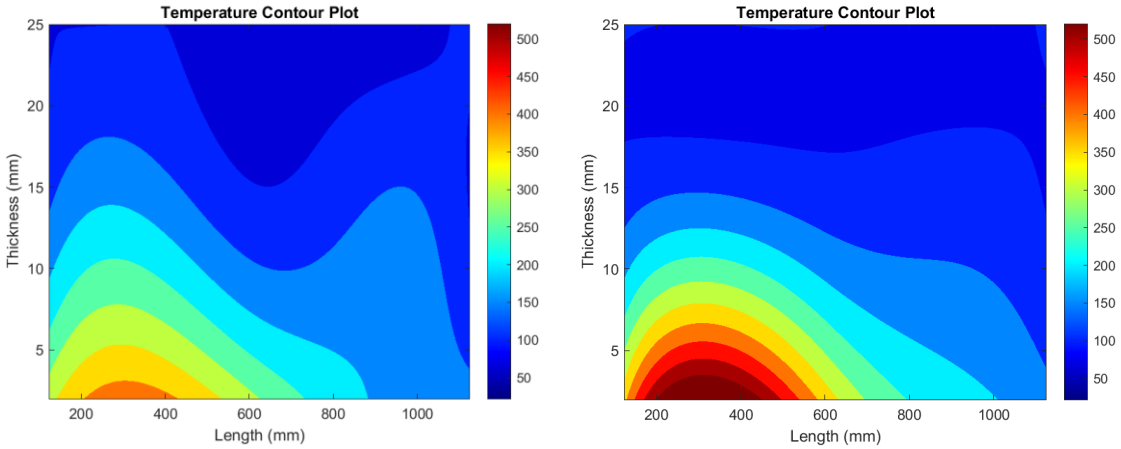

t=40min t=43min

Figure A-5 Temperature penetration contour plots for Test 5

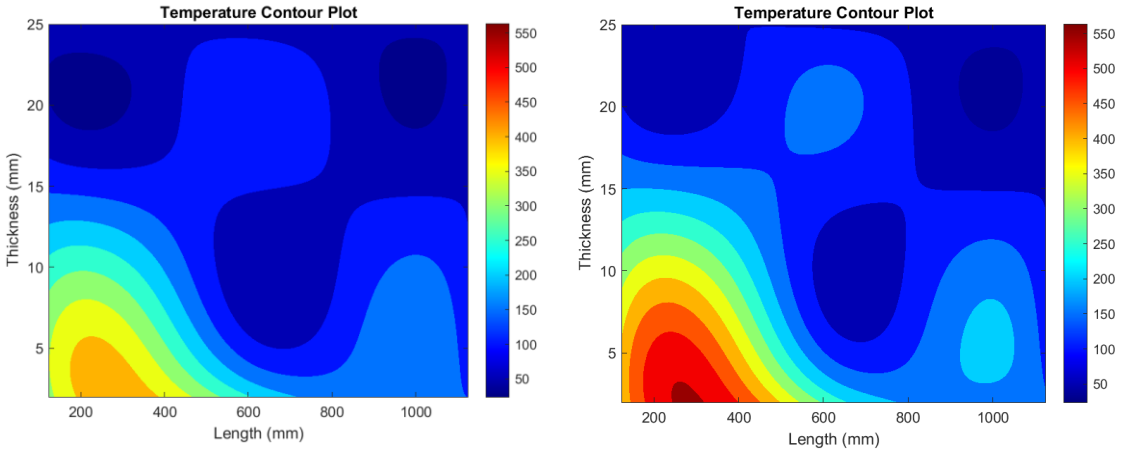

t=40min t=43min

Figure A-6 Temperature penetration contour plots for Test 6

Appendix B

Temperature Time History Plots for Solid Phase TC

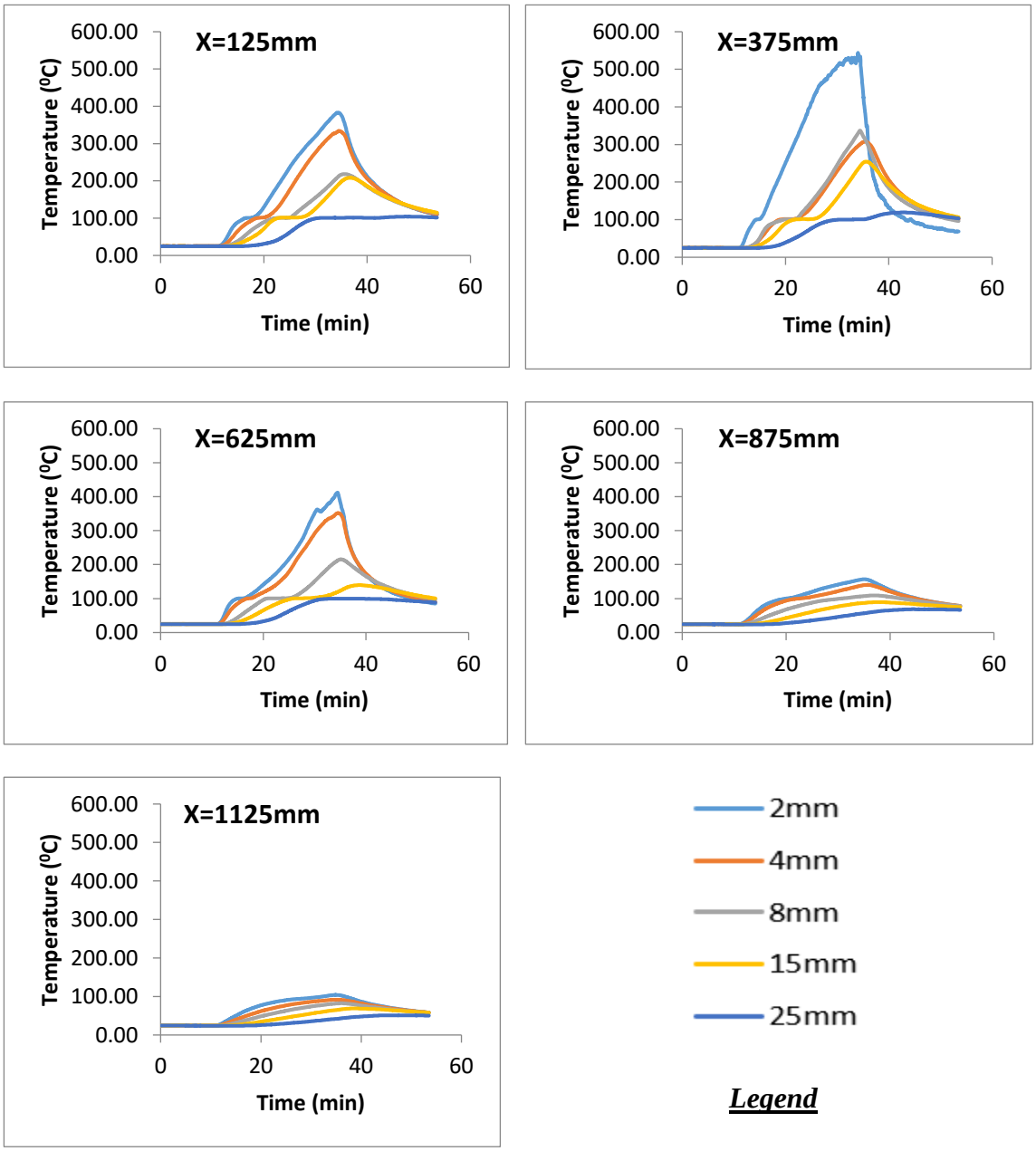

Figure B-1 Temperature histories through thickness for Test 1

d

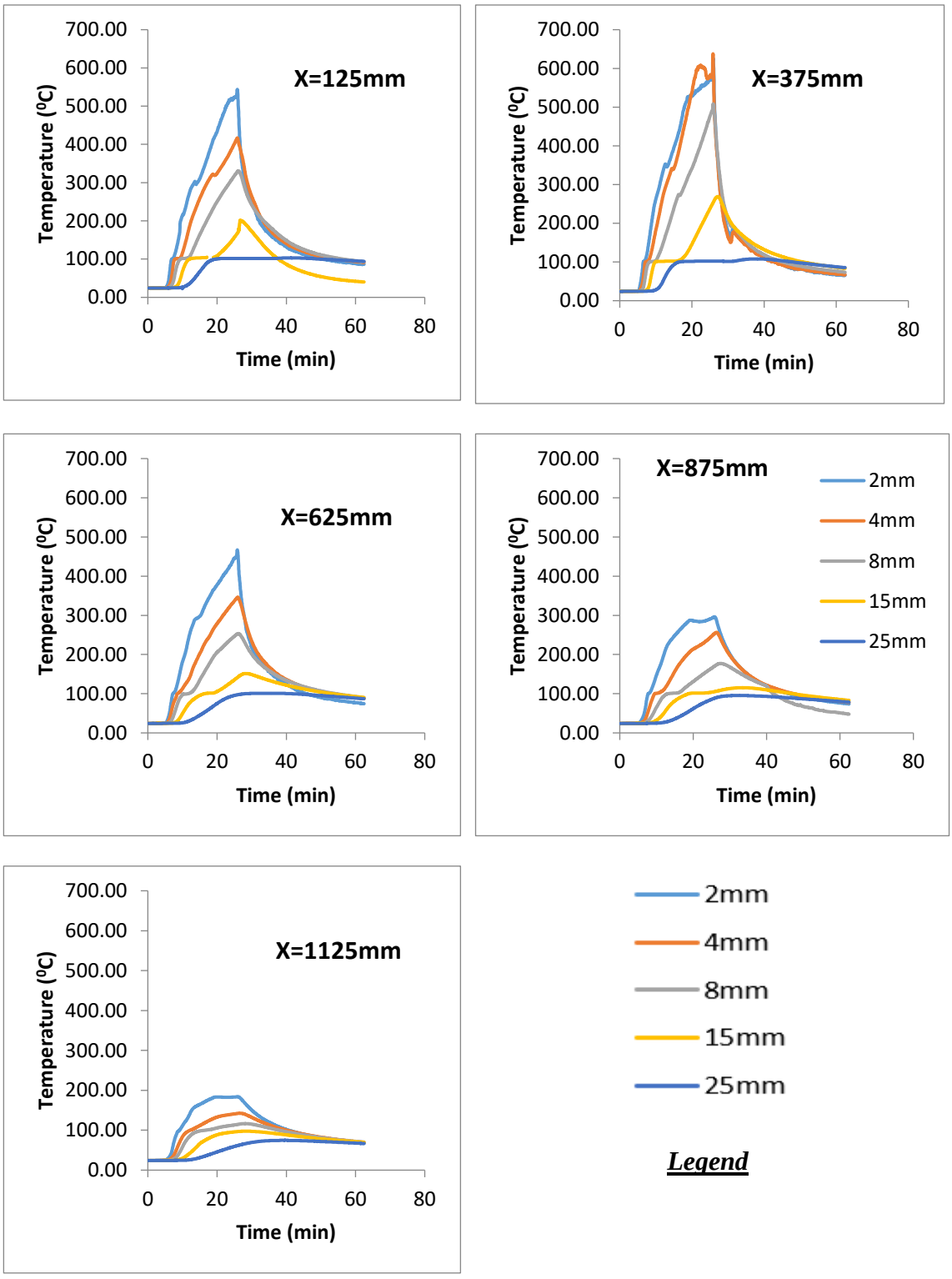

Figure B-2 Temperature histories through thickness for Test 2

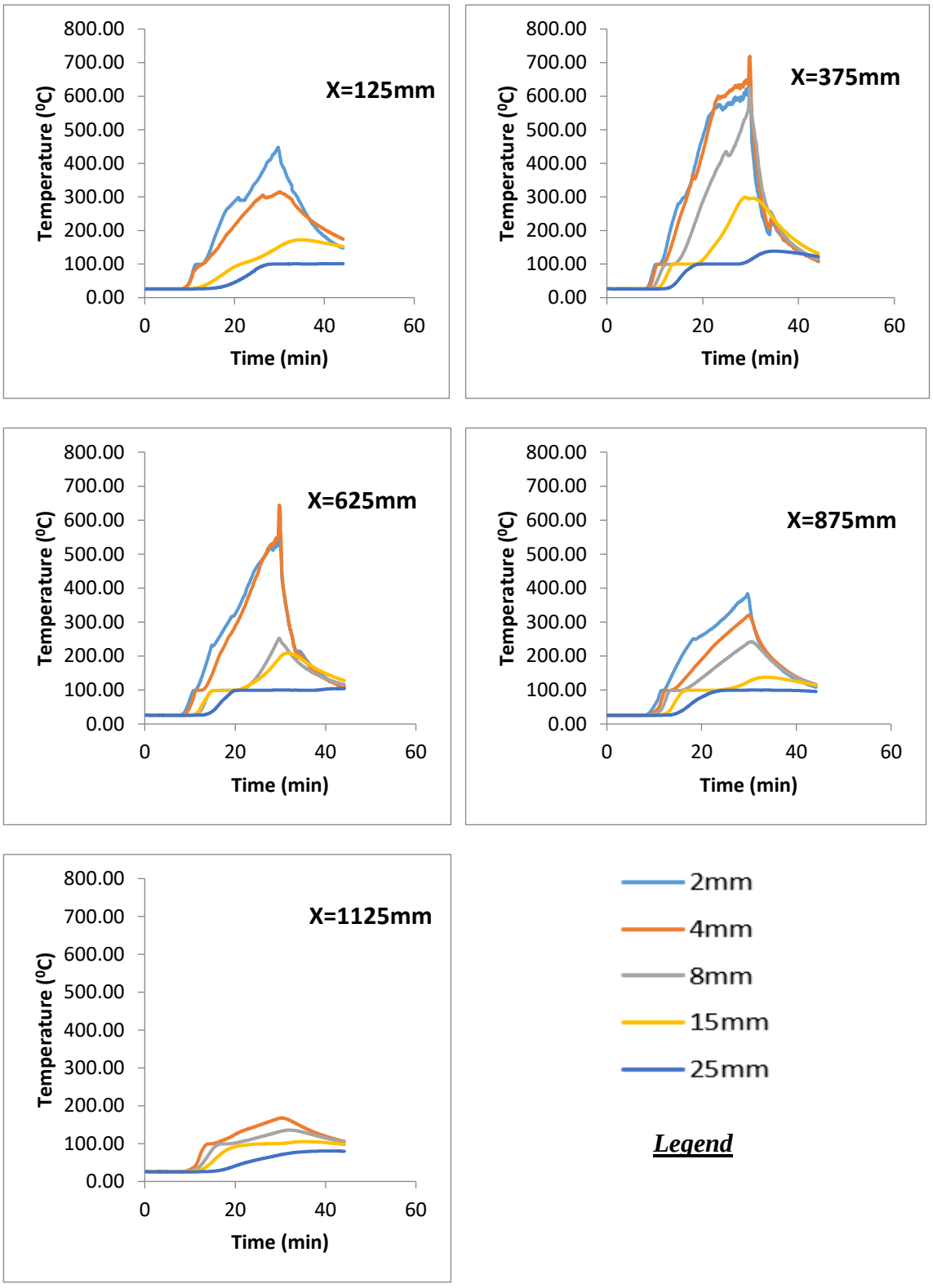

Figure B-3 Temperature histories through thickness for Test 3

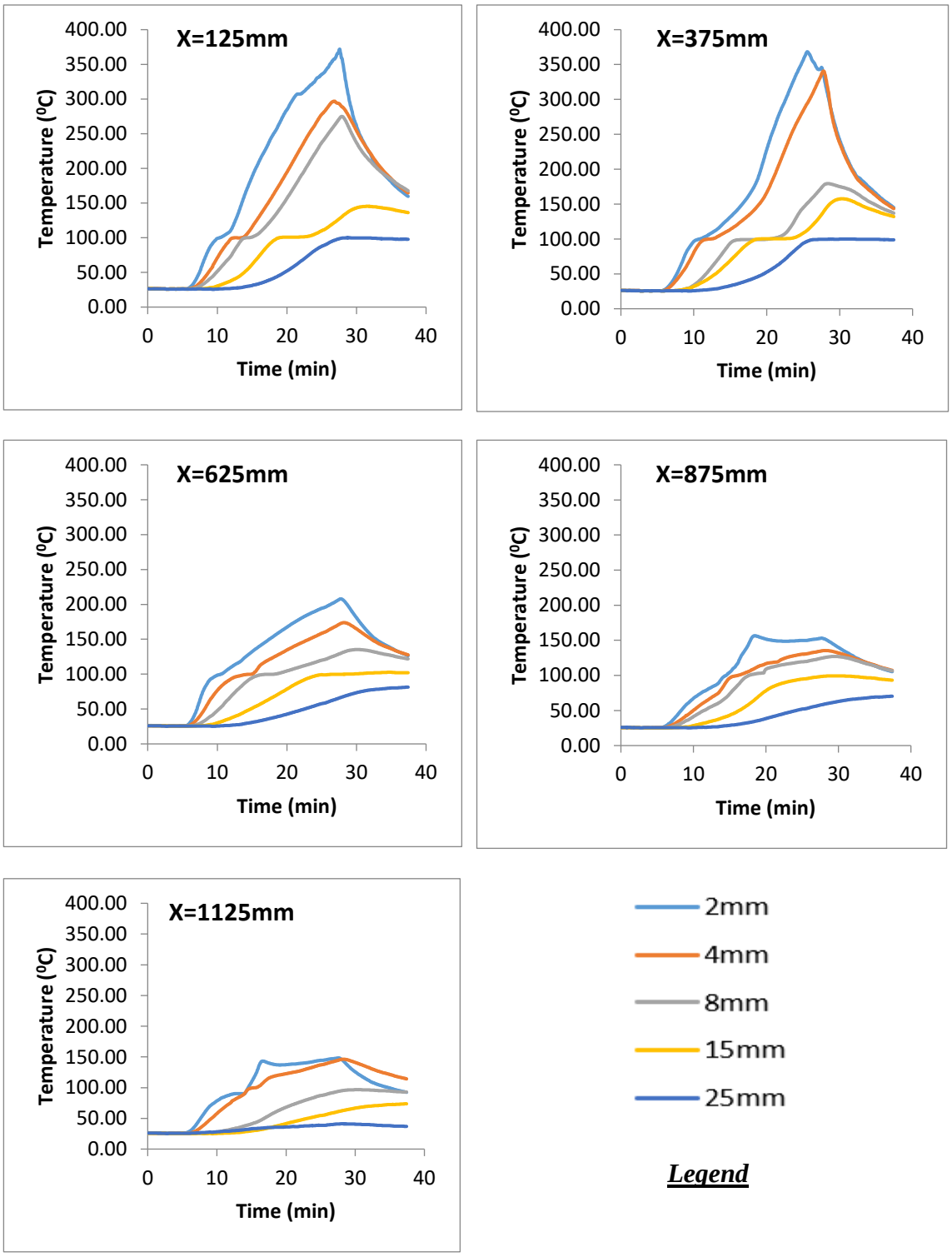

Figure B-4 Temperature histories through thickness for Test 4

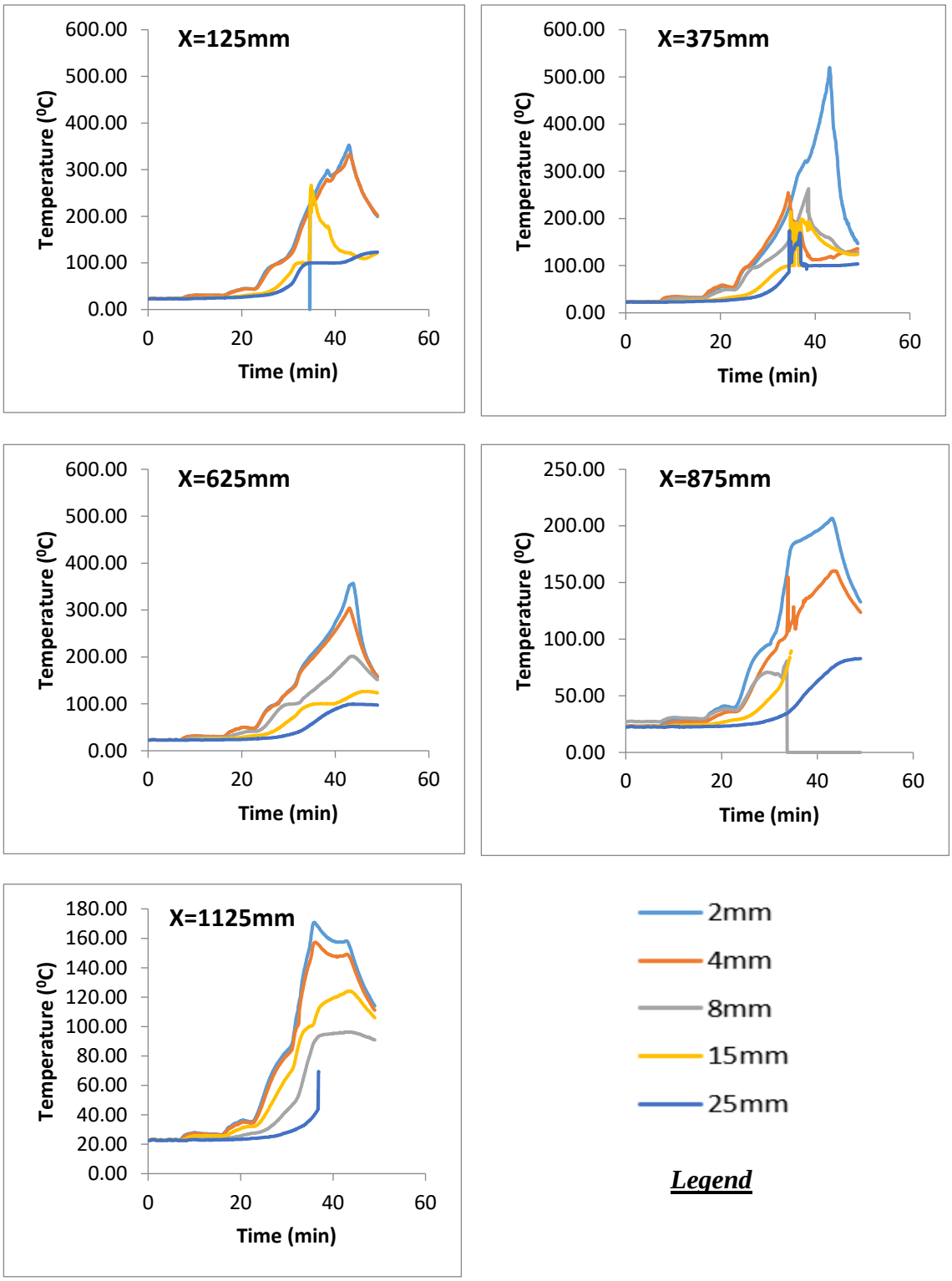

Figure B-5 Temperature histories through thickness for Test 5

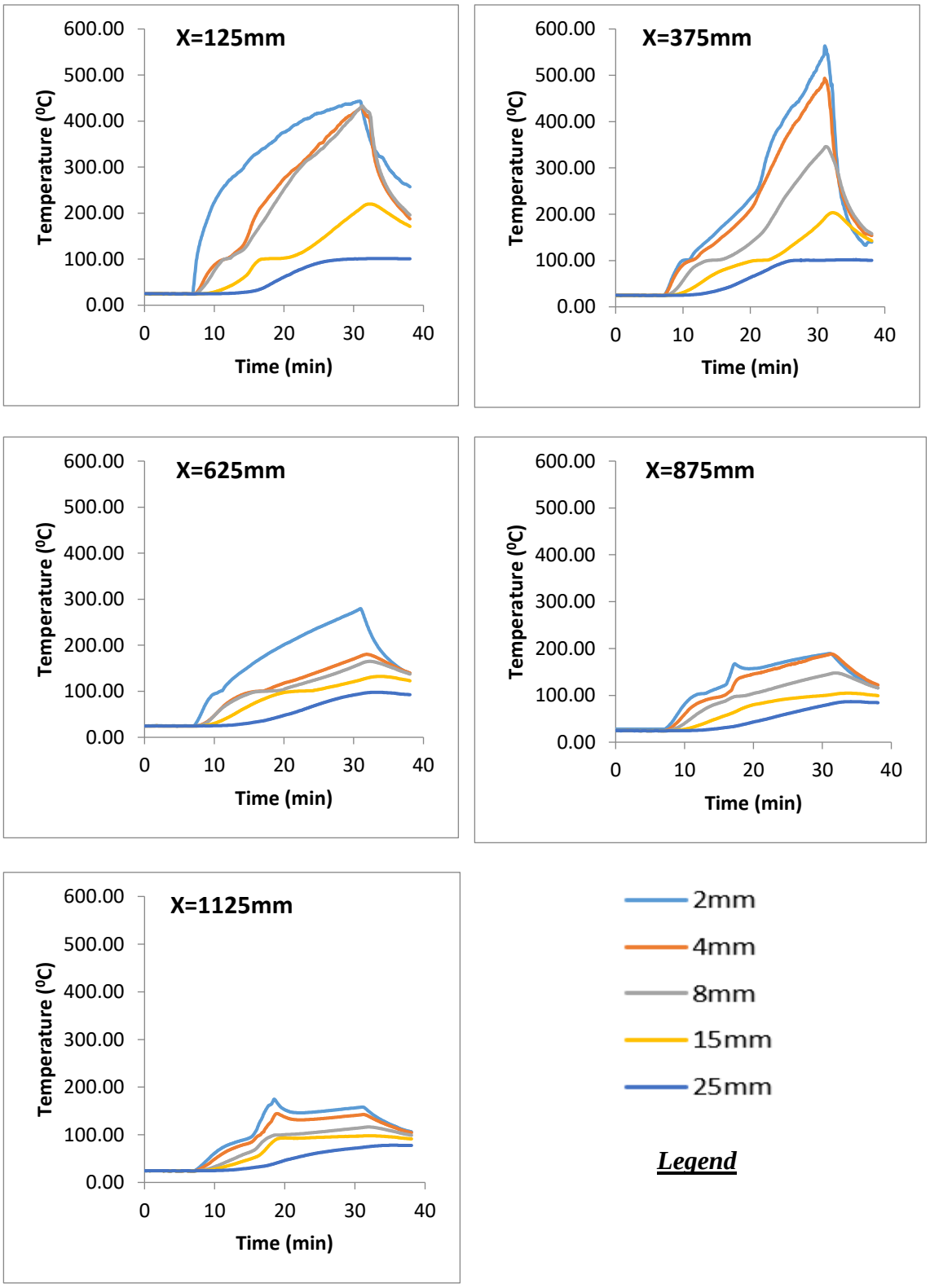

Figure B-6 Temperature histories through thickness for Test 6

Appendix C

Sample Drawing

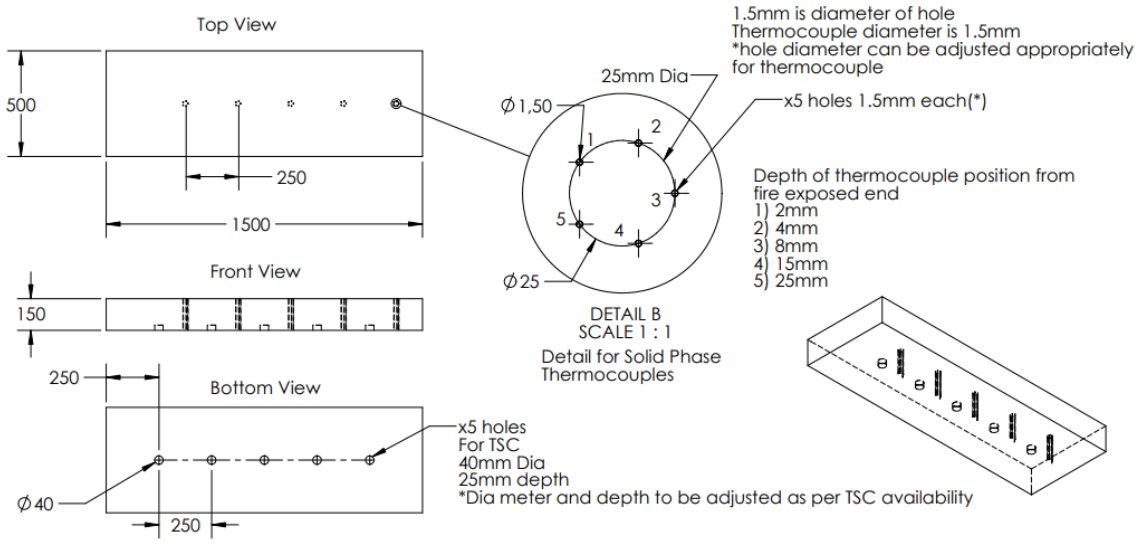

Figure C-1 Sample drawing/drilling template

Appendix D

MATLAB Scripts

Script for flame contours is presented below

```
clc
clear
% Load temperature data from Excel file
data = xlsread('flame spread calc2.xlsx');
x = data(:,1); % x-axis values
y = data(:,2); % y-axis values
T = data(:,3:end); % temperature values
N=size(T,2);
% Reshape temperature data to a 2D array for contour plot
n = length(unique(y));
m = length(unique(x));
a=unique(x);
b=unique(y);

for k=1:N
    my_field = strcat('Tmatrix_',num2str(k));
    variable.(my_field) = reshape(T(:,k), n, m);;
    %T_matrix0 = reshape(T(:,k), n, m);
    [X,Y] = meshgrid(a,b);
    BDmatrix=variable.(my_field);
    newpoints = 100;
    [xq,yq] = meshgrid(linspace(min(a),max(a),newpoints
),linspace(min(b),max(b),newpoints));
    BDmatrixq = interp2(X,Y,BDmatrix,xq,yq,'spline');
    %[c,h]=contourf(xq,yq,BDmatrixq);
    % Create contour plot
    f=figure;

    [c,h]=contourf(xq,yq,BDmatrixq,'edgecolor','none');
    caxis([0,1])
    c = gray(2);
    colormap(flipud(c));
    %colorbar;
    xlabel('Length (mm)');
    ylabel('Width (mm)');
    title('Flame Contour Plot');
    saveas(f, strcat('Test2_',num2str(k)),'png');
end
```

Script for extrapolation for surface temperature is presented below

```
clc
clear
% Load temperature data from Excel file
[num, txt, raw] = xlsread('surftemp.xlsx');
t = num(:,1); % Times in seconds
temp_2mm = num(:,2); % Temperatures at 2mm in degrees Celsius
temp_4mm = num(:,3); % Temperatures at 4mm in degrees Celsius
temp_8mm = num(:,4); % Temperatures at 8mm in degrees Celsius

% Interpolate temperature at x = 0 mm for each time value using quadratic
interpolation
y = [2 4 8];
temp = [temp_2mm temp_4mm temp_8mm];
yq = 0;

N=length(t);
for i=1:N
    tempq1(i) = interp1(y, temp(i,:), yq, 'spline', 'extrap');
    if tempq1(i)<max(temp(i,:))
        tempq1(i)=max(temp(i,:));
    end
end
tempq1=tempq1(:);

% Plot temperature at x = 0 mm as a function of time
% figure;
% plot(t, tempq1);
% hold on
% plot(t, temp);
% hold off
% xlabel('Time (s)');
% ylabel('Temperature (C)');
%title('Temperature at x = 0 mm vs Time');

temp_2mm = num(:,6); % Temperatures at 2mm in degrees Celsius
temp_4mm = num(:,7); % Temperatures at 4mm in degrees Celsius
temp_8mm = num(:,8); % Temperatures at 8mm in degrees Celsius

% Interpolate temperature at x = 0 mm for each time value using quadratic
interpolation
y = [2 4 8];
temp = [temp_2mm temp_4mm temp_8mm];
yq = 0;

N=length(t);
for i=1:N
    tempq2(i) = interp1(y, temp(i,:), yq, 'spline', 'extrap');
    if tempq2(i)<max(temp(i,:))
        tempq2(i)=max(temp(i,:));
    end
end
```

```
tempq2=tempq2(:);

% Plot temperature at x = 0 mm as a function of time
% figure;
% plot(t, tempq2);
% hold on
% plot(t, temp);
% hold off
% xlabel('Time (s)');
% ylabel('Temperature (C)');
%title('Temperature at x = 0 mm vs Time');

temp_2mm = num(:,10); % Temperatures at 2mm in degrees Celsius
temp_4mm = num(:,11); % Temperatures at 4mm in degrees Celsius
temp_8mm = num(:,12); % Temperatures at 8mm in degrees Celsius

% Interpolate temperature at x = 0 mm for each time value using quadratic
interpolation
y = [2 4 8];
temp = [temp_2mm temp_4mm temp_8mm];
yq = 0;

N=length(t);
for i=1:N
    tempq3(i) = interp1(y, temp(i,:), yq, 'spline', 'extrap');
    if tempq3(i)<max(temp(i,:))
        tempq3(i)=max(temp(i,:));
    end
end
tempq3=tempq3(:);

% Plot temperature at x = 0 mm as a function of time
% figure;
% plot(t, tempq3);
% hold on
% plot(t, temp);
% hold off
% xlabel('Time (s)');
% ylabel('Temperature (C)');
%title('Temperature at x = 0 mm vs Time');

temp_2mm = num(:,14); % Temperatures at 2mm in degrees Celsius
temp_4mm = num(:,15); % Temperatures at 4mm in degrees Celsius
temp_8mm = num(:,16); % Temperatures at 8mm in degrees Celsius

% Interpolate temperature at x = 0 mm for each time value using quadratic
interpolation
y = [2 4 8];
temp = [temp_2mm temp_4mm temp_8mm];
yq = 0;

N=length(t);
for i=1:N
    tempq4(i) = interp1(y, temp(i,:), yq, 'spline', 'extrap');
```

```
    if tempq4(i)<max(temp(i,:))
        tempq4(i)=max(temp(i,:));
    end
end
tempq4=tempq4(:);

% Plot temperature at x = 0 mm as a function of time
% figure;
% plot(t, tempq4);
% hold on
% plot(t, temp);
% hold off
% xlabel('Time (s)');
% ylabel('Temperature (C)');
% title('Temperature at x = 0 mm vs Time');

temp_2mm = num(:,18); % Temperatures at 2mm in degrees Celsius
temp_4mm = num(:,19); % Temperatures at 4mm in degrees Celsius
temp_8mm = num(:,20); % Temperatures at 8mm in degrees Celsius

% Interpolate temperature at x = 0 mm for each time value using quadratic
interpolation
y = [2 4 8];
temp = [temp_2mm temp_4mm temp_8mm];
yq = 0;

N=length(t);
for i=1:N
    tempq5(i) = interp1(y, temp(i,:), yq, 'spline', 'extrap');
    if tempq5(i)<max(temp(i,:))
        tempq5(i)=max(temp(i,:));
    end
end
tempq5=tempq5(:);

% Plot temperature at x = 0 mm as a function of time
%figure;
%plot(t, tempq5);
%hold on
%plot(t, temp);
%hold off
%xlabel('Time (s)');
%ylabel('Temperature (C)');
%title('Temperature at x = 0 mm vs Time');

% Find the first time when the temperature crosses 378
time =zeros(1,5);
found = false;
for i = 1:N
    if tempq1(i) >= 378
        found = true;
        break;
    end
end
```

```
if i ~= N
    time(1)=t(i);
end

found = false;
for i = 1:N
    if tempq2(i) >= 378
        found = true;
        break;
    end
end
if i ~= N
    time(2)=t(i);
end

found = false;
for i = 1:N
    if tempq3(i) >= 378
        found = true;
        break;
    end
end
if i ~= N
    time(3)=t(i);
end

found = false;
for i = 1:N
    if tempq4(i) >= 378
        found = true;
        break;
    end
end
if i ~= N
    time(4)=t(i);
end

found = false;
for i = 1:N
    if tempq5(i) >= 378
        found = true;
        break;
    end
end
if i ~= N
    time(5)=t(i);
end

time=time(:)
% Export temperature data to Excel file
output_data = [t tempq1 tempq2 tempq3 tempq4 tempq5];
xlswrite('surftemp_output.xlsx', output_data, 'Sheet1');
output_time=[time];
xlswrite('pyrolysistime.xlsx', output_time, 'Sheet1');
```

Script for temperature contours is presented below

```
clc
clear
% Load temperature data from Excel file
data = xlsread('Book.xlsx');
x = data(:,1); % x-axis values
y = data(:,2); % y-axis values
T = data(:,3:11); % temperature values
N=size(T,2);
% Reshape temperature data to a 2D array for contour plot
n = length(unique(y));
m = length(unique(x));
a=unique(x);
b=unique(y);

for k=1:N
    my_field = strcat('Tmatrix_',num2str(k));
    variable.(my_field) = reshape(T(:,k), n, m);;
    %T_matrix0 = reshape(T(:,k), n, m);
    [X,Y] = meshgrid(a,b);
    BDmatrix=variable.(my_field);
    newpoints = 100;
    [xq,yq] = meshgrid(linspace(min(a),max(a),newpoints
),linspace(min(b),max(b),newpoints));
    BDmatrixq = interp2(X,Y,BDmatrix,xq,yq,'spline');
    %[c,h]=contourf(xq,yq,BDmatrixq);
    % Create contour plot
    f=figure;

    [c,h]=contourf(xq,yq,BDmatrixq,'edgecolor','none');
    caxis([25.36,718.88])
    c = jet();
    colormap(c);
    colorbar;
    xlabel('Length (mm)');
    ylabel('Thickness (mm)');
    title('Temperature Contour Plot');
    saveas(f, strcat('Test3_',num2str(k)),'png');
end
```